ACTA UNIVERSITATIS SZEGEDIENSIS

ACTA PHYSICA ET CHEMICA

NOVA SERIES

TOMUS XXV FASCICULI 3—4

AUSHAF 25 (3—4) (85—210) (1979)

HU ISSN 0324—6523 Acta Univ, Szeged
HU ISSN 0001—6721 Acta Phys. et Chem.

SZEGED, HUNGARIA
1979

ACTA UNIVERSITATIS SZEGEDIENSIS

ACTA PHYSICA ET CHEMICA

NOVA SERIES

TOMUS XXV. FASCICULI 3—4

AUSHAF 25 (3—4) 85—210 (1979)

HU ISSN 0324—6523 Acta Univ, Szeged
HU ISSN 0001—6721 Acta Phys. et Chem

SZEGED, HUNGARIA
1979

Kiadja

a József Attila Tudományegyetem Természettudományi Kara
(Szeged, Aradi vértanuk tere 1.)

Szerkesztő bizottsági titkárok:

ANDOR J., BÁRDI I., MOLNÁR Á., NÉMET B. és SÜLI Á.

Kiadványunk rövidítése:

Acta Phys. et Chem. Szeged

ELECTRON SCATTERING CROSS SECTION OF CH_4; A MULTIPLE SCATTERING CALCULATION

By

ZS. VARGA, I. GYÉMÁNT and M. G. BENEDICT

Department of Theoretical Physics, Attila József University
Szeged

(Received October 10, 1979)

The total cross section of CH_4 molecules for elastic electron scattering is calculated by a multiple scattering method. The scattering potential includes the following terms: a static potential calculated with the X_α method, a free electron gas exchange potential, and a polarization term for which two variants have been used. The results are discussed and compared with previous calculation and experimental total cross section data.

Introduction

Total cross sections for electron-molecule collisions have been investigated experimentally for many years.

Theoretical results which reproduce the characteristic behaviour of the total cross section for elastic electron scattering on polyatomic molecules have been published, however, only recently. One of the difficulties in calculations arises due to the complexity of the multiple scattering effects, even in the rigid molecule approximation.

In this paper we present results on the total cross section of the electron-methane molecule elastic scattering. The method used here is a modified version of the multiple scattering calculations developed by JOHNSON [1] for determining bound electronic states. Namely, it is a generalized partial wave analysis proposed by DEMKOV and RUDAKOV [2] and extended for a cluster of muffin-tin potentials by ZIESCHE and JOHN [3]. A somewhat different formulation of the scattering problem was proposed by DILL and DEHMER [4, 5].

The details of the scheme of present calculations is described in [6] and this formalism of the multiple scattering problem has been applied for the electron SF_6 molecule scattering [6, 7].

In the following, first we describe the construction of the static molecule potentials for the methane molecule, then present the calculated total cross sections comparing them with experimental data [8—11] and previous calculation [12].

Model

For construction of the potential seen by the scattered electron, as a first step, a self-consistent multiple scattering $X\alpha$ calculation was performed for the rigid CH_4 molecule with the parameters of ref. [13].

The molecular field is partitioned into three types of muffin-tin regions: The atomic region consists of atomic spheres of radii b_p around the p-th atomic nucleus at R_p ($p=C, H^{(1)}, \ldots$). The potential V_p in the p-th atomic sphere is taken to be spherically symmetric. The atomic region is enclosed in a sphere of radius b_0, the so-called Watson sphere, centered in this case at R_c. In the interatomic region — the region outside the atomic spheres and inside the Watson sphere — the potential $\overline{V}$ is constant. The outer region is the region outside the Watson sphere, where the potential V_0 is assumed to be spherically symmetric.

The exchange part of the self-consistent $X\alpha$ molecular potential was changed to a more detailed free-electron exhange potential [14]:

$$V_x(r) = -\frac{4}{\pi} K_F \cdot F(K/K_F) \tag{1}$$

where

$$F(\eta) = \frac{1}{2} + \frac{1-\eta^2}{4\eta} \ln \left| \frac{1+\eta}{1-\eta} \right|. \tag{2}$$

The maximum momentum K_F is expressed by the electron density $\varrho(r)$ of the target as

$$K_F(r) = [3\pi^2 \varrho(r)]^{1/3}. \tag{3}$$

For the momentum K of the electron with kinetic energy E, HARA [15] used the following approximation:

$$K^2(r) = E + I + K_F^2(r) \tag{4}$$

which is reasonable at small r. In our case, *i.e.* for CH_4 the ionization potential I has the value of 1.14 Ry [11]. Eqs. (1—4) give the so called Hara free electron gas exchange (HFEGE) potential [16].

The obvious way to correct Eq. (4) for large r is to remove the ionization energy:

$$K^2(r) = E + K_F^2(r) \tag{5}$$

giving a more attractive exchange potential. Combining Eq. (5) with Eqs. (1—3) gives the asymptotically adjusted free electron gas exchange (AAFEGE) potential [16].

The scattering potentials were constructed with the AAFEGE approximation outside of the Watson sphere and with HFEGE approximation inside of it.

To include polarization effects we first added a polarization potential of the form

$$V_{\text{pol}}(r) = -\frac{\alpha}{r^4} \left(1 - e^{-\frac{r}{r_0}}\right)^6 \tag{6}$$

centered on the carbon site, where α is the static molecular polarizability ($\alpha=17.5$ for methane [17]). This type of polarization potential was suggested by GIANTURCO and THOMPSON [12] who chose the "cut-off" r_0 to be 0.84 by fitting calculated total cross sections to experimental data. In this way they could reproduce the experimental total cross section satisfactorily. The potential constructed in this way will be referred to as potential I. We performed the calculation with another type of potential (potential II) as well. Here the dipole part $-\alpha/r^4$ of the "true" polarization potential was added to the potential in the outer region. Inside the Watson sphere we simply modified the potential by $-\frac{\alpha}{b_0^4}$ in the interatomic and in the hydrogen regions.

Results and Discussion

In the wave function of the scattered electron mixed of partial waves with different angular momenta the $l=6$ term gave the highest contribution to be taken into account in our calculations.

The total scattering cross section calculated with potential I does not even qualitatively reproduce the results of Ref. [12] or the experimental results of Ref. [11]. This discrepancy is due to the polarization which is clearly overestimated having a deep minimum within the carbon site. In fact, as mentioned by GIANTURCO and THOMPSON [12], the polarization potential of Eq. (6) is essentially chosen by appeal to experiment and not to the polarization effect itself.

Potential II with a more flat polarization, as described in the previous section, produces the total scattering cross section plotted in Fig. 1; for comparison the recent experimental values of [11] are also given. The total cross section is a sum

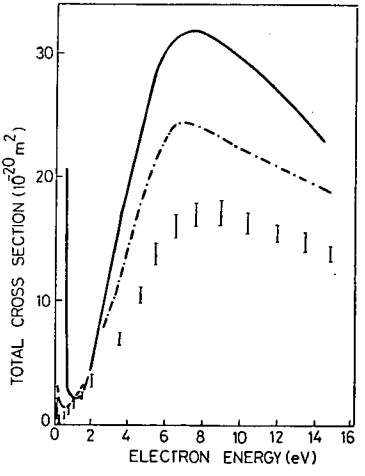

Fig. 1. Total scattering cross section calculated with potential II (solid line). Experimental values of Ref. [11] (error bars), Ref. [9] (dashed line) Ref. [10] (dash-dotted line)

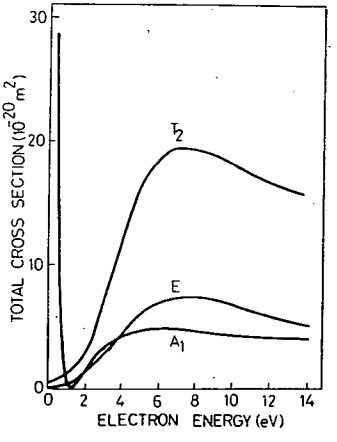

Fig. 2. The cross sections of different symmetry for potential II.

of contributions of cross sections belonging to the A_1, E, T_2 irreducible representations (IR) of the T_d symmetry group of the CH_4 molecule. (The other two IRs do not appreciably contribute in this energy range.) This decomposition is shown in Fig. 2. It can be seen that the broad maximum near 7.5 eV is dominated by T_2 symmetry. The minimum in Fig. 1 at 1.2 eV is in qualitative agreement with the experimental total cross section. At low energies there appears a sharp increase of A_1 origin in accord with the calculation in [12].

These results show that an essential point in the calculations is the choice of the potential seen by the scattered electron. The muffin-tin approximation, on one hand, turns out to be appropriate for molecular calculations and for electron scattering on 'nearly spherical' molecules, *e.g.* on SF_6 [6]. As to the exchange and especially the polarization part of the potential on the other hand we are left to rough approximations.

Nevertheless, the characteristic features of the experimental total cross section for electron-methane elastic scattering can be reproduced. Better agreement, however, can be achieved by using more reasonable potentials; this needs further investigations.

References

[1] *Johnson, K. H.:* Adv. Quant. Chem. **7**, 143 (1973).
[2] *Demkov, Yu., N. V. S. Rudakov:* Zh. Eksp. Teor. Fiz. **69**, 2035 (1970).
[3] *Ziesche P., W. John:* J. Phys. B: Atom. Molec. Phys. **9**, 333 (1976).
[4] *Dill, D., J. L. Dehmer:* J. Chem. Phys. **61**, 692 (1974).
[5] *Dehmer, J. L., J. Siegel and D. Dill:* J. Chem. Phys. **69**, 5205 (1978).
[6] *Gyemánt, I., Zs. Varga, M. G. Benedict:* Int. J. Quant. Chem. **XVII.**, 255 (1980).
[7] *Benedict, M. G., I. Gyemánt:* Int. J. Quant. Chem. **XIII.**, 597 (1978).
[8] *Brode, R. B.:* Phys. Rev. **25**, 636 (1925).
[9] *Brüche E.:* Ann. Phys. (Leipzig) **4**, 387 (1930).
[10] *Ramsauer C., R. Kollath: ibid:* **4**, 91 (1930).
[11] *Barbarito E., M. Basta, M. Calicchio, G. Tessari:* J. Chem. Phys. **71**, 54 (1979).
[12] *Gianturco, F. A., D. G. Thompson:* J. Phys. B: Atom. Molec. Phys. **9**, L383 (1976).
[13] *Danese, J. B.:* Int. J. Quant. Chem. **6S**, 209 (1972).
[14] *Gombás, P.:* Die Statistische Theorie des Atoms (Springer, Wien, 1949).
[15] *Hara, S.:* J. Phys. Soc. Japan **22**, 710 (1967).
[16] *Riley, M., D. Truhlar:* J. Chem. Phys. **63**, 2182 (1975).
[17] *Landolt—Börnstein:* Zahlenwerte und Funktionen (Springer, Berlin, 1951), Vol. I. pt 3, p. 511

СЕЧЕНИЕ ЭЛЕКТРОННОГО РАССЕЯНИЯ CH_4: РАСЧЕТ МЕТОДОМ МНОГОКРАТНОГО РАССЕЯНИЯ

Ж. Варга, И. Деманит и М. Г. Бенедикт

Рассчитано полное сечение молекулы CH_4 для упругого электронного рассеяния методом многократного рассеяния. Потенциал рассеяния состоит из следующих частей: статический потенциал рассчитанный методом X_α, обменной потенциал типа свободного электронного газа и поляризационный член, для которого было применено два варианта. Обсуждаются результаты и сравниваются с предыдущими рассчетами и с экспериментальными сечениями.

LOW TEMPERATURE ELECTRON PARAMAGNETIC STUDIES IN VANADIUM PHOSPHATE GLASSES

By

L. I. HORVÁTH

Institute of Biophysics, Biological Research Center, Szeged

and

T. SZÖRÉNYI

Institute of Experimental Physics, Attila József University, Szeged

(Received September 10, 1979)

In vanadium phosphate glasses the paramagnetism is due to the conducting 3d electrons of V^{4+} centers and, thus, the electron exchange frequency between V^{4+} and V^{5+} ions as followed by EPR lineshape analysis can furnish direct information on the mobility of the charge carrier. In the central region of the spectrum where the parallel and perpendicular lines overlap the characteristic hopping frequency can be followed through two orders of magnitude. If spin-spin interaction should also be taken into account, the temperature dependence of paramagnetic susceptibility provides useful structural data.

Introduction

The diverse application of semiconducting glasses results in a need for deeper understanding of the physical events in these materials; a challenge which has initiated both thorough theoretical and experimental work. In vanadium phosphate (V_2O_5—P_2O_5) glasses the conduction mechanism can be described in terms of phonon assisted hopping of electrons between V^{4+} and V^{5+} ions [1, 2]. Since electron paramagnetic resonance (EPR) provides information about the 3d electron of the V^{4+} ion, it has been widely used to study the short range order around the V^{4+} centers. However, the lineshape analysis of the EPR spectra which can furnish information about the dynamical behaviour of the conducting 3d electrons gained less interest. LIVAGE *et al.* found that in amorphous vanadium pentoxide the paramagnetic resonance exhibited hyperfine splitting (hfs), whereas in crystallized samples no hyperfine splitting could be resolved. They interpreted this phenomenon by considering the electron delocalization to an adjacent vanadium nucleus, and gave an upper limit for the hopping frequency [3, 4]. A complete EPR analysis can, thus, reveal not only structural aspects but also dynamical features. From EPR theoretical point of view V^{4+} is one of the most extensively studied transition metal ions and its application is not limited to vanadium containing systems as it is indicated by the current interest of introducing V^{4+} spin probes into different materials.

Since we are interested in the anomalous conductivity properties of vanadium phosphate glasses which may be of both microstructural and dynamical origin [5, 6], in a series of investigations we analysed the EPR lineshape of these glasses. It turned out that for glasses with low V^{4+} content the lineshape analysis could be quantitatively done, but beyond a certain V^{4+} content the hfs analysis broke down due to the concomitant line broadening of spin-spin interaction. LIVAGE and his coworkers observed no exchange narrowing down to liquid nitrogen temperature [3, 4]. On theoretical basis, however, exchange narrowing might be anticipated at low temperatures, and thus we extended the temperature range down to 20 K.

Experimental

EPR measurements were made with a JES-PE-IX (Jeol, Japan) X-band spectrometer using 100 kHz standard or 100 kHz/80 Hz double modulation techniques. For cryogenic work we applied a closed-cycle He cryostat (DISPLEX™, Air Products, USA; model CSW-202), which very economically extended our temperature range down to 20 K. This system permits flexibility by having a small expander conveniently mounted above the EPR cavity while compressor and controls are remotely located. The expander module consists of a two-stage piston: the first stage maintains the "warm" end of the second stage at low temperature (90 K). The samples are attached to the cold end of the second stage. The rate of cool down depends on the mass which is attached to the cold end and also the conductance of the heat path between the sample and the cold end. The system is thermally insulated from ambient conditions with a vacuum shroud. A vacuum of 5×10^{-4} torr or better is required to achieve good performance, which was done by connecting the expander module to a PST-60 E vacuum pumpstand (Balzers, Liechtenstein). The inevitable mechanical vibration of the sample due to the moving piston was minimized by mounting the expander module onto a bulky $\varphi-z$ translator.

The temperature was measured with a Chromel *vs.* gold — 0.07 at. % iron thermocouple at the cold end of the second stage. The heat path was manufactured from a single piece copper rod in order to minimize wrong heat conductance due to copper-to-copper soldering. The temperature was varied with a kanthal heating coil attached to the cold end of the second stage. As the kanthal coil warms up the cold end it reduces the cooling rate and, thus, the sample — through the heat path — equilibrates very fast with the cold end. The time period to establish any heat equilibria was monitored by the EPR signal intensity and a typical value of about 10 minutes was found (in 10 K steps).

During EPR measurements both the vacuum shroud and the cooled sample should be inserted into the cavity. Since the Q factor (which is proportional to the sensitivity) largely depends on the dielectric constant of the sample, only moderate amount of metal can be applied inside the cavity. This requirement was met by using a 1 mm dia. copper wire at the end of the heat path and a 11 mm O.D. quartz vacuum shroud (Fig. 1a).

The vanadium phosphate glasses were prepared from V_2O_5 and H_3PO_4 (Reanal, Hungary, purum grade). The V^{4+}/V_{total} $(=c)$ ratio was varied by melting the mixtures at various temperatures. As shown in Fig. 1a the samples were made by

immersing the end of the copper wire into the melt. The obtained material proved to be totally amorphous by X-ray diffraction and scanning electron microscopy.

Thermostatic analysis of the experimental set-up

From thermostatic point of view the set-up can be represented by the flow diagram given in Fig. 1b. Three factors determine the actual temperature of the sample: firstly the rate of the heat transmission between the cold end (heat sink) and the sample (denoted by 4→3→1 in Fig. 1b), secondly the rate of the radiation heat of the ambient heat reservoir which warms up the sample (5→4), and thirdly the heating rate of the coil which reduces the heat sinking efficiency of the cold end (2→1). Obviously an EPR application of the system is the most critical test, since in this case the sample is relatively far from the cold end and no silvered quartz extension tube can be applied to minimize the radiation heat. Less apparently, this transparent tube has other disadvantages too, for its geometrical sizes make very troublesome to provide a really efficient vacuum isolation. Needless to say whenever there was a heat conductance coupling between the ambient heat reservoir and the sample (Fig. 1b, dotted line 5→4), with its moderate heat sinking capacity (2 Watts) the cold end could hardly lower the temperature of the sample below room temperature. A typical case repeatedly experienced occurred when the sample touched the inner surface of the extension tube. However, with careful alignment of the sample this error could be prevented.

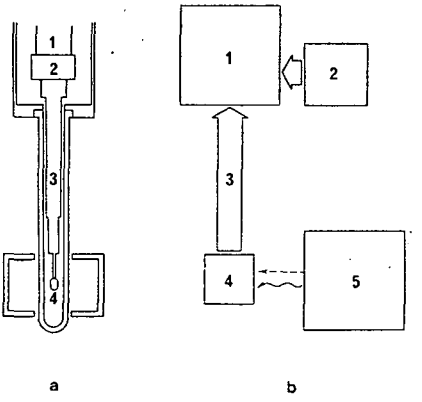

Fig. 1. The lay-out of mounting the glassy sample onto the cold end of the He-cryostat (a) and its thermostatic flow diagram (b). (1) — cold end, (2) — heating coil, (3) — heat transferring copper rod, (4) — glassy sample inside the EPR cavity, (5) — ambient heat reservoir (including the cavity).

Another weak point of this system is to obtain maximum heat coupling between the sample and the cold end. As far as vanadium phosphate glass is concerned this is an almost ideal substance since the melted glass wets the copper wire. Still, the good heat contact becomes worse at low temperatures due to differences between the linear expansion's coefficient of the copper wire and the glassy substance. In some cases the glass chipped off when exposed to cooling. This problem could be best overcome by applying a special cryogenic heat conducting grease (CRY—CON, Air Products, USA) which provided good heat contact on the outer surface of the glass-metal joint.

Results and discussion

LIVAGE and his coworkers found that the EPR lineshape of amorphous V_2O_5 and V_2O_5—P_2O_5 glasses with more than 92 mol % V_2O_5 strongly depended on temperature: the hfs linewidth changed by one order of magnitude between 273 K and 77 K [4, 7]. To interpret the results they considered the electron delocalization

to an adjacent vanadium nucleus, cf. the motion of the magnetic electron towards the nearest hopping center. Since the hopping motion is a thermally activated process, at higher temperatures more complete electron delocalization and, thus, worse hfs resolution can be anticipated.

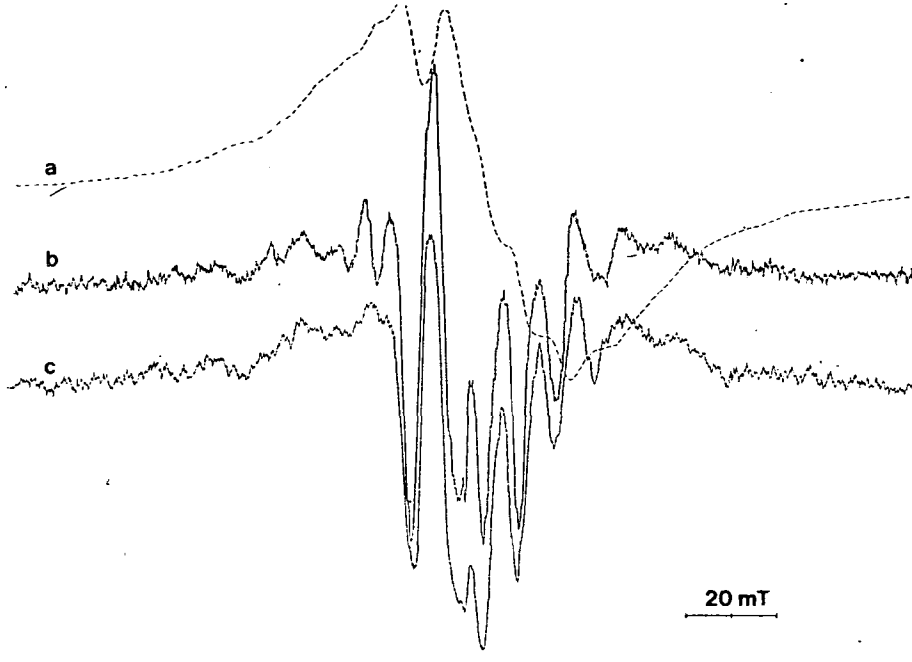

Fig. 2. Temperature dependence of the hyperfine structure in a 90−10 glass, $c=0.05$. Curve a (dotted line) first derivative spectrum, curves b and c second derivative spectra recorded at 20 and 300 K, respectively.

In Fig. 2 the temperature dependence of the EPR spectrum is shown for a 90 mol % V_2O_5−10 mol % P_2O_5 (90−10) glass. Since the hfs could be resolved only partially at room temperature, second derivative representation was chosen which is very sensitive to changes in the overall lineshape. As seen in Fig. 2 (curves b and c) the hfs resolution could slightly be improved when the sample was cooled down to 20 K. To make a quantitative estimation in this respect we assume that two overlapping spectral lines can only be resolved if their midpoint is not closer to each other than their spectral linewidth. According to LIVAGE ET AL. when this condition is met, the hopping frequency cannot be higher than the linewidth expressed in frequency units. However, it should be noted that this analysis holds in this simple form for a spectral doublet only. The V^{4+} axial spectrum represents a much more complicated case where a full lineshape analysis is not straightforward.

The EPR spectrum of the same glass dissolved in 38 wt % sulphuric acid is shown in Fig. 3. This exhibits characteristic hyperfine splitting due to the ^{51}V

nucleus $\left(I=\frac{7}{2}\right)$ which is in an axially distorted crystal field. The spin-Hamiltonian can be written in the following form:

$$\hat{H} = \beta g_{\parallel} B_z S_z + \beta g_{\perp}(B_x S_x + B_y S_y) + A_{\parallel} S_z I_z + A_{\perp}(S_x I_x + S_y I_y) \qquad (1)$$

where $g_{\parallel}, g_{\perp}$ and $A_{\parallel}, A_{\perp}$ denote the axial components of the $\hat{g}$- and $\hat{A}$-tensor, respectively; S_x, S_y, S_z and I_x, I_y, I_z are the three components of the electron and nuclear spin operators, B_x, B_y, B_z denote the magnetic field strength along the principal axes, and β is the Bohr magneton [4, 7]. In good agreement with the literature data we found $g_{\parallel}=1.936$, $g_{\perp}=1.987$, $A_{\parallel}=20.1$ mT, and $A_{\perp}=6.7$ mT.

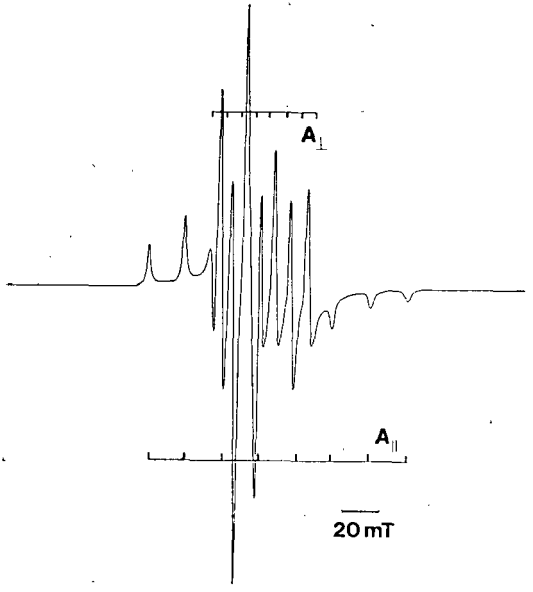

Fig. 3. The EPR spectrum of a frozen solution of V^{4+} recorded at 77 K.

As schematically shown in Fig. 3 the $\hat{A}$-tensor exhibits large anisotropy resulting in many overlapping lines. Using second order perturbation formulae we calculated the position of each parallel and perpendicular line and determined the positional differences in frequency units (Table I). It is very interesting to realize that in the central region where the parallel and perpendicular features overlap a few lines are much closer than those in the wings. As a necessary consequence an ideally resolved hfs spectrum should first collapse in this region indicating slow hopping rate. It is straightforward to extend the analysis of the wings [7] to the whole spectrum since with a careful analysis of the hfs particularly in the central region the increase of the hopping frequency can be followed quantitatively through almost two orders of magnitude. To illustrate the method we analyzed the spectra

Table I

The position and differences of the parallel and perpendicular features in the axial spectrum of V^{4+} ions

Position in mT units	Assignment	Difference	
		in mT	in MHz
417.63	$\parallel \left(-\frac{7}{2}\right)$		
397.14	$\parallel \left(-\frac{5}{2}\right)$	20.49	567.
376.78	$\parallel \left(-\frac{3}{2}\right)$	20.36	564.
360.89	$\perp \left(-\frac{7}{2}\right)$	15.89	440.
356.54	$\parallel \left(-\frac{1}{2}\right)$	4.35	120.
352.21	$\perp \left(-\frac{5}{2}\right)$	4.33	120.
344.19	$\perp \left(-\frac{3}{2}\right)$	8.02	222.
337.22	$\parallel \left(+\frac{1}{2}\right)$	6.97	193.
336.82	$\perp \left(-\frac{1}{2}\right)$	0.4	11.
330.12	$\perp \left(+\frac{1}{2}\right)$	6.7	185.
324.09	$\perp \left(+\frac{3}{2}\right)$	6.03	167.
318.71	$\perp \left(+\frac{5}{2}\right)$	5.38	149.
316.73	$\parallel \left(+\frac{3}{2}\right)$	1.98	55.
312.83	$\perp \left(+\frac{7}{2}\right)$	3.9	108.
296.37	$\parallel \left(+\frac{5}{2}\right)$	16.46	456.
276.14	$\parallel \left(+\frac{7}{2}\right)$	20.23	560.

shown in Fig. 2. In the left side of the spectra two lines (assigned to $m=+\frac{7}{2}$ perpendicular and $m=+\frac{3}{2}$ parallel transitions) are clearly resolved at 20 K (curve b) whereas at 300 K (curve c) this pattern can hardly be recognized. According to Table I we can conclude that the exchange frequency is about 100 MHz at 300 K. Analyzed in very much the same way for other linepairs we can establish

that this frequency value drops to its half at 20 K. From these values the activation energy of the hopping process can be estimated [8]: $E_h = 1.2$ meV.

We investigated a series of 90−10 and 75−25 glasses with varying c-values. At higher V^{4+} content no hfs could be resolved at all even at 20 K (Fig. 4a—d). Therefore we concluded that apart from lifetime broadening dipole broadening should also contribute to the linewidth. In fact in the case of glasses with low c-values we are already in the region where the contribution of lifetime and dipole broadening to the resultant linewidth is comparable in size, whereas at higher c-values the linewidth is entirely governed by dipolar broadening. This is a reasonable explanation whenever $V^{4+}-V^{4+}$ interaction cannot be neglected. [5].

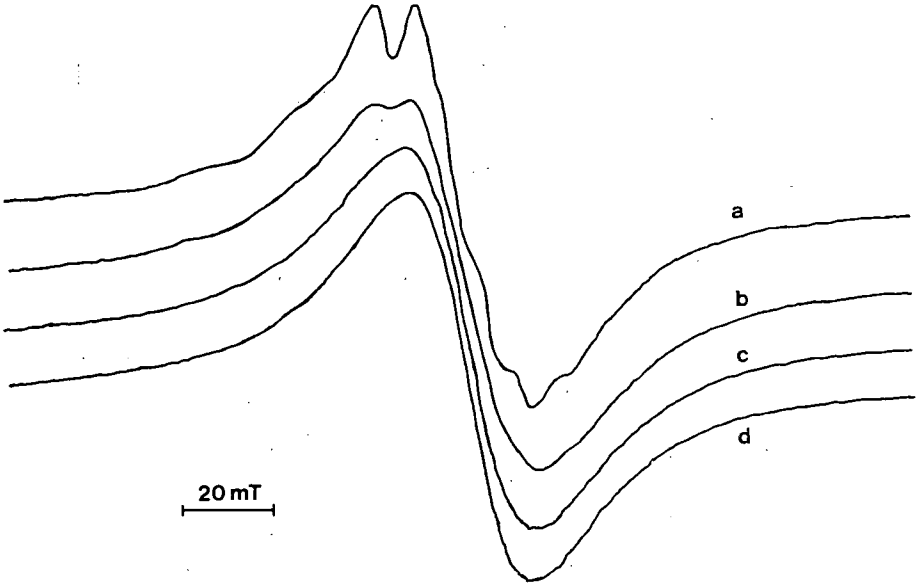

Fig. 4. EPR spectra of V_2O_5—P_2O_5 glasses: (a) 90—10, $c=0.07$; (b) 75−25, $c=0.10$; (c) 90−10, $c=0.14$; (d) 75−25, $c=0.28$

In this case an additional term should be included into the spin-Hamiltonian ($\hat{H}$) given in Eq. (1). Assuming pairwise spin-spin interaction between the nearest neighbours 1 and 2 we can write:

$$\hat{H}' = \hat{H} + J(c)\bar{S}_1\bar{S}_2 \qquad (2)$$

where $\bar{S}$ denotes the spin operator, $J(c)$ is the triplet-singlet separation energy (in eV) which depends on the average distance of the V^{4+} centers. (No anisotropic exchange was observed.) $J(c)$ can be obtained from the temperature dependence of EPR signal intensities (*cf.* paramagnetic susceptibility). As seen in Fig. 5 the paramagnetism of this 75−25 glass does not follow Curie-law (*i.e.* reciprocal temperature dependence), but exhibits slight spin exchange.

It turned out quite apparently that the lineshape analysis may be applied only to few exceptional glasses (with very low c-values) but no data can be obtained for the majority of the vanadium phosphate glasses since the dipolar broadening do-

minates the resultant linewidth. In glasses rich in V^{4+} the $J(c)$ value can be introduced which is related to the average spacing of the hopping centers. This is a geometric factor and is, thus, a static parameter; still it should be noted that the hopping frequency — apart from the degree of level matching and the barrier height — also depends on the hopping distance. Therefore, the $J(c)$ value furnishes useful information on the structure of the glass. A systematic investigation of $J(c)$ in the same $V_2O_5-P_2O_5$ glass series will be reported in a forthcoming publication.

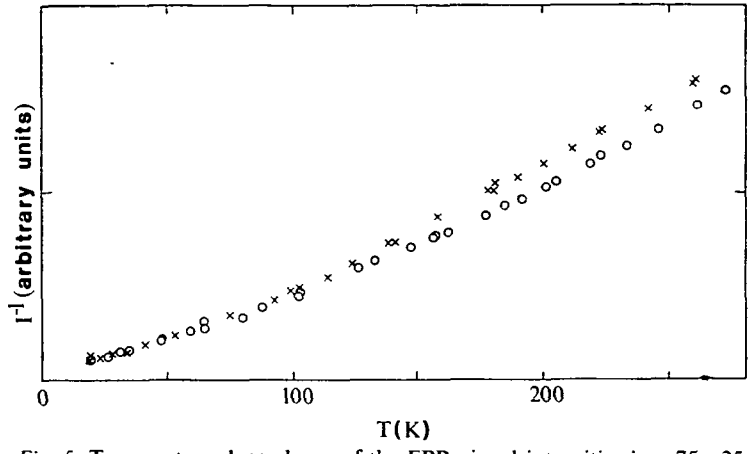

Fig. 5. Temperature dependence of the EPR signal intensities in a 75 – 25 glass, $c=0.26$. The two sets of experimental points illustrate the reproducibility of this measurement from one sample to another.

Summing up we can conclude that EPR can also provide a means to derive dynamical parameters, not necessarily limited to the $V_2O_5-P_2O_5$ system. For glasses with very low V^{4+} content the lineshape analysis can be applied; the limit and, thus, the applicability of which depends on the hyperfine coupling constant of the transition-metal ion studied. Beyond this limit the hfs analysis breaks down due to the spin-spin interaction; an effect which provides an alternative way to analyze the hopping conditions.

References

[1] *Mott, N. F.:* J. non-crystall. Solids **1**, 1 (1968).
[2] *Sayer, M., A. Mansingh:* Phys. Rev. **6B**, 4629 (1972).
[3] *Livage, J., R. Collongues:* Mater. Sci. Eng. **23**, 297 (1976).
[4] *Rivoalen, L. A., Revcolevschi, J. Livage, R. Collongues:* J. non-crystall. Solids **21**, 171 (1976).
[5] *Kinser, D. L., L. K. Wilson:* 2. Solid State Conf. Recent Advances in Sci. and Technology of Materials, Cairo 1973.
[6] *Bogomolova, L. D., T. F. Dolgolenko, V. N. Lazukin, I. V. Filatova:* Fiz. tverd. Tela **16**, 1486 (1974).
[7] *Livage, J., P. Pineau, M. C. Leroy, M. Michaud:* phys. stat. sol. (a) **39**, 73 (1977).
[8] *Michaud, M., M. C. Leroy, J. Livage:* Mat. Res. Bull. *11*, 1425 (1976).

ИЗУЧЕНИЕ СТЕКОЛ ФОСФАТА ВАНАДИЯ МЕТОДОМ ЭПР ПРИ НИЗКИХ ТЕМПЕРАТУРАХ

Л. И. Хорват и Т. Сереньи

Частота электронного обмена между V^{4+} и V^{5+} ионами, определенная из анализа форм ЭПР линий, дает непосредственную информацию о подвижности носителей заряда.

ИЗУЧЕНИЕ ВНУТРИМОЛЕКУЛЯРНЫХ ПЕРЕХОДОВ В РАСТВОРАХ ОРГАНИЧЕСКИХ КРАСИТЕЛЕЙ

И. ХАМОРИ, Э. ФАРКАШ и Л. КОЗМА

Институт экспериментальной физики университета им. Аттилы Йожефа, Сегед

(Поступило в редакцию 28 октября 1979 г.)

Экспериментально определен квантовый выход люминесценции нескольких ксантеновых и акридиновых красителей. Зная время затухания люминесценции определялись вероятности излучательных и безызлучательных переходов молекул. Эти данные сравниваются с результатами расчетов полученных основе на формул Форстера и Стриклера-Берга.

Для определения вероятности излучательных и безызлучательных внутримолекулярных процессов разработано несколько методов, которые можно разделить на две группы. Во-первых, исследуются процессы, происходящие с возбужденного состояния, так, например, $S_1 \rightarrow S_2$ и $T_1 \rightarrow T_2$ поглощения или фотохимические процессы. Во-вторых, экспериментально измеряется квантовый выход (Φ) и время затухания (τ_M) флуоресценции на основе которых определяется по соотношению $\tau_0 = \frac{\tau_M}{\Phi}$ естественное время затухания флуоресценции τ_0, обратное значение которого равно вероятностям излучающих переходов. Так как Φ и τ_M трудно определить экспериментально, из феноменологической теории люминесценции выведены соотношения, с помощью которых можно определить значение τ_0 на основе спектров поглощения и люминесценции. Цель настоящей работы, исспользуя точные экспериментальные данные, исследовать справедливость применимости разных методов определения k и показать связь хода раичитанных данных с другими параметрами исследованных растворов.

Показано, что в том случае если не отличается атомная конфигурация молекул в основном и возбужденном состояниях, то τ_0 определяется по формулам Форстера [1]:

$$\tau_{01} = [1{,}067 \cdot 10^{-40} n^2 \int_0^\infty \nu^{-1}(2\nu_0 - \nu)^3 \varepsilon(\nu) d\nu]^{-1}, \quad (1)$$

или Стриклера-Берга [2]:

$$\tau_{02} = [1{,}067 \cdot 10^{-40} n^2 \langle \nu_f^{-3} \rangle^{-1} \int_0^\infty \nu^{-1} \varepsilon(\nu) d\nu]^{-1}. \quad (2)$$

Здесь $\varepsilon(\nu)$-молярный коеффисиент поглощения, $f_q(\nu)$ — квантовый спектр люми-

несценции, n — показатель преломления раствора, ν_0 — частота электронного перехода и $\langle \nu_f^{-3} \rangle^{-1} = \int_0^\infty [\nu^{-3} f_q(\nu) d\nu]^{-1} \cdot f_q(\nu) d\nu$.

Результаты ранее опубликованных исследований [3, 4, 5, 6] показывают, что значения τ_{0i}, полученные по соотношениям (1) или (2), в большинстве случаев близки друг к другу и меньшие чем значения τ_0, вычисленные из Φ и τ_M. В исследованных случаях отношение τ_0/τ_{0i} меняется от 0,9 до 2. В случае нескольки групп люминофоров (например, бром производные флуоресцеина [5], производные антрацена [7] и дифенилен полиены [9]) проводили детальные исследования для определения влияния структуры молекул на вероятности внутримолекулярных переходов и на отношение τ_0/τ_{0i}. Полученные результаты показывают, что изменение структуры молекул меньше меняет отношение τ/τ_{0i} чем зеркальную симметрию спектров. Значение τ_0/τ_{0i} может быть равным единице и втом случае, когда зеркальная симметрия спектров не выполняется из-за ротационного уширения спектров. У дифенил полиенов наблюдали, что τ_0/τ_{0i} пропорциональнь увеличивается с разницей средних час тот спектров поглощения и люминесценции.

Нами исследовалась вышеописанная проблема для нескольких растворов органических соединений, состав которых представлен в таблице 1.

Спектры поглощения измеряли на спектрофлуориметра OPTON PMQ 3. При малых концентрациях родамина 6Ж применяли в [13] описанный метод используя сферическую кювету. Спектры люминесценции при малых консентрациях растворов измерялись на спектрофотометре PERKIN ELMER MPF 44A, применяя перпендикулярное наблюдение, а при больших концентрациях использовали прибор, описанный в [10], у которого осуществлено антипараллелное наблюдение. В каждом случае проводили расчеты для учета влияния реабсорбции, и осуществляли такие экспериментальные условия, что влиянием вторичной флуоресценции мы могли пренебрегать. Квантовый выход растворов измерялся методом Вавилова описанным в работе [10] прибором. Применялись такие толщины слоев исследованных растворов, что влияние вторичной люминесценции не играло роли. Независимость значения квантового выхода от концентрации растворов проверяли относительным методом, применяя эталоном водный раствор кининсульфата. Спектр квантового выхода определялся на спектрофотометре PERKIN ELMER, применяя квантовым счетчиком родамин Б и метилен синий, расворенные в этиленгликоле. Красители флуоресцеин, родамин 6Ж (фирма MERCK) очищались методом описанным в [11], а красители родамин 6Ж (фирма NEN) и крезил фиолетовый (фирма EASTMAN) исследовали без очистки. Из акридиновых красителей трипафлавин (3,6-диамино-10-метилакридинклорид) фирмы HOECHST и 3,6-диаминоакридин фирмы MERCK оказались однородными при тонкослойной хроматографии.

В качестве растворителей применялись этанол, метанол спектроскопической чистоты и вода, с добавкой $NaOH \cdot 10^{-2}$ моль/л концентрации. Концентрация растворов менялась в пределах $10^{-7} - 10^{-4}$ моль/л.

Результаты наших измерений представлены на русинках 1—4. Спектры поглощения, люминесценции и квантового выхода, а также значения абсолютного квантового выхода оказались независимыми от концентрации в исследованном интервале. У растворов родамин 6Ж и акридиновых красителей кван-

Таблица I

Вещество и растворитель	Φ	$\tau_м$ (нс)	$\nu_п$ ($10^{14}\,c^{-1}$)	$\nu_п$ ($10^{14}\,c^{-1}$)	$\Delta\nu$ ($10^{14}\,c^{-1}$)	ν_0 ($10^{14}\,c^{-1}$)	τ_0 (нс)	τ_{01} (нс)	τ_{02} (нс)	τ_0/τ_{02}	k_T ($10^8\,c^{-1}$)
Родулин оранжевый этанол	0,44	4,38	6,38	5,60	0,40	5,94	10,0	8,11	8,06	1,24	1,28
Трипафлавин этанол	0,64	5,12	6,76	5,89	0,43	6,30	8,0	4,72	4,74	1,69	0,70
9-Аминоакридин этанол	0,79	18,5	7,49	6,63	0,44	7,04	23,4	13,83	14,02	1,67	0,11
3,6 Диаминоакридин этанол	0,50	5,47	6,85	5,84	0,51	6,33	10,9	4,40	4,43	2,46	0,91
Флуоресцеин 10^{-2} NaOH вода	0,92	3,97	6,53	5,77	0,38	5,95	4,32	4,60	4,38	0,99	0,202
Родамин 6Ж* этанол	0,98	3,80	5,79	5,28	0,25	5,44	3,88	4,17	4,17	0,93	0,053
Родамин 6Ж* метанол	0,91	3,80	5,81	5,31	0,25	5,56	4,18	4,92	4,39	0,95	0,237
Родамин 6Ж** этанол	0,94	2,90	5,81	5,29	0,26	5,55	3,09	3,77	3,49	0,89	0,207
Крезил фиолетовый этанол	0,54	2,95	5,11	4,59	0,26	4,85	5,46	6,06	5,84	0,94	1,56

фирма: *MERCK **NEN

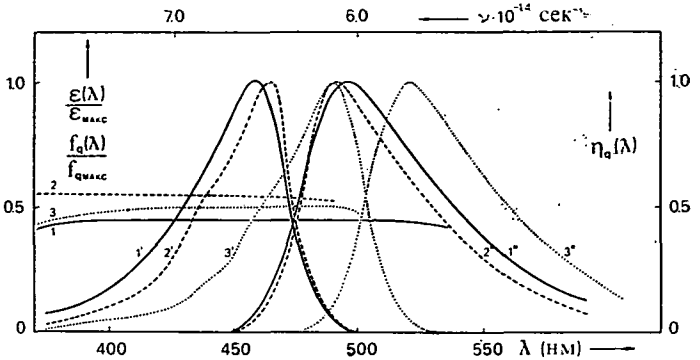

Рис. 1. Спектры поглощения (′), люминесценции (″), и квантового выхода без штриха; 3,6-диаминоакридин (1), трипафлавин (2), родулин оранжевый (3). Растворитель этанол.

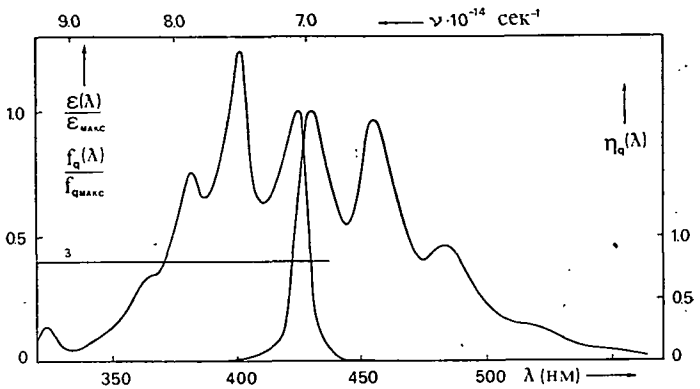

Рис. 2. Спектры поглощения (1), люминесценции (2), квантового выхода (3) раствора 9- аминокридина. Растворитель этанол.

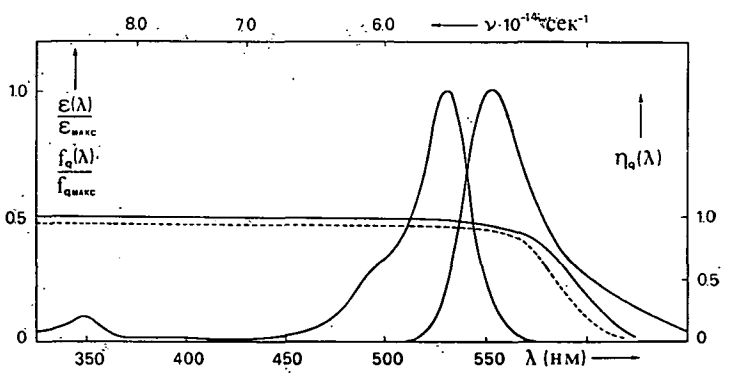

Рис. 3. Спектры поглощения, люминесценции и квантового выхода родамина 6Ж; (—) фирма MERCK, (— — —) фирма NEN PILOT 559 P. Растворитель этанол.

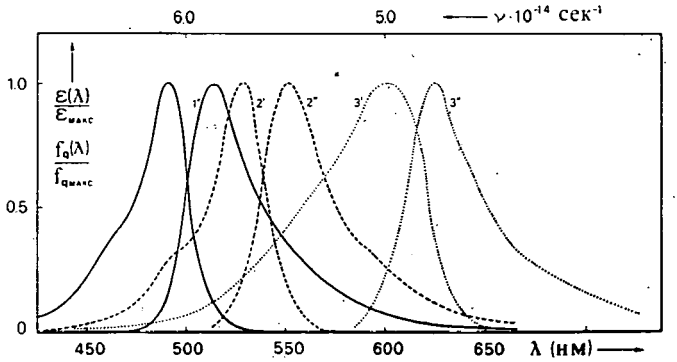

Рис. 4. Спектры поглощения (′), люминесценции (″); флуоресцеина в воде $+10^{-2}$ моль/л NaOH, родамин 6Ж в метаноле (2), крезилфиолетовый в этаноле (3).

товый выход оказался независимым от длины волны возбуждающего света до места максимума спектра люминесценции. Спектр квантового выхода обоих родаминовых красителей измеряли и при возбуждении в антистоксовой области. Из рисунка 3. видно, что квантовой выход красителя фирмы NEN быстрее падает с ростом длины волны возбуждающего света чем очищенного вещества фирмы MERCK, спектр поглощения которого быстрее падает в этой области. Измерения проводились при концентрациях $5 \cdot 10^{-7} - 5 \cdot 10^{-6}$ моль/л, поэтаму спад выхода не могут вызывать димеры. Анализ экспериментальных результатов показывает, что поглощение фотопродуктов, возникающих в растворе очищенных красителей не вызывает падение выхода.

Измеренные и вычисленные результаты представлены в таблице 1. Время затухания люминесценции экспериментально определено в работе [12]. Из таблицы видно, что у ксантеновых красителей и у крезилового фиолетового значения τ_{01} и τ_{02}, вычисленные по формулам (1) и (2) хорошо совпадают с рассчитанными результатами из измеренных значений длительности люминесценции и выхода. У акридиновых красителей отношение τ_0/τ_{02}, характеризующее отклонение определенных разными методами значений, пропорционально растут растоянем максимумов спектров поглощения и люминесценции. Это показан другими авторами для ретинолполиеных соединений. На основе нашего материала нельзя детально рассмотреть связь между изменением отношения τ_0/τ_{0i} и зеркалной симметрией, так как в исследованных нами случаях зеркалная симметрия выполнается всего лишь между максимумами спектров поглощения и люминесценции. Особенно интересно было бы провести исследование на основе экспериментальных результатов τ и Φ, полученных при возбуждении в антистоксовой области, однако из-за экспериментальных трудностей соответствующие данные по τ оотсутствуют.

На основе определенных нами с большой точностю экспериментальных данных можно установить, что соотношения Форстера и Стриклера—Берга дают практически одинаковые результаты для значения τ_0. Изменение структуры молекул не вызывает никаких регулярных изменених в спектрах и в значениях Φ и τ_M, тем не менее зависимость отношение τ_0/τ_{02} от стоксового сдвига оказывается регулярным, а именно, получается линейный ход.

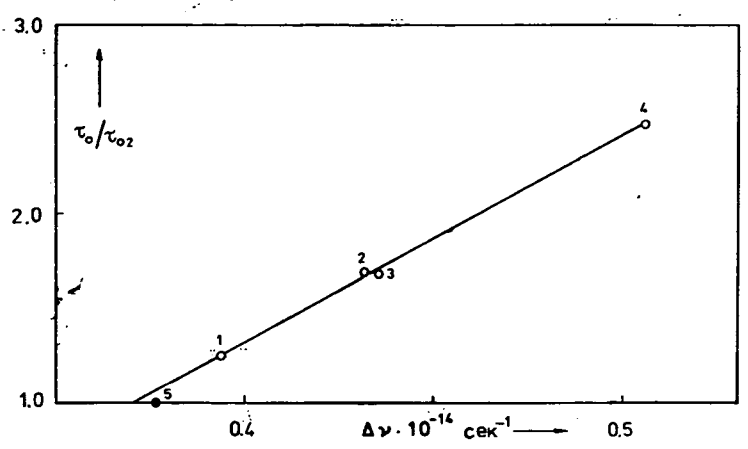

Рис. 5. Зависимость отношения τ_0/τ_{02} от значения антистоксового сдвига $\Delta\nu$. ($\Delta\nu = \frac{1}{2}(\bar{\nu}_\pi - \bar{\nu}_л)$, где $\bar{\nu}_\pi$ и $\bar{\nu}_л$ средная частота спектров поглощения и люминесценции). (1) — родулин оранжевый в этаноле, (2) — трипафлавин в этаноле, (3) — 9-аминоакридин в этаноле, (4) — 3,6-диаминоакридин в этаноле, (5) — флуоресцеин в воде.

Авторы выражают благодарность профессору И. Кечкемети за постоянный интерес к их работе и сотрудникам М. Хилберт и К. Сюч за помощь в экспериментальной работе.

Литература

[1] *Förster, Th.:* Fluoreszenz Organischer Verbindungen, Vanderhoeck und Ruprecht, Göttingen 1951.
[2] *Strickler, S. J., R. A. Berg:* J. Chem. Phys. **37**, 814 (1962).
[3] *Birks, J. B., D. J. Dyson:* Proc. Roy. Soc. A **275**, 135 (1963).
[4] *Ware, W. R., B. A. Baldwin:* J. Chem. Phys. **40**, 1703 (1964).
[5] *Seybold, P. G., M. Gouterman, J. Callis:* Photochem. Photobiol. **9**, 229 (1969).
[6] *Berlman, J. B.:* Handbook of Fluorescence Spectra of Aromatic Molecules Acad. Press N. Y. 1965.
[7] *Birks, J. B.:* Photophysics of Aromatic Molecules, Wiley N. Y. 1970.
[8] *Birks, J. B., D. J. S. Birch:* Chem. Phys. Lett. **31**, 608 (1975).
[9] *Dalle, J. P., B. Rosenberg:* Photochem. Photobiol. **12**, 151 (1970).
[10] *Ketskeméty, I., J. Dombi, R. Horvai, J. Hevesi, L. Kozma:* Acta Phys. et. Chem. Szeged **7**, 17 (1961).
[11] *Варга, З.;* Дисс. Сегед 1978. *Домби, Й.;* Канд. дисс. Сегед 1967.
[12] *Szücs, K., B. Rácz, B. Német, L. Kozma, I. Sánta, M. Hilbert:* Acta Phys. et Chem. **24**, 437 (1978).
[13] *Ketskeméty, I., L. Kozma:* Acta Phys. Hung. **29**, 331 (1970).

STUDY ON INTRAMOLECULAR TRANSITIONS OF ORGANIC DYE SOLUTIONS

I. Hámori, É. Farkas and L. Kozma

We measured the absolute quantum yield of fluorescence of some xanthene and acridine dyes, experimentally. The radiative and non-radiative transitional probabilities were calculated from the fluorescence lifetime and quantum yield. The results are compared with quantities calculated by application of Strickler—Berg and Förster equations.

MEASUREMENT OF FLUORESCENCE DECAY OF RHODAMINE 6G SOLUTIONS BY TEA uv N_2 LASER EXCITATION

By

B. NÉMET, K. SZÜCS, M. HILBERT and L. KOZMA

Institute of Experimental Physics, Attila József University
Szeged

(Received October 28, 1979)

Fluorescence decay of Rhodamine 6G solutions in wide dye concentration and layer thickness was investigated by a pulse fluorometer based on TEA uv N_2 laser. Deviations in τ results obtained in different experimental conditions are explained by the effect of secondary fluorescence. The molecular fluorescence decay time of Rhodamine 6G in methanol was found 4.1 ± 0.1 ns by extrapolating the experimental results to zero γ_{max}.

Introduction

There is a great deviation (3.1—6.8 ns) in decay times as measured by different investigators for Rhodamine 6G (Rh 6G) [1—4]. The measurements were performed using nitrogen and mode-locked lasers as exciting light source. When the intensity of the laser pulse is small, a bulky cuvette and considerable dye concentration is required. Fluorescence decay times (τ') as measured at various concentrations using a single cuvette (*i.e.* no variation in layer thickness) show a marked dependence on the concentration, and the $\tau'(c)$ function has a maximum [9, 10]. This effect has been explained by the present authors by self-absorption of the dye [11] and suggested a necessary correction. Although this effect was previously described for fluoresceine dye [5—7] and rigorously explained in refs, [6—8] on the basis of the theory of secondary fluorescence, the exact correction is a very difficult calculation in the general case and so it is usually neglected.

In this paper we report our experimental results concerning decay time measurements of Rh 6G (in methanol) in a wide range of dye concentration (c) and layer thickness (l). A simple experimental method is suggested to determine the molecular or true decay time (τ) of Rh 6G from the measured values (τ'); the obtained data are explained qualitatively on the basis of the theory of secondary fluorescence.

Material and experimental method

For measuring fluorescence decay time we applied the single pulse method using a transverselly excited atmospheric pressure nitrogen (TEA N_2 laser $\lambda_{ex} = 337$ nm) laser as exciting light source. The experimental arrangement and the evaluation method were described in our previous paper [10]. Rh 6G was purchased from Merck (Switzerland) and purified by chromatographic method. As solvent methanol, (MeOH) free of water, was used.

Results

The experimental results of the fluorescence decay time for Rh 6G solutions are summarized in Table I as a function of dye concentration and layer thickness. For every solution the maximum of the extinction coefficient ($\gamma_{max}=2.3\cdot\varepsilon_{max}\cdot c\cdot l$) is also given in Table I to include the γ_{max} dependence of τ'.

The measured τ' values of Rh 6G in MeOH versus the logarithm of concentration are shown in Fig. 1. As seen a great variety of τ' values (full trace) can be

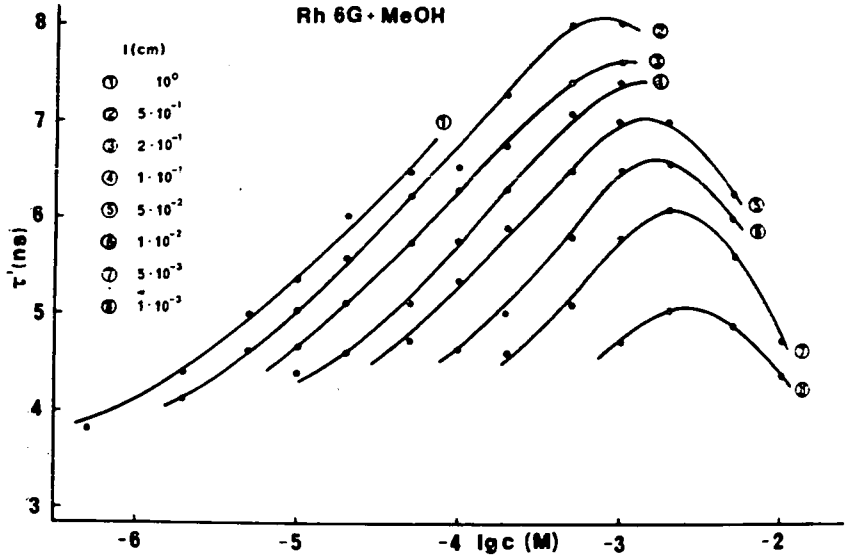

Fig. 1. Fluorescence decay time values (τ') of Rhodamine 6G in methanol (Rh 6G+MeOH) measured at several layer thickness (l) ($l=10^{\circ}-10^{-3}$ cm, ①–⑧, solid lines) versus the logarithm of dye concentration (lg c).

obtained with varying c and l values. For comparison solid lines connect the τ' values obtained for the same cuvette thickness. The curves increase gradually from 4—4.5 ns to a maximum of 5—8 nsec (at the concentration of 1—$2\cdot10^{-3}$ M), and then decrease due to concentration quenching. We could not measure τ' values at very low concentration part of these curves.

As the Fig. 1. shows the dependence on c is not a true one, because of curves are different varying the layer thickness. A re-plot is shown in Fig. 2 where τ' values (full trace) versus cuvette thickness are shown. For comparison again solid lines connect the experimental points obtained at the same concentration. As seen the measured data decrease if the thickness tends to zero, and this effect is more pronounced at higher concentrations. The curves tend to the same limit value of decay time, about 4.0—4.2 ns, when decreasing the cuvette thickness. The dependence on l is also not a true connection between τ' and l.

We plotted the decay time data as a function of γ_{-max} (a parameter which contains the product of c and l). The measured τ' values belonging to the same extinction coefficient are a little different, namely the diameter (d) of the laser beam in

Table I

	τ' (*ns*) $\gamma_{max} = 2.3 \cdot \varepsilon_{max} \cdot c \cdot l$									
l (cm)	10^{0}	$5 \cdot 10^{-1}$	$2 \cdot 10^{-1}$	10^{-1}	$5 \cdot 10^{-2}$		10^{-2}	$5 \cdot 10^{-3}$		10^{-3}
lg l	0	−0.3	−0.7	−1.0	−1.3		−2.0	−2.3		−3.0
$m = R/l$	0.5	1.0	2.5	5.0	10		50	100		500
c (M)										
$5 \cdot 10^{-7}$	3.8 *0.11*									
$2 \cdot 10^{-6}$	4.3 *0.45*	4.1 *0.23*								
$5 \cdot 10^{-6}$	5.0 *1.15*	4.6 *0.6*								
$1 \cdot 10^{-5}$ ①	5.35 *2.3*	5.0 *1.15*	4.65 *0.45*	4.4 *0.23*						
$2 \cdot 10^{-5}$ ②	6.0 *4.5*	5.55 *2.3*	5.1 *0.9*	4.55 *0.45*						
$5 \cdot 10^{-5}$ ③	6.45 *11.5*	6.2 *5.75*	5.7 *2.3*	5.1 *1.15*	4.7 *0.6*					
$1 \cdot 10^{-4}$ ④		6.5 *11.5*	6.3 *4.5*	5.7 *2.3*	5.35 *1.15*		4.6 *0.23*			
$2 \cdot 10^{-4}$ ⑤		7.3 *23.0*	6.7 *9.0*	6.3 *4.5*	5.9 *2.3*		5.0 *0.45*	4.6 *0.23*		
$5 \cdot 10^{-4}$ ⑥		*8.0*	7.4 *23.0*	7.1 *11.5*	6.45 *5.75*		5.8 *1.15*	5.1 *0.6*		
$1 \cdot 10^{-3}$ ⑦			7.65	7.4 *23.0*	7.0 *11.5*		6.5 *2.3*	5.8 *1.15*		4.7 *0.23*
$2 \cdot 10^{-3}$ ⑧					7.0 *23.0*		6.55 *4.5*	6.1 *2.3*		5.05 *0.45*
$5 \cdot 10^{-3}$					6.25		6.0 *11.5*	5.6 *5.75*		4.9 *1.15*
$1 \cdot 10^{-2}$								4.7 *11.5*		4.4 *2.3*

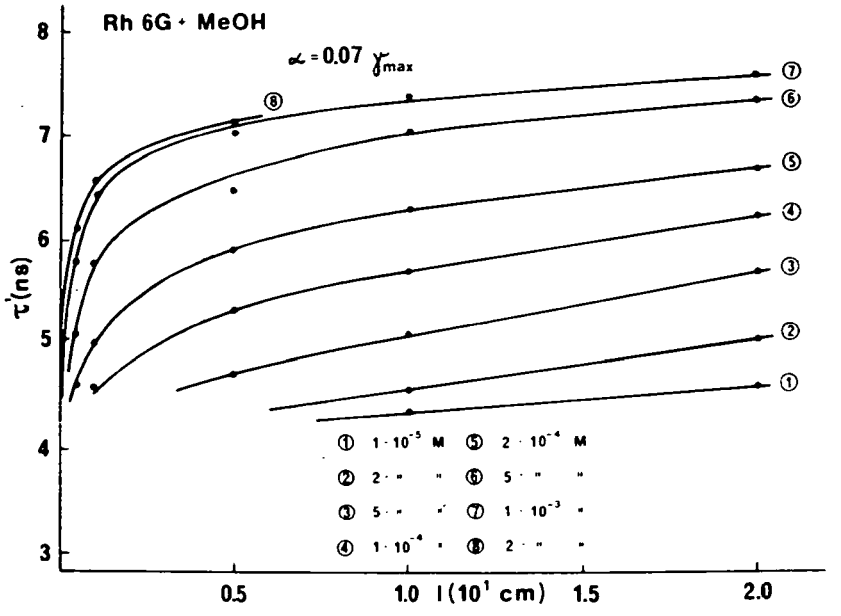

Fig. 2. Fluorescence decay time values (τ') of Rhodamine 6G in methanol (Rh 6G+MeOH) measured at several dye concentrations *(c)* ($c = 10^{-5} - 2 \cdot 10^{-3}$ M, ①–⑧, solid lines) versus the layer thickness *(l)*.

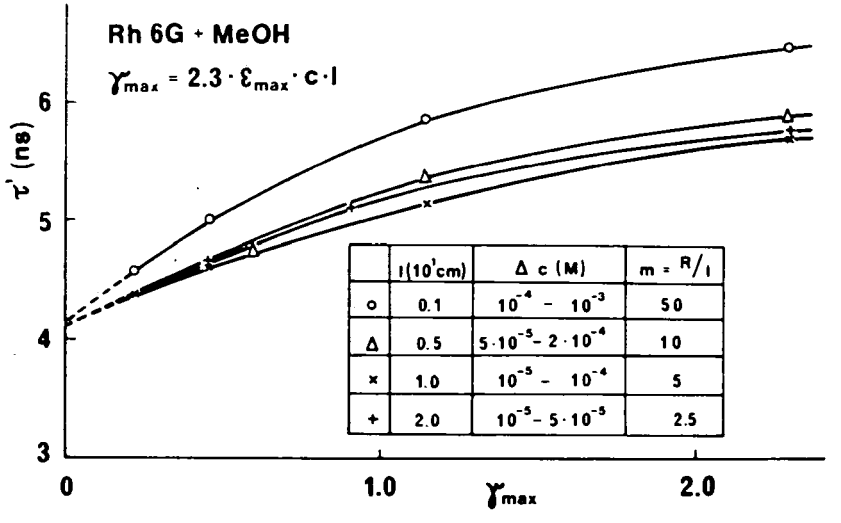

	l(10¹cm)	Δ c (M)	m = R/l
o	0.1	$10^{-4} - 10^{-3}$	50
Δ	0.5	$5 \cdot 10^{-5} - 2 \cdot 10^{-4}$	10
×	1.0	$10^{-5} - 10^{-4}$	5
+	2.0	$10^{-5} - 5 \cdot 10^{-5}$	2.5

Fig. 3. Fluorescence decay time values (τ') of Rhodamine 6G in methanol (Rh 6G+MeOH) ($0, \Delta, x, +$) as a function of the maximum extinction coefficient (γ_{max}). The solid lines connect the τ' values obtained at the same layer thickness *(l)*, so at the same *m* parameters ($m = R/l$). Δc is the concentration range used for measurements when $0.2 < \gamma_{max} \leqq 2.3$.

every case was constant ($d=1$ cm, so $R=0.5$ cm), and at the same time the layer thickness decreased with increasing concentration, *i.e.* the geometrical circumstances continuously changed, and so the $m=R/l$ ratio rapidly increased. Thus we connected those τ' data, which belong to the same layer thickness. By means of this representation we can determine the molecular fluorescence decay time when extrapolating these curves to zero γ_{max}; and a value of 4.1 ± 0.1 ns is obtained.

Discussion

The overlap of the absorption and fluorescence spectra, as well as the fluorescence absolute quantum yield, of Rh 6G is basically similar to the corresponding parameters of fluorescein dye. Our results regarding Rh 6G, also described by others [9, 10] (*i.e.* significant dependence of the measured time τ' on concentration, layer thickness, and geometrical circumstances), can be explained by taking secondary fluorescence into account; the relevant theory was worked out a long time ago. In this study we give a qualitative interpretation of our experimental results referring to [6—8, 13—15].

According to the theory of secondary fluorescence the primary fluorescence is followed by the self-absorption and then the secondary fluorescence of the dye molecules, *etc.* This effect lengthens the molecular or true decay time τ, and the relation between τ and τ' can be written as follows [6, 8]:

$$\tau = \tau'(1-\varkappa),$$

where $\varkappa$ is the ratio of the intensity of secondary and primary fluorescence. This $\varkappa$ correction is a very complicated function of α, β, γ and m parameters. We can say about these parameters in the case of our experiments the followings:

(1) $\alpha=2.30\cdot\varepsilon(\lambda_{ex})\cdot c\cdot l$ (where $\lambda_{ex}=337$ nm) is the optical density of the solution at the exciting wavelength; in every case approximately 7% of the maximum optical density (*i.e.* $\alpha=0.07\gamma_{max}=0.07\beta_{max}$, Table I).

(2) $\beta(\lambda')=2.30\cdot\varepsilon(\lambda')\cdot c\cdot l$ is a function of the optical density in the investigated part of the fluorescence spectrum. During the measurement the photodiode observed the total fluorescence spectrum, so β_{max} is equal to the value obtained at the maximum of the absorption spectrum. This fact makes $\varkappa$ correction more difficult.

(3) $\gamma(\lambda'')=2.30\cdot\varepsilon(\lambda'')\cdot c\cdot l$ is a function of the optical density between the short wavelength part of the fluorescence and the long wavelength part of the absorbance. Since the maximum of the absorption spectrum is in the range of the overlap, γ_{max} is also equal to the value obtained at the absorption maximum, so $\gamma_{max}=\beta_{max}$.

(4) $m=R/l$, where R denotes the radius of the exciting light beam after the diaphragm (and the cuvette). Since R was constant, m is inversely proportional to the layer thickness l (Table I, Fig. 3.).

According to [6, 8, 13, 15] the $\varkappa$ correction is a monotonously varying function of γ_{max} and $m\cdot\beta(\lambda)$ was the same as compared to α and γ in every case and thus we conclude that if the $\tau'(\gamma_{max}, m)$ function is known from experiments (Fig. 3.) and $\gamma_{max}<0.5$ as well as $m<5$ holds, then the τ' values do not deviate from τ more than 4—5%; this is the experimental error of our measurements.

Summing up we reported (*a*) a graphic method for the estimation of τ from experimentally obtained τ'; (*b*) an experimental verification of the theory of secondary fluorescence by measuring τ' of Rh 6G dye in different solutions.

References

[1] *Kashnow, R. A., J. A. Sousa:* J. Appl. Phys. **42**, 2128 (1971).
[2] *Alfano, R. R., S. L. Shapiro, W. Yu:* Opt. Commun. 7, 191 (1973).
[3] *Mourou, G., M. M. Malley:* Opt. Commun. **11**, 282 (1974).
[4] *Harris, J. M., F. E. Lytle:* Rev. Sci. Instrum. **48**, 1649 (1977).
[5] *Schmillen, A.:* Z. Phys. *135*, 294 (1953); Z. Angew. Phys. *6*, 260 (1954).
[6] *Budó, Á., L. Szalay:* Z. Naturforsch. **18a**, 90 (1963).
[7] *Gáti, L., I. Szalma:* Acta Phys. et Chem. Szeged **14**, 3 (1968).
[8] *Budó, Á., I. Ketskeméty:* Acta Phys. Hung. **7**, 207 (1957).
[9] *Cirkel, H. J., L. Ringwelski, F. P. Schäfer:* Z. Physik. Chem. Neue Folge **81**, 158 (1972).
[10] *Selanger, K. A., J. T. Falnes, T. Sikkeland:* J. Phys. Chem. **81**, 1960 (1977).
[11] *Birks, J. B.:* Photophysics of Aromatic Molecules (Wiley Interscience, London, 1970).
[12] *Szücs, K., B. Rácz, B. Német, L. Kozma, I. Sánta, M. Hilbert:* Acta Phys. et Chem. Szeged **24**, 437 (1978).
[13] *Dombi, J., R. Horvai:* Acta Phys. et Chem. Szeged **2**, 9 (1956).
[14] *Budó, Á., J. Dombi, R. Horvai:* Acta Phys. et Chem. Szeged **3**, 3 (1957).
[15] *Dombi, J., J. Hevesi, R. Horvai:* Acta Phys. et Chem. Szeged **5**, 20 (1959).

ИЗМЕРЕНИЕ ВРЕМЕНИ ЗАТУХАНИЯ ФЛУОРЕСЦЕНЦИИ РАСТВОРОВ РОДАМИНА 6Ж ВОЗБУЖДЕННОЙ «uv» TEA N_2 ЛАЗЕРОМ

Б. Немет, К. Сюч, М. Хилберт и Л. Козма

Зависимость времени затухания флуоресценции растворов родамина 6Ж от концентрации растворов и толщины образца, изменяющихся в широкой области, была исследована с использованием атмосферического азотного лазера. Различия между получаемыми результатами при разных экспериментальных условиях объяснены по теории вторичной флуоресценции. Молекулярное время затухания флуоресценции родамина 6Ж в метаноле получалось $4{,}1 \pm 0{,}1$ нс экстраполяцией экспериментальных данных когда $\gamma_{\text{макс}}$ стремится к нулю.

О КИНЕТИКИ ФОТОПРОДИМОСТИ МОНОКРИСТАЛЛОВ V_2O_5 ПОД ВЛИЯНИЕМ ЛАЗЕРНОГО ИЗЛУЧЕНИЯ

Л. НАНАИ, Ю. К. ЮШИН*, Э. СИЛ и И. ХЕВЕШИ

Институт Экспериментальной Физики Университета им. А. Йожефа, г. Сегед
* Институт Кристаллографии им. А. С. Шубникова, г. Москва, СССР

(Поступило в редакцию в 15 июля 1979 г.)

Генерация и рекомбинация фотоносителей исследуется на кристаллических пластинках V_2O_5. Установлено, донор центры играют важную роль в генерации фототока, так генерация фототока хорошо описывается моделью, предложенной Гудденом—Полем, а для релаксации фототока дается гипотеза о ее термическом происхождении.

Известно, что высший окисел ванадия, V_2O_5 является полупроводником *n*-типа, полупроводниковые свойства которого определяются дефектами по кислороду [1, 2] обладающий довольно низкой подвижностью носителей [2], шириной зоны $\sim 2{,}3$ эВ и активационной энергии $\sim 0{,}45$ эВ [4, 5]. Отклонения в стехиометрическом составе, дефекты по окислу выступают как донорные центры и во многом определяют механизм проводимости V_2O_5. Известно, что V_2O_5 при температурах ниже точки плавления не показывает собственную проводимость [5]. Фотопроводящие свойства материала практически не изучены. По данным [6] в красной области спектра при обычных интенсивностях обладает незначительной фоточувствительностью.

Цель настоящей работы, изучить фотопроводящие свойства V_2O_5 на длине волны рубинового лазера ($\lambda = 0{,}694$ мк) при высоких интенсивностях возбуждения.

Эксперимент

Монокристаллы выращивались из расплава и из них по плоскостям (010) были сколоты образцы размерами порядка $15 \times 5 \times 0{,}2$ мм. Контактированные образцы помещались в путь излучения рубинового лазера. Относительное изменение тока регистрировалось с помощью осциллографа. Одновременно измерялась лучевая энергия, падающая на образец.

Результаты экспериментов показывают, что фототок экспоненциально растет во время действия лазерного излучения После прекрашения импульса излучения амплитуда сигнала экспоненциально падает, притом время спада достигает очень большие значения (рис. 1).

По измеренным данным следует, что амплитуда сигнала «фотоответа» линейно увеличивается с ростом падающей на образец лучевой энергии при фиксированном напряжении на нем (рис. 2).

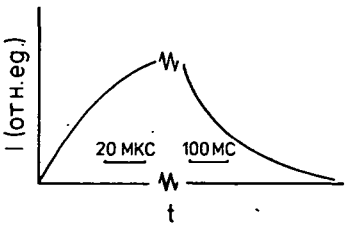

Рис. 1. Зависимость нарастания и спада фототока от времени.

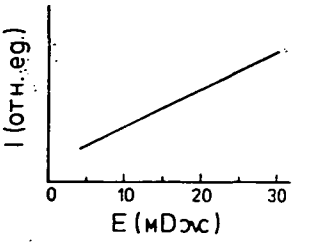

Рис. 2. Зависимость силы фототока от уровня возбуждения.

Дискуссия результатов

Поскольку энергия кванта рубинового лазера ($h\nu$ = 1,78 эВ) меньше ширины запрещенной зоны, то причиной поглощения света является оптическое возбуждение электронов донорных центров в зону проводимости. Заброщенные электроны будут горячими и избыток энергии расходуется в столкновениях с фононами.

Если предложить, что фотопроводимость, наблюдаемая во время действия лазерного импульса связана с электронами возбужденными светом с донорных уровней, то можно использовать для оценок формулу, предложенную еще Гудденом и Полем [7] для «первичных» фототоков,

$$\Delta i = Fe\frac{x_-}{d}, \tag{1}$$

где Δi — фототок, F — скорость генерации свободных носителей, e — заряд электрона, d — расстояние между электродами, x — расстояние в направлении противоположном полу, проходимое свободным отрицательным заряженным носителем до захвата. Если к электродам приложено напряжение V, а μ_n и τ_n соответственно подвижность и время жизни в зоне проводимости, то

$$x_- = \mu_n \frac{V}{d}\tau_n.$$

Так как коэффициент поглощения образца на этой длине волны ~ 120 см$^{-1}$ и тольщина его превышает α^{-1}, можно считать, что величина F совпадает со скоростью поглощения фотонов которая равна $\sim\frac{\varepsilon}{\hbar\omega\Delta t}$, где $\hbar\omega$ = 1,78 эВ, ε — энергия лазерного импульса $\sim 10^{-2}$ Дж, Δt — его длительность $\sim 10^{-4}$ сек$^{-1}$. Для F так получается значение $F \approx 4\cdot 10^{20}$ сек$^{-1}$. Относительное изменение тока по сравнению с темновым током состовляет $\sim 0{,}5\cdot 10^{-4}$ А, поэтому для x_- получаем $x_- \sim 10^{-6}$ (V=30 В и d=0,8 см). Если воспользоваться величиной подвижности $\mu_n \approx 1$ см^2 сек$^{-1}$В$^{-1}$, то получаем $\tau_n \approx 3\cdot 10^{-8}$ сек. Для величины подвижности взятых из [3] $\sim 10^{-2}$ см^2 сек$^{-1}$В$^{-1}$, получаем $\tau_n \approx 3\cdot 10^{-6}$ сек. Отме-

тим, что для разогретых электронов подвижность может отличаться от подвижности приведенной в работе [3].

Полученные оценки времени жизни показывают, что высказанное выше предположение о природе фотопроводимости во время действия лазерного импульса вполне правдоподобно. Электрон проводимости в свою очередь может быть захвачен донорным центром если последний не занят электроном. В модели одного глубокого донорного уровня зависимость концентрации электронов проводимости $n(t)$ с учетом процессов возбуждения и захвата

$$\frac{dn}{dt} = (N_d - n)D - n^2 vS, \tag{2}$$

где

$$D = AI + w.$$

Здесь N_d — концентрация донорных центров, AI — вероятность возбуждения электрона в единицу времени светом интенсивностью I, w — вероятность теплового возбуждения, vS — среднее значение произведения скорости электрона на сечения захвата. Предположим, что лазерный пучок начинает действовать на образец при $t=0$. Стационарное решение (2) будет

$$n = \frac{\sqrt{D^2 + 4vSN_dD} - D}{2vS}. \tag{3}$$

Учитывая начальное условие $n(0)=n_0$, и тот факт, что переменные в дифференциальном уравнении (2) разделяются, находим его решение

$$n(t) = \frac{n_2(n_1 - n_0) + n_1(n_0 - n_2)e^{\beta t}}{(n_1 - n_0) + (n_0 - n_2)e^{\beta t}}, \tag{4}$$

здесь

$$n_2 = \frac{-D - \sqrt{D^2 + 4vSN_dD}}{2vS}$$

и

$$\beta = vS(n_1 - n_2) = \sqrt{D^2 + 4vSN_dD}.$$

Поскольку проводимость $\sigma \sim e\mu_n n$, то экспериментально наблюдаемая зависимость силы фототока находится в соответствии уравнении (4).

Как видно из рис. 1. спад фототока длится намного дольше, чем его нарастание. Экспоненциальный его характер и также линейная зависимость силы фототока от уровня возбуждения указывают на линейную рекомбинацию. Чрезмерная длительность спада обрашает внимание на учет возможных тепловых эффектов. При облучении кристалла высокими интенсивностьями света поверхность его значительно нагревается. В нашем случае прирашение температуры может достигать значений 50—70 град. Цельсия. Итак можно думать, что рекомбинированные на донорных центрах носители под влиянием температуры снова забрасываются в зону проводимости. Уменьшение фототока хорошо согласуется законом охлаждения Ньютона, что потдверждает вышесказанное о тепловом характере затухания фототока.

Литература

[1] *Доржко, Ф. В., В. Г. Савицкий:* ФТТ **19**, 953 (1977).
[2] *Bodó, Z., I. Hevesi:* Phys. stat. sol **20**, K45 (1967).
[3] *Neuberger, M.:* EPIC IR 79 Reports, Kansas City, 1971.
[4] *Йоффе, В. А.:* Автореферат докторской диссертации, Ленинград, 1967.
[5] *Hevesi, I.:* Candidate Dissertation, Szeged, 1967.
[6] *Hevesi, I., J. Lang, G. G. Chemeresyuk:* Acta Phys. et Chem. Szeged **19**, 25 (1973).
[7] *Бьюб, Р.:* Фотопроводимость твердых тел, ИЛ, Москва, 1962.

KINETICAL INVESTIGATION OF LASER-INDUCED PHOTOCONDUCTION OF V_2O_5 SINGLE CRYSTALS

L. Nánai, Yu. K. Yushin, E. Szil and I. Hevesi

The photoconduction of V_2O_5 single crystals has been studied. It has been found that the donor impurities have important role in the generation of photocurrent, according to the GOUDDEN—POHL theory. The relaxation may be in connection with temperature effects.

SIMULATED SEMIEMPIRICAL MOLECULAR ORBITAL CALCULATIONS I.

*Transferability of Fock matrix elements**

By

M. I. BÁN, I. BÁLINT and M. RÉVÉSZ

Institute of General and Physical Chemistry, Attila József University, Szeged

(Received October 25, 1979)

Converged Fock matrix elements over Slater-type atomic orbitals and hybridized orbitals obtained in semiempirical (EHT, CNDO, INDO and MINDO) quantum chemical calculations have been compared in case of alkanes, olefins, O-containing polar molecules and various closed-shell and open-shell molecules and molecular fragments. Good agreements between parallel Fock matrix elements in different molecules foreshadow their transferability from one molecule to another. Successful transference has been proved for alkanes. The aim of this series of studies is to establish the principles, rules, possibilities and limitations of transferability. The findings by semiempirical procedures will very likely be applicable in general by more rigorous approximations and may find their use in the approximate calculations of very large organic and inorganic (such as transition metal complex) systems by reasonable computing times.

The principle of transference is of great significance in chemistry; everywhere and everytime this principle is functioning and is exploited for the advantages which are arising from its use. This is happening whenever a given chemical bond is regarded to be essentially the same independently of the nature of the molecule in which it appears and of its location in the molecule. The additivities of bond moments and covalent bond radii, the use of characteristic bond frequencies in the *i.r.* spectroscopy and the concept of chromophoric groups in the visible-*u.v.* spectroscopy are all examples of the manifestations of this principle. The "chemical sense" or the "chemist's intuition" is quite often based upon the implicit transference of chemical bonds or characteristic chemical features.

All this make it quite comprehensible why the theoretical chemist has long been kept employed by the question of transferability and is searching partly for suitable "building blocks" which consistently carry the essential chemical properties and informations transferable from one molcule to another without any fundamental change and partly for the electronic structural reasons, evidences and explanations of transferability.

---

* Parts of this work were presented at the Quantum Chemistry Seminar held in Visegrád, Nov. 8—10, 1978 and at the Conference on Structure of Matter and Molecules held in Mátrafüred, Oct. 8—10, 1979.

It seems to be obvious to find the ultimate "building blocks" in the wave functions of the molecule by presuming the similarities in the wave functions of similar molecules or similar parts of molecules. According to some quantum chemical sense one could expect that localized MO orbitals will be transferable with greater success than fully delocalized orbitals which extend over the whole molecule so being more strongly affected by structural changes even though the molecules or molecular fragments to be compared are more or less similar to one another.

A number of quite recent studies [1—7] has really shown that the transference of localized orbitals can in numerous cases be carried out with success especially if the transfer takes place between similar environments. DEPLUS and others [8] proved the transferability of Fock matrix elements over localized orbitals on an orthogonal basis, however transference through localization of non-orthogonal orbitals may be of particular interest [9].

In the MO theory, *"ab initio"* quantum chemical calculations have given very useful results for relatively small molecules. Nevertheless, such calculations for larger molecules are prohibitively lengthy and expensive owing mainly to the large number of two-electron repulsion integrals which have to be evaluated. Calculations on very large organic molecules and transition metal coordination compounds are rather time-consuming and money-wasting even by semiempirical methods. The SCF—LCAO—MO scheme, in none of its approximation levels utilizes the fundamental fact that the physical and chemical properties of a molecular fragment or functional group are almost entirely independent of the particular molecule in which such molecular pieces occur, therefore, each molecule is treated as a new case even though several molecules have identical or similar common parts. However, this very fact suggests the possibility of developing procedures in which results of accurate calculations on smaller molecules could be used in the approximate calculation of larger molecules containing the same molecular fragments or functional groups. Thus, in spite of the expectations by mere speculations, transferable features of molecules can truly be revealed even when using completely delocalized canonical orbitals obtained in MO calculations. The process of expanding the molecular orbitals in terms of atomic orbitals and optimizing the linear combinations of atomic orbitals through the iterative solution of the Hartree—Fock—Roothaan eigenvalue equation brings to light the transferable properties of molecules. Transference in MO theory was first used in the work of ORLOFF and FITTS [10] who approximated the Hamiltonian diagonal matrix elements in the Hückel MO calculation of large molecules by appropriate matrix elements obtained from *ab initio* calculations on smaller molecules. This concept was extended to σ-electrons and off-diagonal matrix elements in the nonempirical molecular orbital (NEMO) procedure [11] and transference of molecular orbitals themselves was applied in the "Molecules in Molecules" (MIM) approach [12]. The "Simulated Ab Initio Molecular Orbital" (SAMO) method [13—22] utilizes the transferability of *ab initio* Fock matrix elements of small molecules in the construction of Fock matrices of large molecules. The SAMO method has been successfully applied to aliphatic hydrocarbons [14], polymers, polyethylene and polyene [15], a large biologically active (carcinogenic) substance [16], organic radicals using a spin unrestricted open-shell formalism [17], saturated cyclic hydrocarbons [18], aromatic molecules [19], polar molecules such as alcohols, amines, aldehydes and acids [20], large poly-

nuclear aromatic hydrocarbons [21] and open-shell radicals, ionized and excited states using a spin restricted Hartree—Fock scheme [22].

The SAMO method seems to have the widest applicability among the transference methods therefore we decided to perform semiempirical (EHT, CNDO, INDO, MINDO, etc.) calculations following the SAMO suggestions. Thus, when assemblying the Fock matrix of a large (target) molecule, the converged Fock matrix elements of small (pattern) molecules containing the same fragments or functional groups as the large molecule are transferred from direct semiempirical calculations. Both diagonal and off-diagonal matrix elements can be transferred from semiempirical calculations. The synthetic Fock matrix of the target molecule thus constructed can be used in two different ways: either to generate the molecular orbitals and orbital energies for the target molecule by a single non-iterative solution of the eigenvalue problem or to use it as a starting Fock matrix in the SCF iteration procedure. In the first case approximate results less accurate than those of the pattern molecules can be obtained for the large target molecule in computer times which are only the fractions of those for the direct calculations. In the second case a solution of comparable accuracy to the direct semiempirical calculations can be achieved but still for less expense, regarding the decrease in the number of iteration cycles owing to better convergence.

The aim of our simulated semiempirical MO calculations is to establish, at a lower cost than the original SAMO version of transference does, the principles, rules, possibilities and limitations concerning the transferability of Fock matrix elements and perhaps to find other transferable properties (*e.g.* density matrix blocks, etc.) overlooked so far. Another purpose of this series of our studies is to attempt finding evidences for the transferability among transition metal complexes. It can easily be realized that the reason why works on transference methods keep away from this subject so that practically no reference on successful transference can as yet be found in this field is to be looked for mainly in financial motives: the expense of repeating *ab initio* calculations at a range of different geometries would be enormous even for relatively small transition metal complexes or fragments of such containing the metal with its many orbitals and electrons.

The first paper of this series is mainly dealing with results obtained by CNDO/2 calculations [23] since this method — using its CLACK's version [24] — can easily be extended to studying coordination compounds of transition elements. Our preliminary investigations, however, have justified the transference of Fock matrix elements obtained in EHT, INDO and MINDO calculations as well. Next papers will give wider account on uses of such results. It is hoped that most of the conclusions on transference properties drawn by semiempirical methods will also be applicable by more rigorous (*e.g.* various level *ab initio*) calculations.

The Fock matrix elements are critically dependent on molecular configuration, the choice of the coordinate system, the orientation of the molecule relative to an external coordinate system, geometry factors, bonding data (internal coordinates: bond distances and angles), conformation of the molecule, presence or absence of net charges on the molecule as a whole, multiplicity of the ground state of the molecule, and the nature and location of neighbouring atoms or groups. Individually or collectively these factors may drastically affect the magnitude of matrix elements.

To test for similarities the parallel matrix elements in different molecules and molecular fragments, complete semiempirical (EHT, CNDO/2, INDO and MINDO/1) calculations were performed for a number of molecules and molecular fragments using standardized geometries and unhybridized and standard hybridized bases.

In Table I typical Fock matrix elements over Slater-type AO-s calculated by CNDO/2 for ethane in two different orientations are presented. In orientation 1

Table I

Typical Fock matrix elements over AO-s calculated by CNDO/2 for ethane in 2 different orientations

Interacting* orbitals	Orientation** 1	Orientation** 2
$C_s - C_s$	−0.5203	−0.5203
$C_s - C_{p_x}$	0.0062	0.0000
$C_s - C_{p_y}$	0.0062	0.0036
$C_s - C_{p_z}$	0.0062	0.0101
$C_s - C'_s$	−0.3048	−0.3048
$C_s - C'_{p_x}$	0.2064	0.0000
$C_{p_x} - C'_{p_x}$	0.0065	−0.1767
$C_{p_x} - C'_{p_y}$	0.1832	0.0000
$C_{p_y} - C'_{p_y}$	0.0065	−0.1157
$C_{p_y} - C'_{p_z}$	0.1832	0.1726
$C_{p_z} - C'_{p_z}$	0.0065	0.3119

* C − C denotes intragroup elements and C − C′ neighbouring group elements.
** The values of Fock matrix elements are in hartrees.

one of the C-atoms of the ethane molecule is located in the origin of the coordinate system and the C—C bond is directed towards direction (1, 1, 1). In orientation 2 one of the H-atoms is placed in the origin the neighbouring C-atom being in the y-axis and the C—C bond in the yz-plane. From the data of Table I it is evident that most of the correspondent matrix elements are differring from one another thus upsetting the possibility of their uses in transference procedures. To avoid such difficulties the transferability can in general be ensured in two alternative ways: *i*) by maintaining the same relative orientations for both the pattern molecules and the target molecule; in this case even matrix elements over AO-s can be transferred, and *ii*) by employing ideally hybridized bases; in this case matrix elements over hybridized atomic orbitals (HAO-s) can be transferred. The use of HAO-s facilitates the accurate comparisons between the corresponding Fock matrix elements because the HAO-s are determined by the internal reference framework of the molecule whereas unhybridized AO-s are defined by reference to the external coordinate system.

In Table II Fock matrix elements over AO-s calculated by CNDO/2 method for aliphatic hydrocarbons oriented identically and in Table III matrix elements over HAO-s calculated by CNDO/2 method for the same first four members in

the homologous series of alkanes oriented differently are compared. The numbering of hybrid orbitals and the H 1s orbitals is displayed on Fig. 1. As one can see, in case of hybrid orbitals no matter whatever orientation is in effect, the corresponding matrix elements can always be parallelled.

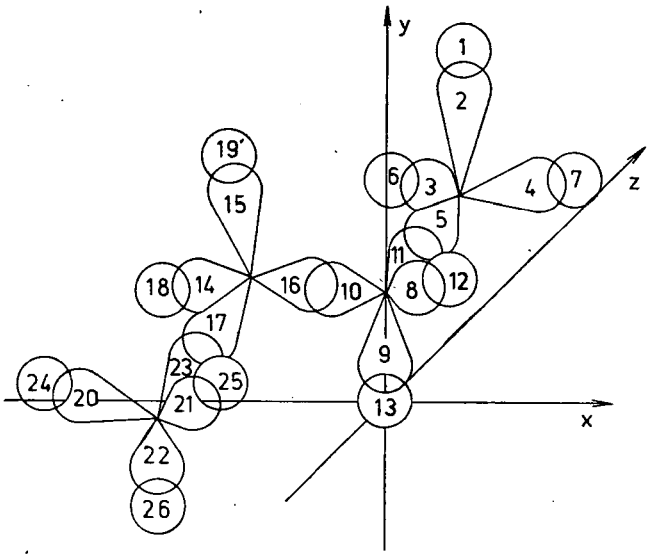

Fig. 1. Numbering of hybrid atomic orbitals in alkanes

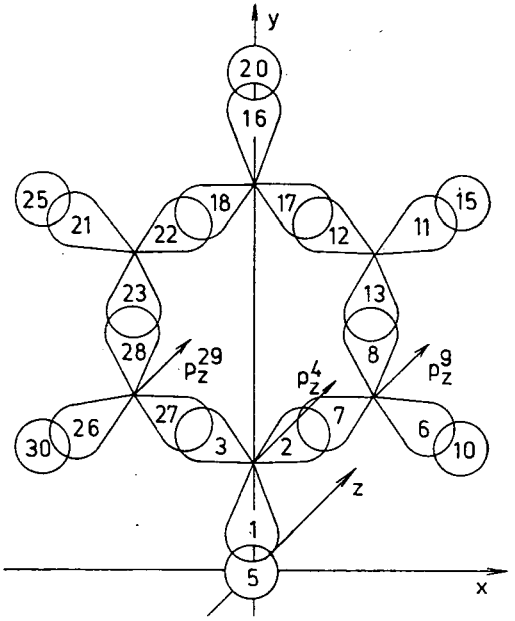

Fig. 2. Numbering of hybrid atomic orbitals in olefins

Table II

Typical parallel Fock matrix elements over AO-s calculated by CNDO/2 for alkanes (in hartrees)

Interacting* orbitals	Methane	Ethane	Propane	Butane
		Methyl intragroup		
C_s —C_s	−0.5271	−0.5203	−0.5232	−0.5226
C_{p_x}—C_{p_x}	−0.1958	−0.1959	−0.1982	−0.1972
C_s —C_{p_y}	0.0000	0.0036	0.0040	0.0038
H_i —H_i	−0.2580	−0.2628	−0.2631	−0.2630
H_i —H_j	−0.0573	−0.0557	−0.0553	−0.0553
C_s —H	−0.3907	−0.3890	−0.3882	−0.3879
C_{p_z}—H	0.2625	0.2164	0.2162	0.2160
		Methylene intragroup**		
C_s —C_s	—	(−0.5203)	−0.5159	−0.5189
C_{p_x}—C_{p_x}	—	(−0.1959)	−0.1976	−0.2001
C_s —C_{p_y}	—	(0.0036)	0.0055	0.0053
H_i —H_i	—	(−0.2628)	−0.2595	−0.2603
H_i —H_j	—	(−0.0557)	−0.0545	−0.0547
C_s —H	—	(−0.3890)	−0.3871	−0.3874
C_{p_z}—H	—	(−0.2164)	−0.2157	−0.2158
		First neighbour groups		
C_s —C'_s	—	−0.3048	−0.3042	−0.3039
C_{p_x}—C'_{p_x}	—	−0.1767	−0.1760	−0.1760
C_{p_y}—C'_{p_y}	—	−0.1157	−0.1125	−0.1126
C_{p_z}—C'_{p_z}	—	0.3119	0.3108	0.3112
H —H′	—	−0.0160	−0.0160	−0.0160
C_s —H′	—	−0.0650	−0.0645	−0.0644
C_{p_z}—H′	—	−0.0723	−0.0716	−0.0714
		Second neighbour groups		
C_s —C''_s	—	—	−0.0568	−0.0569
C_{p_x}—C''_{p_x}	—	—	−0.0211	−0.0212
C_{p_y}—C''_{p_y}	—	—	−0.0594	−0.0592
C_{p_z}—C''_{p_z}	—	—	0.0183	0.0167
H —H″	—	—	−0.0100	−0.0100
C_s —H″	—	—	−0.0219	−0.0219
C_{p_z}—H″	—	—	−0.0077	−0.0077

* Atomic orbitals with prime and double prime denote those on first and second neighbour group atoms, with respect to the group whose atoms bear on no prime.

** For sake of comparisons ethane methyl intragroup values are displayed in brackets.

Other than CNDO/2 semiempirical calculations exhibit similar possibilities concerning transferences of matrix elements. When comparing the results of CNDO/2, EHT, INDO and MINDO/1 calculations for alkanes in Table II and Table IV, it can be seen that perhaps the best transferabilities can be expected from

MINDO/1 and the worst from EHT calculations. Table V and Table VI show comparisons of parallel matrix elements for olefins using AO-s and HAO-s as bases. The numbering of hybrid orbitals, the H 1s and C $2p_z$ orbitals is as in Fig. 2. A number of typical equivalent Fock matrix elements over AO-s in CNDO/2 calculations for some polar carbon compounds containing a carbonyl group listed in Table VII show transferabilities comparable to those found for alkanes and olefins.

Table III

Typical parallel Fock matrix elements over HAO-s calculated by CNDO/2 for alkanes (in hartrees)

Interacting* orbitals	Methane	Ethane	Propane	Butane
1—1	−0.2580	−0.2628	−0.2631	−0.2624
1—2	−0.5890	−0.5867	−0.5869	−0.5869
1—3	−0.0640	−0.0651	−0.0647	−0.0647
1—5	−0.0640	−0.0609	−0.0598	−0.0595
1—6	−0.0572	−0.0557	−0.0553	−0.0553
2—2	−0.2786	−0.2817	−0.2830	−0.2820
2—3	−0.0828	−0.0857	−0.0861	−0.0861
1—9	—	−0.0277	−0.0270	−0.0270
1—10	—	0.0185	0.0160	0.0160
1—11	—	−0.0930	−0.0927	−0.0927
1—12	—	−0.0148	−0.0149	−0.0150
1—16	—	−0.0181	−0.0180	−0.0180
2—5	—	−0.0734	−0.0749	−0.0750
2—9	—	−0.0629	−0.0626	−0.0625
2—10	—	0.1137	0.1115	0.1117
2—11	—	−0.0861	−0.0868	−0.0871
2—12	—	−0.0277	−0.0276	−0.0276
5—8	—	−0.0862	−0.0871	−0.0867
5—11	—	−0.6655	−0.6642	−0.6644
5—16	—	—	−0.1232	−0.1230
5—17	—	—	0.0299	0.0280
1—15	—	—	−0.0030	−0.0031
1—17	—	—	0.0019	0.0023
2—15	—	—	0.0190	0.0189
2—17	—	—	−0.0179	−0.0176
8—17	—	—	−0.0627	−0.0609
8—18	—	—	0.0181	0.0184
12—14	—	—	0.0187	0.0184
12—17	—	—	−0.0922	−0.0920
12—18	—	—	−0.0179	−0.0176

* The numbering of orbitals is as in Fig. 1.

For transference purposes even fictitious or hypothetical pattern molecules or molecular fragments can effectively be used. In Table VIII some typical Fock matrix elements over AO-s for four heavy centers including fluorine atom in a number of fragments in closed-shell and open-shell states of different spin-multiplicities and in monofluorobenzene and salicylidene-4-fluoro-aniline are collected. Open-shell calculations were carried out by CNDO/2-level spin unrestricted Hartree-Fock (DODS) method. To be able to compare the results of closed-shell and open-

Table IV

Typical parallel Fock matrix elements over AO-s calculated by EHT, INDO and MINDO/1 methodes for alkanes (in hartrees)

Interacting* orbitals	EHT**			INDO			MINDO/1		
	Ethane	Propane	Butane	Ethane	Propane	Butane	Ethane	Propane	Butane
Methyl intragroup									
C_s —C_s	0.2888	0.2645	0.2603	−0.5618	−0.5637	−0.5630	−0.5465	−0.5475	−0.5475
C_{p_x}—C_{p_x}	−0.5464	−0.6264	−0.6209	−0.1780	−0.1799	−0.1789	−0.1640	−0.1658	−0.1657
H_i —H_i	−0.3646	−0.4115	−0.4123	−0.2723	−0.2724	−0.2715	−0.2730	−0.2724	−0.2697
C_s —H	0.2970	0.3215	0.3165	−0.3842	−0.3878	−0.3875	−0.3132	−0.3124	−0.3125
C_{p_z}—H	0.4367	0.4655	0.4723	0.2650	0.2636	0.2639	0.1625	0.1603	0.1603
Methylene intragroup *)**									
C_s —C_s	(0.2888)	0.2613	0.2406	(−0.5618)	−0.5612	−0.5641	(−0.5465)	−0.5588	−0.5599
C_{p_x}—C_{p_x}	(−0.5464)	−0.6341	−0.6938	(−0.1780)	−0.1875	−0.1892	(−0.1640)	−0.1692	−0.1692
H_i —H_i	(−0.3646)	−0.4574	−0.4776	(−0.2723)	−0.2764	−0.2779	(−0.2730)	−0.2695	−0.2691
C_s —H	(0.2970)	0.3041	0.2932	(−0.3842)	−0.3865	−0.3868	(−0.3132)	−0.3124	−0.3122
C_{p_z}—H	(0.4367)	0.5036	0.5088	(0.2650)	0.2590	0.2588	(0.1625)	0.1594	0.1594
First neighbour groups									
C_s —C'_s	0.1060	0.1008	0.1095	−0.3040	−0.3035	−0.3032	−0.2008	−0.2024	−0.2025
C_{p_x}—C'_{p_x}	0.5250	0.5129	0.5194	−0.1696	−0.1748	−0.1736	−0.1232	−0.1190	−0.1191
H —H′	0.1167	0.0848	0.0820	−0.0250	−0.0323	−0.0296	−0.0128	−0.0242	−0.0195
C_s —H′	0.0174	0.0316	0.0339	−0.0728	−0.0706	−0.0702	−0.0436	−0.0462	−0.0450
C_{p_z}—H′	−0.1610	−0.1208	−0.1171	−0.0582	−0.0645	−0.0633	−0.0469	−0.0552	−0.0526
Second neighbour groups									
C_s —C''_s	—	0.0174	0.0142	—	−0.0564	−0.0565	—	−0.0349	−0.0352
C_{p_x}—C''_{p_x}	—	0.0626	0.0631	—	0.0395	0.0388	—	0.0137	0.0140
H —H″	—	0.0307	0.0221	—	−0.0031	−0.0031	—	−0.0075	−0.0075
C_s —H″	—	0.0174	0.0081	—	−0.0219	−0.0219	—	−0.0252	−0.0253
C_{p_z}—H″	—	−0.0738	−0.0528	—	−0.0122	−0.0121	—	−0.0095	−0.0096

* Atomic orbitals with dash and double dash denote those on first and second neighbour group atoms, with respect to the group whose atoms bear on no prime.

** Though the orientations of ethane, propane and butane are identical among themselves in EHT they differ from those in INDO and MINDO/1 calculations.

*** Ethane methylene elements in brackets taken as the corresponding methyl intragroup elements in ethane demonstrate their interchangeability.

Table V

Typical parallel Fock matrix elements over AO-s calculated by CNDO/2 for conjugated hydrocarbons (in hartrees)

Interacting* orbitals	Ethylene	*s-cis*-Butadiene	Benzene
	Intragroup		
C_s —C_s	−0.5239	−0.5238	−0.5235
C_{p_x}—C_{p_x}	−0.1948	−0.2026	−0.2045
H —H	−0.2570	−0.2554	−0.2601
C_s —H	−0.4158	−0.4143	−0.4102
C_{p_x}—H	0.3947	0.3938	0.3928
	First neighbour groups		
C_s —C'_s	−0.3730	−0.3724	−0.3710
C_s —C'_{p_x}	0.3585	0.3563	0.3525
C_{p_x}—C'_{p_x}	0.2169	0.2158	0.2191
C_{p_z}—C'_{p_z}	−0.3671	−0.3548	−0.3540
C_s —H′	−0.0662	−0.0660	−0.0656
	Second neighbour groups		
C_s —C''_s	—	−0.0666	−0.0668
C_s —C''_{p_x}	—	−0.0443	−0.0441
C_{p_x}—C''_{p_x}	—	0.0092	0.0087
C_{p_z}—C''_{p_z}	—	−0.0263	−0.0267
	Third neighbour groups		
C_s —C'''_s	—	−0.0299	−0.0291
C_{p_x}—C'''_{p_x}	—	−0.0106	−0.0096
C_{p_z}—C'''_{p_z}	—	0.0227	0.0199

* Atomic orbitals with prime, double dash and triple dash denote those on first, second and third neighbour group atoms, with respect to the group whose atoms bear on no prime.

shell calculations, the corresponding elements of Fock matrices have been averaged for α and β spins. Though there are better agreements between the corresponding matrix elements of higher members of homologous series or between molecules and molecular fragments of comparable sizes, still acceptable differences occur especially when Fock matrix elements of small fragments assumed to be radicals with one or more unpaired electrons and parts of large molecules are compared.

Usually, matrix elements are decreasing in magnitude with increasing spatial separation of the functions involved. When using hybrid orbitals most matrix elements are negative but at larger separations some elements are positive indicating net repulsions. As a result of our preliminary investigations concerning the changes in the Fock matrix elements over AO-s for mononuclear transition metal complexes and their fragments, containing isoelectronic diatomic ligands (*e.g.* CN^-, NO^+, CO, N_2, *etc.*) arranged around the central metal with the same symmetry, as a function of net charge on the complex molecules, by maintaining other parameters

Table VI

Typical parallel Fock matrix elements over HAO-s calculated by CNDO/2 for conjugated hydrocarbons (in hartrees)

Interacting* orbitals	Ethylene	*s-cis*-Butadiene	Benzene
1—1	−0.3044	−0.2969	−0.3129
1—2	−0.1051	−0.1069	−0.1099
1—3	−0.1224	−0.1236	−0.1099
1—5	−0.6078	−0.6080	−0.6062
1—6	−0.1061	−0.1055	−0.1052
1—7	−0.1003	−0.1011	−0.1029
1—8	0.1201	0.1167	0.1166
1—10	−0.0341	−0.0338	−0.0332
2—5	−0.0506	−0.0489	−0.0501
4—4	−0.1948	−0.2004	−0.2073
4—9	−0.3671	−0.3547	−0.3076
5—5	−0.2575	−0.2513	−0.2648
5—10	−0.0120	−0.0121	−0.0117
1—11	—	−0.0133	−0.0129
1—13	—	0.0299	0.0295
1—15	—	0.0019	0.0018
2—11	—	0.0298	0.0295
2—12	—	−0.0495	−0.0489
2—13	—	−0.1549	−0.1549
5—12	—	−0.0043	−0.0032
5—13	—	−0.0197	−0.0197
5—15	—	0.0013	0.0011

* The numbering of orbitals is as in Fig. 2.

constant, we found that mostly similar matrix elements only appear when the resultant net charges on the molecules to be compared are identical. Less conspicuous changes can be observed in the matrix elements when complexes carrying the same net charges but having ligands different in quality and number are compared. In most cases the use of pattern molecules (fragments) comprising at least three heavy atoms seems to give satisfactory results in semiempirical transference procedures.

The proper criteria for transferability are, of course, lying far more in the results arising from the solutions of the eigenvalue problem, by transferring Fock matrix elements from small pattern molecules or fragments to construct matrices of large target molecules, than in the one by one comparisons of parallel matrix elements for different molecules or fragments, therefore, we completed CNDO/2 calculations for butane in a direct way and also by using synthetic Fock matrices constructed by transference from direct calculations on ethane and propane. When constructing butane from ethane by using Fock matrix element transference, methylene group elements occur in butane which are not found in ethane. On the basis of the similarities of matrix elements in Table II and III it is presumed that the necessary methylene elements can be reasonably approximated by appropriate ethane methyl group elements. Clearly butane elements between non-neighbouring carbon atoms are unavailable from ethane and have been assumed to be negligible, thus all elements

Table VII

Typical parallel Fock matrix elements over AO-s calculated by CNDO/2 for polar carbon molecules (in hartrees)

Interacting orbitals	Formic acid	Acetaldehyde	Acetic acid
	Carbonyl intragroup		
C_s —C_s	−0.5723	−0.5663	−0.5709
C_{p_x}—C_{p_x}	−0.2149	−0.2162	−0.2082
O_s—O_s	−1.1335	−1.1381	−1.1299
O_{p_x}—O_{p_x}	−0.3542	−0.3496	−0.3518
C_s —O_s	−0.4085	−0.4075	−0.4083
C_{p_x}—O_{p_x}	−0.3622	−0.3605	−0.3583
C_{p_z}—O_{p_z}	0.2540	0.2570	0.2532
	Hydroxyl intragroup		
O_s —O_s	−1.1450	—	−1.1391
O_{p_x}—O_{p_x}	−0.6152	—	−0.6135
H —H	−0.2383	—	−0.2345
O_s —H	−0.4568	—	−0.4548
O_{p_x}—H	0.0000	—	0.0000
O_{p_y}—H	−0.4706	—	−0.4688
O_{p_z}—H	−0.1595	—	−0.1639
	Carboxyl intragroup*		
O_s —O'_s	−0.0268	—	−0.0275
O_{p_x}—O'_{p_x}	0.0324	—	0.0329
C_s —O'_s	−0.3347	—	−0.3335
C_s —H	−0.1004	—	−0.1120
	Methyl intragroup*		
C_s —C_s	—	−0.5464	−0.5550
C_{p_x}—C_{p_x}	—	−0.2241	−0.2348
C_s —C_{p_y}	—	0.0024	0.0027
H_i —H_i	—	−0.2750	−0.2776
H_i —H_j	—	−0.0579	−0.0580
C_s —H	—	−0.3890	−0.3891
C_{p_z}—H	—	0.0036	0.0034
	Methyl first neighbour intergroup*		
C_s —C'_s	—	−0.3110	−0.3126
C_{p_x}—C'_{p_x}	—	−0.1727	−0.1714
C_{p_y}—C'_{p_y}	—	−0.1246	−0.1237
C_{p_z}—C'_{p_z}	—	0.3020	0.2997
C_s —C'_{p_x}	—	0.0027	0.0032
C_s —C'_{p_y}	—	0.1172	0.1166
C_s —C_{p_z}	—	0.3317	0.3298
C_{p_y}—C'_{p_z}	—	0.1723	0.1709
H —C'_s	—	−0.0652	−0.0639
H —C'_{p_x}	—	−0.0342	−0.0353
H —C'_{p_y}	—	0.0012	0.0014
H —C'_{p_z}	—	0.0736	0.0747

* Dash denotes orbitals on atoms neighbouring to an atom on which the orbitals bear no dash.

Table VIII

Typical parallel Fock matrix elements over AO-s calculated by CNDO/2 for salicylidene-4-fluoro-aniline and its fragments (in hartrees)*

Interacting** orbitals	Formula 1 singlet	Formula 2 quartet	Formula 3 singlet	Formula 4 quartet	Formula 5 singlet	Formula 6 singlet
$F_s - F_s$	−1.4739	−1.5030	−1.5159	−1.4681	−1.4623	−1.4554
$F_{p_x} - F_{p_x}$	−0.7536	−0.7805	−0.7730	−0.7382	−0.7395	−0.7330
$F_s - F_{p_z}$	0.0132	0.0122	0.0110	0.0120	0.0121	0.0121
$F_s - C^3_s$	−0.3243	−0.3238	−0.3232	−0.3240	−0.3245	−0.3245
$F_s - C^3_{p_y}$	−0.4677	−0.4658	−0.4709	−0.4708	−0.4705	−0.4705
$F_{p_y} - C^3_{p_y}$	0.4201	0.4153	0.4236	0.4235	0.4238	0.4237
$F_{p_y} - C^1_{p_y}$	0.0505	0.0419	0.0302	0.0314	0.0317	0.0317
$F_s - C^2_{p_y}$	−0.0415	−0.0377	−0.0364	−0.0362	−0.0362	−0.0362
$C^3_s - C^3_s$	−0.5431	−0.5499	−0.6251	−0.5525	−0.5540	−0.5460
$C^3_{p_y} - C^1_s$	0.1666	0.1770	0.1656	0.1660	0.1666	0.1666
$C^3_{p_y} - C^1_{p_y}$	−0.1341	−0.1376	−0.1201	−0.1168	−0.1186	−0.1186
$C^3_{p_z} - C^2_{p_y}$	0.2830	0.2779	0.2786	0.2786	0.2783	0.2783
$C^3_{p_z} - C^2_{p_y}$	0.1695	0.1765	0.1728	0.1735	0.1746	0.1745
$C^1_{p_y} - C^1_{p_z}$	−0.1214	−0.1591	−0.2032	−0.2257	−0.2286	−0.2234
$C^1_s - C^1_{p_y}$	−0.0159	−0.0240	−0.0223	−0.0114	−0.0103	−0.0099
$C^2_{p_z} - C^2_{p_z}$	−0.1705	−0.2031	−0.2239	−0.2120	−0.2179	−0.2120
$C^2_{p_z} - C^2_s$	0.0200	0.0179	0.0141	0.0114	0.0108	0.0103
$C^1_{p_z} - C^2_{p_z}$	−0.0758	−0.0314	−0.0171	−0.0242	−0.0285	−0.0289
$C^1_{p_x} - C^2_{p_x}$	0.1266	0.1164	0.1139	0.1141	0.1145	0.1145
$H^4_{p_z} - H^4_{p_z}$	−0.2444	−0.2621	−0.2754	−0.2705	−0.2668	−0.2632
$H^4 - F_s$	−0.0111	−0.0133	−0.0126	−0.0130	−0.0128	−0.0128
$H^4 - F_{p_z}$	0.0127	0.0134	0.0177	0.0125	0.0128	0.0128
$H^4 - C^3_s$	−0.0705	−0.0687	−0.0715	−0.0702	−0.0680	−0.0680
$H^4 - C^1_{p_z}$	0.0109	0.0142	0.0147	0.0157	0.0153	0.0153
$H^4 - C^2_s$	−0.4007	−0.4147	−0.4026	−0.4029	−0.4026	−0.4024

* Only interactions of orbitals on the most critical five atoms are presented.

** The superscripts of orbitals correspond with the numbering of atoms in Fig. 3.

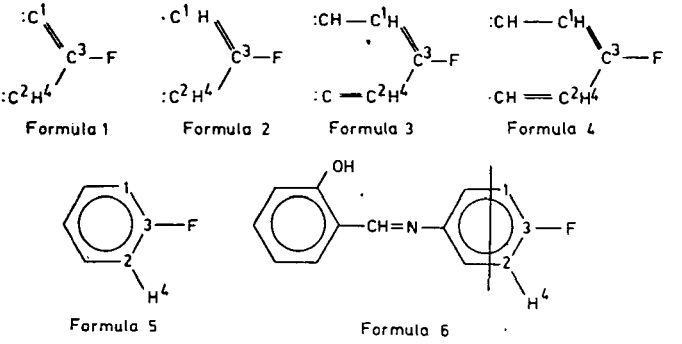

Fig. 3. Structures of fragments and molecules denoted by Formulae 1—6 and numbering of atoms whose orbitals have been considered as interacting orbitals

Table IX

Butane orbital energies (in hartrees)

No.*	Direct CNDO/2 7. step	Simulated CNDO/2**			
		from ethane		from propane	
		non-iterative	2. step	non-iterative	2. step
1.	−1.6646	−1.5605	−1.6675	−1.6573	−1.6647
2.	−1.3901	−1.3996	−1.3896	−1.3975	−1.3900
3.	−1.0883	−1.1408	−1.0874	−1.0884	−1.0879
4.	−1.0651	−1.0145	−1.0665	−1.0650	−1.0652
5.	−0.9840	−0.9542	−0.9847	−0.9831	−0.9836
6.	−0.8399	−0.8471	−0.8408	−0.8392	−0.8410
7.	−0.7879	−0.8075	−0.7882	−0.7930	−0.7875
8.	−0.7814	−0.7754	−0.7800	−0.7822	−0.7805
9.	−0.6618	−0.7010	−0.6627	−0.6611	−0.6630
10.	−0.6205	−0.6448	−0.6195	−0.6190	−0.6198
11.	−0.5727	−0.6242	−0.5741	−0.5712	−0.5721
12.	−0.5588	−0.5354	−0.5596	−0.5588	−0.5585
13.	−0.5434	−0.5331	−0.5431	−0.5366	−0.5440
14.	0.2623	0.2506	0.2612	0.2633	0.2625
15.	0.2771	0.2708	0.2754	0.2784	0.2767
16.	0.2896	0.2854	0.2889	0.2895	0.2891
Total energy	−36.1922	−36.1947	−36.1981	−36.1827	−36.1915
Relative comput. time	1	1/10	1/7	1/10	1/7

* No. 1.—No. 13. orbitals are occupied.

** By using Fock matrix elements over HAO-s of ethane and propane pattern molecules, calculated by CNDO/2 method.

between non-nearest neighbour groups are taken zero. When butane is constructed from propane only the largest distance methyl-methyl (third neighbour) terms have been neglected and some methylene (second neighbour) terms have been approximated by appropriate propane methyl matrix elements, however, all the other terms required in the calculations have directly been taken from propane. In Table IX the orbital energies of butane are presented: in the first column those obtained by direct calculation at the 7. cycle of iterations, in the second and fourth columns those from the non-iterative solution of the synthetic problems constructed from ethane and propane elements and in the third and fifth columns the solutions of the synthetic matrices from ethane and propane elements after the 2. iteration step. The advantages of the semiempirical method transferring Fock matrix elements are most striking when comparing the relative computing times of the calculations in the last row of Table IX. The time requirements of selecting the matrix elements needed and constructing the matrix of the target molecule are not included in the computing times. The gain in computing time is due to the fact that when using the transference method the calculations of molecular orbitals and total energy do not necessitate the repeated lengthy evaluation of two-electron repulsion integrals. It is expected that the benefits of Fock matrix element transferences within semiempirical methods will become much more evident if used to much larger systems but starting with the same pattern molcules. Of such results we will give accounts in following papers of this series after having finished developing our computer library program which would render possible the automatic transfer of matrix elements. The construction of large matrices from elements of pattern molecules by hand is not only exhausting and tedious but also an extensive source of errors.

References

[1] *Trindle, C., O. Sinanoğlu:* in "Sigma Molecular Orbital Theory" (O. Sinanoğlu and K. Wiberg eds.) p. 214. Yale University Press, 1970, New Haven and London.
[2] *Magnasco, V., A. Perico:* J. Chem. Phys. **47**, 971 (1967), ibid **48**, 800 (1968).
[3] *Rothenberg, S.:* J. Chem. Phys. **51**, 3389 (1969).
[4] *Degand, P., G. Leroy, D. Peeters:* Theor. Chim. Acta **30**, 243 (1973).
[5] *Leroy, G., D. Peeters:* in "Localization and Delocalization in Quantum Chemistry" (O. Chalvet et al. eds.) Vol. 1. pp. 207—221. Reidel Publishing Company, 1975, Dordrecht, Netherlands.
[6] *Peeters, D., G. Leroy:* Theor. Chim. Acta **50**, 135 (1978).
[7] *Klessinger, M.:* Theor. Chim. Acta **49**, 77 (1978).
[8] *Deplus, A., G. Leroy, D. Peeters:* Theor. Chim. Acta **36**, 109 (1974).
[9] *Mayer, I., M. Révész:* Presented at the Conference on Structure of Matter and Molecules held in Mátrafüred, October 8—10, 1979.
[10] *Orloff, M. K., D. D. Fitts:* J. Amer. Chem. Soc. **85**, 3721 (1963).
[11] *Newton, M. D., F. P. Boer, W. N. Lipscomb:* J. Amer. Chem. Soc. **88**, 2353, 2361, 2367 (1966), Palke, W. E., W. N. Lipscomb: ibid **88**, 2384 (1966), Boyd, D. B., W. N. Lipscomb: J. Chem. Phys. **48**, 4955 (1968).
[12] *von Niessen, W.:* J. Chem. Phys. **55**, 1948 (1971).
[13] *O'Leary, B., B. J. Duke, J. E. Eilers:* in "Advances in Quantum Chemistry" (P-O. Löwdin ed.) Vol. 9. pp. 1—67. Wiley, 1975, New York. (an excellent review on the SAMO method and other transference procedures).
[14] *Eilers, J. E., D. R. Whitman:* J. Amer. Chem. Soc. **95**, 2067 (1973).
[15] *Duke, B. J., B. O'Leary:* Chem. Phys. Lett. **20**, 459 (1973).
[16] *O'Leary, B., B. J. Duke, J. E. Eilers, E. W. Abrahamson:* Nature **246**, 166 (1973).
[17] *Duke, B. J., J. E. Eilers, B. O'Leary:* J. Chem. Soc. (Faraday II) **70**, 386 (1974).

[18] *Eilers, J. E., B. O'Leary, B. J. Duke, A. Liberles, D. R. Whitman:* J. Amer. Chem. Soc. **97**, 1319 (1975).
[19] *Eilers, J. E., B. O'Leary, A. Liberles, D. R. Whitman:* J. Amer. Chem. Soc. **97**, 5979 (1975).
[20] *Duke, B. J., B. O'Leary:* in "Quantum Chemistry — The State of Art" (V. R. Saunders and J. Brown eds.) Proceedings of the Atlas Computer Conference, No. 4. p. 157. Science Research Council, 1975, London,
Duke, B. J., M. Pickering, B. O'Leary, J. E. Eilers: J. Chem. Soc. (Faraday II) **71**, 1401 (1975).
[21] *Duke, B. J., D. R. Eilers, J. E. Eilers, S. Kang, A. Liberles, B. O'Leary:* Int. J. Quantum Chem. Quantum Biology Symp. **2**, 155 (1975).
[22] *Collins, M. P. S., B. J. Duke:* Int. J. Quant. Chem. **10**, 629 (1976), and B. J. Duke: Personal communication.
[23] *Pople, J. A., D. L. Beveridge:* Approximate Molecular Orbital Theory. McGraw Hill, 1970, New York.
[24] *Clack, D. W., N. S. Hush, J. R. Yandle:* J. Chem. Phys. **57**, 3503 (1972).

ИМИТАЦИОННЫЕ СЕМИЭМПИРИЧЕСКИЕ РАСЧЕТЫ МОЛЕКУЛЯРНЫХ ОРБИТАЛЕЙ, I

М. И. Бан, И. Балинт и М. Ревес

Сравнены конвергированные Фокк матрикс элементы атомных орбиталей типа Слэтера и гибридизированных орбиталей, получаемых семиэмпирическими (РМГ, ППДП, ЧПДП, и МЧПДП) квантово-химическими методами расчетов для алканов, олефинов, кислородсодержащих полярных молекул и различных молекул и молекулярных фрагментов с закрытыми и открытыми электронными оболочками. Хорошее совнадение между параллельными элементами матрикса Фокка, предсказывает их трансферабельность с одной молекулы в другую. Успешно проведена трансферация для алканов. Цель серии работ заключается в представлении принципов, законов, возможностей и ограничений трансферабелбности.

SPECTRAL STUDIES OF SCHIFF BASES DERIVED FROM AROMATIC ALDEHYDES AND ALIPHATIC AMINES

By

J. CSÁSZÁR

Institute of General and Physical Chemistry, Attila József University, Szeged, Hungary

(Received 12th September, 1979)

The spectral behaviour of Schiff bases derived from salicylaldehyde, resorcylaldehyde, naphthaldehyde, resacetophenone and *n*-alkylamines (C_{10}, C_{12}, C_{16}, C_{18}) was investigated. From the ultraviolet, infrared and ^1H NMR spectral data it can be established that the alkyl chains have only a small effect on the other part of the molecules.

The electronic spectra of Schiff bases derived from salicylaldehyde and aromatic or aliphatic amines are interesting from the point of view of inter- and intramolecular hydrogen-bond formation, as well as substituent effects. In the solid state the N-salicylidene-anilines have planar [1] or non-planar [2, 3] configurations. With respect to possible deviations from the planar configuration, these compounds can exist with different conformations in solution. The possible tautomeric equilibria are discussed in several papers [4—8]. The aim of the present work is a spectral study of some Schiff bases of aromatic aldehydes and long-chain aliphatic amines (structures I and II).

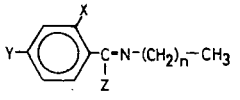

I.

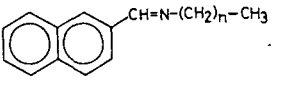

II.

No.	X	Y	Z	n
1	OH	H	H	15
2	OH	H	H	17
3	OH	OH	H	11
4	OH	OH	H	17
5	OH	OH	CH_3	9
6	OH	OH	CH_3	11
7	OH	OH	CH_3	15
8	OH	OH	CH_3	17

No.	n
9	9
10	11
11	15

Experimental

The Schiff bases were prepared by mixing equivalent amounts of methanolic solutions of the respective aldehydes and amines. The samples were purified by repeated recrystallization from methanol. The m.p. (uncorrected) and analytical data are presented in Table I.

Table I

Analytical data on the Schiff bases

No.	m.p.	C %		H %	
		calc.	found	calc.	found
1	34.2	79.93	79.79	11.37	11.34
2	42.7	80.35	80.31	11.60	11.50
3	52.4	74.71	74.65	10.33	10.18
4	70.8	77.07	77.01	11.13	11.08
5	123.2	74.18	74.08	10.03	10.00
6	111.1	75.19	75.15	10.41	10.34
7	106.3	76.75	76.71	11.00	10.88
8	93.4	77.36	77.25	11.24	11.19
9	47.2	85.35	85.30	9.89	9.85
10	53.8	85.37	85.29	10.28	10.24
11	62.0	85.41	85.36	10.88	10.85

The absorption spectra were measured with a Specord UV—VIS apparatus, using spectrally pure solvents. The ^1H NMR spectra were recorded with a Perkin—Elmer R12 60 MHz spectrometer in $CDCl_3$ at room temperature (TMS as internal standard).

The equilibrium constants K of the tautomeric equilibria were calculated as described previously [8].

Results

In the ultraviolet spectral range the aromatic Schiff bases show several well-defined bands which can be assigned to $\pi \rightarrow \pi^*$ transitions [9—13]. The spectra of the compounds studied in this paper may be divided into three types: derivatives of 1) salicylaldehyde, 2) resorcylaldehyde and resacetophenone, and 3) naphthaldehyde.

The spectra of methanolic solution of *1* and *2* show five bands at 398 (ν_1), 314 (ν_2), 276 (ν_3), 254 (ν_4) and 215 (ν_5) nm, with increasing intensity. In cyclohexane or in other non-polar solvents the bands ν_1, ν_2 and ν_4 can be found at almost the same energies, but ν_3 and ν_5 are absent (Fig. 1, Table II) (see *e.g.* [14]).

In mixtures of polar and non-polar solvents the intensities of ν_3 and ν_5 change, depending on the composition of the solvent mixture (Fig. 2). The equilibrium constants K (*e.g.* in the methanol/benzene binary solvent system), calculated on the basis of such a set of curves, are as expected very similar for the two compounds (Table II).

Table II

No.	a)	Spectral data (nm and lg ε) measured in different solvents						^{1}H NMR data[b] δ CH$_2$	δ CH$_3$[c]	δ CH$_3$[d]	δ CHN	K
Hsal—N—CH$_3$[c]	M	408(3.02)	311(3.65)	282(3.40)	253(4.11)		214(4.44)					
1	M	399(3.38)	314(3.57)	276(3.70)	254(4.09)		216(4.44)	1.32		3.47; 3.58; 3.67	8.27	0.6
	B		315(3.76)									
2	H		318(3.73)		255(4.14)		217(4.44)	1.25		3.43; 3.54; 3.63	8.26	0.7
	M	397(3.40)	315(3.56)	277(3.70)	253(4.06)		217(4.40)					
	B		317(3.89)									
3	M	367(3.94)	303(4.24)	250(3.91)	245(3.92)	232(4.10)	220(4.18)	1.19		3.24; 3.34; 3.43	7.64	5.8
	B		309(4.01)									
4	H		308(3.91)	274(4.24)			221(4.45)	1.26		3.33; 3.44; 3.53	7.74	5.7
	M	367(4.02)	302(4.33)	252(4.00)	246(4.00)	232(4.19)	220(4.27)					
	B		310(4.01)									
5	M	366(4.11)	297(4.32)	250(4.08)	244(4.10)		227(4.37)	1.19	2.21	3.28; 3.39; 3.47		28.0
	B		307(4.01)									
6	M	365(4.18)	296(4.38)	249(4.14)	243(4.15)		227(4.43)	1.18	2.20	3.27; 3.37; 3.48		29.3
	B		307(3.96)									
7	M	366(4.07)	297(4.28)	249(4.02)	244(4.04)		228(4.32)	1.24	2.24	3.34; 3.44; 3.53		17.5
	B		306(3.94)									
8	H		304(4.05)	271(4.18)			227(4.38)	1.23	2.24	3.30; 3.41; 3.50		18.0
	M	365(4.04)	297(4.25)	249(3.99)	244(4.01)		228(4.28)					
	B		306(3.83)									
9	M	293(4.15)	283(4.24)	273(4.14)	251(4.84)	243(4.82)		1.23		3.47; 3.59; 3.69	8.30	
10	M	293(4.09)	282(4.18)	272(4.08)	251(4.78)	244(4.76)		1.21		3.48; 3.59; 3.70	8.30	
11	H	293(4.04)	281(4.17)	272(4.08)	251(4.85)	242(4.85)		1.23		3.50; 3.61; 3.72	8.34	
	M	294(4.04)	283(4.13)	273(4.03)	251(4.74)	244(4.72)						

[a] H: cyclohexane; M: methanol; B: benzene
[b] $CHCl_3$;
[c] $C_6H_4(OH)CH=N-CH_3$;
[d] CH_3 signal;
[e] $-C(CH_3)=N-$ signal

A dramatic change can be observed in the spectra measured in glacial acetic acid, and in methanol containing NaOH or acetic acid (Fig. 3). With increasing acid content two new bands develop (277 and 352 nm) with high and medium intensity, respectively; there is a linear relationship between lg[acid] and ε (Table III).

The NMR spectra of *1* and *2* are similar to those of the other Schiff bases of salicylaldehyde [8]; the methine, methylene and methyl proton signals are observed at 8.27 and 8.26 (singlet), at 1.32 and 1.25, and at 3.58 and 3.54 ppm (triplet), re-

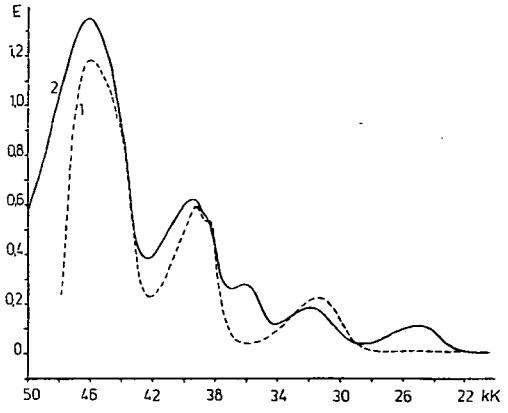

Fig. 1. Electronic spectra of *2*. 1: in cyclohexane; 2: in methanol. $c=4.3\cdot10^{-4}$ M; d=0.1 cm.

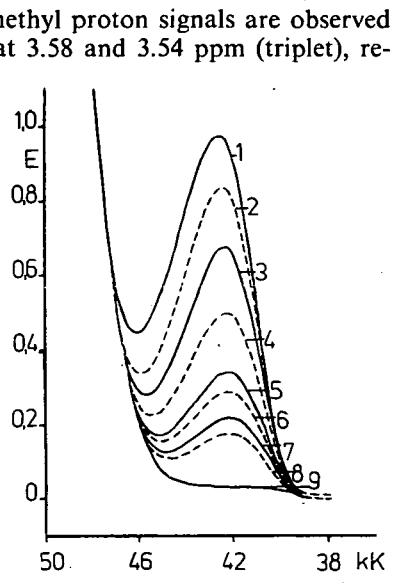

Fig. 2. Absorption spectra of *1* in CH_3OH/C_6H_6 mixtures. $c=5\cdot10^{-4}$ M; d=1.0 cm. 1: in methanol; 2-8 in methanol -benzene mixtures; 2: 0.114; 3: 0.303; 4: 0.683; 5: 1.365; 6: 1.820; 7: 2.578; 8: 3.682; 9: in benzene.

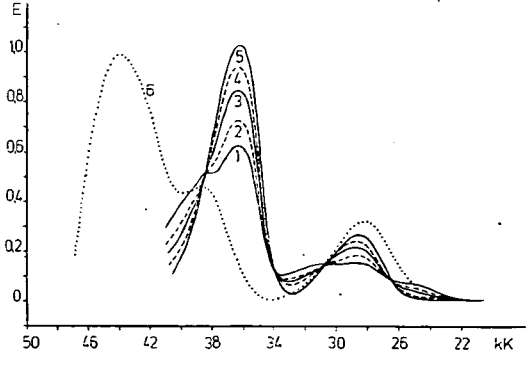

Fig. 3. Absorption spectra of *2* in methanol/glacial acetic acid mixtures. [acid]=1: 0.333; 2: 0.666; 3: 1.332, 4: 2.664 M; 5: in pure acid; 6: in methanol containing 0.02 M NaOH. $c=4.3\cdot10^{-4}$; d=0.1 cm.

Table III

*Spectral change of 1 with the glacial acetic acid concentration in methanolic medium**

[acid]	ε_{275}	ε_{350}
0	6 250	980
0.333	14 550	3 510
0.500	16 100	3 950
0.666	16 900	4 250
1.000	18 500	4 650
1.332	19 700	5 000
2.000	20 900	5 350
2.664	21 950	5 650
⋮	⋮	⋮
14.470	23 950	6 250

* [SB] = $4.3 \cdot 10^{-4}$ M; d = 0.1 cm.

spectively. It can be stated that these bases (*3*—*8* too) exist solely in the phenol-imine form (III) in non-hydroxylic solvents at normal temperatures.

As seen from Table II and Fig. 4, the absorption spectra of *3*—*8* are quite different from those of the two former compounds; the methanolic solutions of *3* and *4*, and *5*—*8*, showed six and five bands, respectively. In glacial acetic acid a new high-intensity band developed at 302 nm, with a shoulder at about 355 nm.

The equilibrium constants calculated for *3* and *4* (5.8 and 5.7), as well as for *5*—*8* (17.5—29.3) are high; this fact suggests that the 5—OH group and the methyl substituent on the azomethine carbon atom favour formation of the quinone-imine tautomer. The significant difference between the *K* values of *5* and *6* and those of *7* and *8* is difficult to interpret. The CHN proton signals of *3* and *4* were observed at 7.64 and 7.74 ppm; for *5*—*8* the —$C(CH_3)$= signals appear at 2.20—2.24 ppm.

The absorption spectra of *9*—*11* are quite similar to those of β-naphthaldehyde or other naphthalene derivatives (Fig. 5); in the range 270—300 nm a band system characteristic of such molecules occurs. In cyclohexane, in glacial acetic acid, or in alkaline methanol the structure of the absorption curves remains almost unchanged; also, the ^{1}H NMR spectra of all three Schiff bases are practically the same (Table II).

Discussion

In the molecules studied there are two chromophores, the phenyl and the azomethine groups [15, 16]. The band of the $n \rightarrow \pi^*$ transition of the unconjugated azomethine group lies at 236 nm, with an extinction coefficient of about 100 [17], but this band is hidden under the more intense bands occurring at around the same energy. The absorption spectra of the compounds studied are essentially slightly modified spectra of the aldehydes in question; *e.g.* in cyclohexane solution the spectra of *1* (Fig. 1) shows bands at 217, 255 and 318 nm, and those of salicylaldehyde (in the same solvent) at 215, 257 and 328 nm. This observation is supported by the

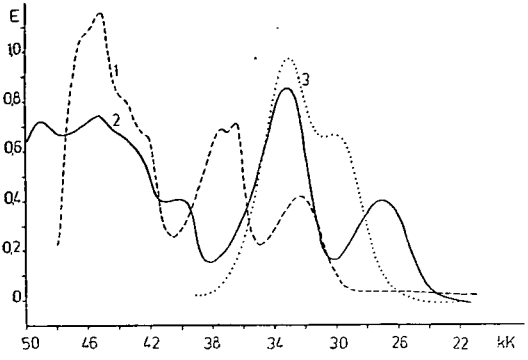

Fig. 4. Spectra of *4*. 1: in cyclohexane; 2: in methanol; 3: in glacial acetic acid. $c = 4.1 \cdot 10^{-4}$; d = 0.1 cm.

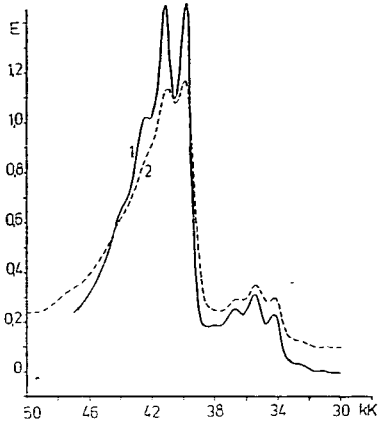

Fig. 5. Absorption spectra of *11*. 1: in cyclohexane; 2: in methanol. $c = 2 \cdot 10^{-4}$ M; d = 0.1 cm.

finding [18] that the spectra of $C_6H_5 \cdot CH{=}N{-}CH_3$ and benzaldehyde are very similar. According to several authors (*e.g.* [18]) the 245 nm band of N-benzylimine and probably of our compounds corresponds to the 262 nm band of benzylideneaniline. This band corresponds to a transition to a charge-transfer state in which the phenyl and the azomethine groups act as electron donor and electron acceptor, respectively. Replacing the phenyl group by an alkyl group increases the electronegativity of the nitrogen atom, making the azomethine group a better electron acceptor. We found that these *N*-salicylidene-alkylamines are extremely sensitive to the nature of the solvent. In polar solvents the tautomeric form IV exists pre-

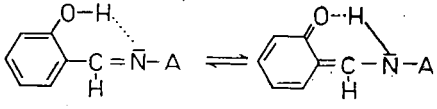

III. IV.

dominantly; due to the conjugation between the azomethine group and the aldehyde ring, two new medium-intensity bands appear, at 276 and 400 nm. In a benzene/methanol binary solvent system the III↔IV equilibrium shifts to the right with increasing concentration of the polar component.

In alkaline and in acidic medium the ionic (V) and the protonated (VI) (the nitrogen lone-pair is localized) forms of the Schiff base molecules are present. In both cases the possible tautomeric forms (V/a and VI/a) must be taken into con-

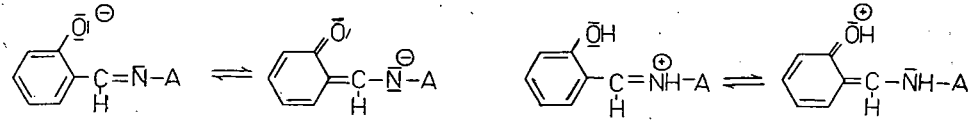

V. Va. VI. VIa.

sideration, too. On the basis of the spectral change observed it may be stated that the III↔V(VI)↔V/a (VI/a) equilibrium shifts to the right with increasing alkaline and acid concentration.

From the results discussed it is obvious that the long alkyl chains have only a small effect on the other part of the molecules and on their spectra. This is proved by the experimental result that the spectra of the methylamine, 2-aminopropane [14] and octadecylamine derivatives of salicylaldehyde differ only very slightly.

References

[1] *Bergman, J., L. Leiserowitz, G. M. J. Schmidt:* J. Chem. Soc., 2068 (1964).
[2] *Bergman, J., L. Leiserowitz, K. Osaki:* J. Chem. Soc., 2086 (1964).
[3] *Minkin, V. I. et al.:* Zh. Fiz. Khim., **38**, 938 (1964).
[4] *Holm, R. H., G. W. Everett:* Progr. Inorg. Chem., **7**, 83 (1966).
[5] *Dudek, G. O., E. P. Dudek:* J. Amer. Chem. Soc., **88**, 2407 (1966).
[6] *Dudek, G. O., E. P. Dudek:* Chem. Comm., 464 (1965).
[7] *Bakerek, V.:* Coll. Czech. Chem. Comm., **33**, 994 (1968).
[8] *Császár, J. et al.:* Acta Chim. Hung., **86**, 9, 101 (1975).
[9] *Jaffé, H. H., S. Jung Yeh, R. W. Gardner:* J. Mol. Spectr., **2**, 120 (1958).
[10] *Kristek, F., J. Klicnar, P. Vetesnik:* Coll. Czech. Chem. Comm., **36**, 3608 (1971).
[11] *Smith, W. F.:* Tetrahedron, **19**, 445 (1963).
[12] *Brocklehurst, P.:* Tetrahedron, **18**, 299 (1962).
[13] *Ismailski, V. A., E. A. Smirnov:* J. Gen. Chem. USSR, **26**, 3389 (1956).
[14] *Charette, J., G. Falttlhansl, Ph. Teyssie:* Spectrochim. Acta, **20**, 597 (1964).
[15] *Minkin, V. I. et al.:* Tetrahedron, **23**, 3651 (1966).
[16] *Houlden, S. A., I. G. Csizmadia:* Tetrahedron, **25**, 1137 (1969).
[17] *Bonett, R., N. J. David, J. Hamlin, P. Smith:* Chem. Ind. (London), **46**, 1836 (1963).
[18] *El-Aasser, M., F. Abdel-Halim, M. Ashraf El-Bayoumi:* J. Amer. Chem. Soc., **93**, 590 (1971).
[19] *Chatterjee, K. K., B. E. Douglas:* Spectrochim. Acta, **21**, 1625 (1965).

СПЕКТРАЛЬНОЕ ИЗУЧЕНИЕ ШИФ — ОСНОВАНИЙ, ПОЛУЧЕННЫХ ИЗ АРОМАТИЧЕСКИХ АЛЬДЕГИДОВ И АЛИФАТИЧЕСКИХ АМИНОВ

Й. Часар

Изучены Шиф — основания, полученные из салицилальдегида, резорцилальдегида, нафталальдегида, резацетофенона и алкил-аминов с различной длиной цепи (C_{10}, C_{12}, C_{16}, C_{18}). На оснований УФ, ИК и ^1H- ЯМР спектроскопических данных можно прийти к заключению, что алкильные цепи мало влияют на основные свойства изученных молекул.

SPECTRA OF SCHIFF BASES OF THE TYPE X,Y-BENZYLIDENE-4-Z-ANILINE

By

J. CSÁSZÁR

Institute of General and Physical Chemistry, Attila József University, Szeged, Hungary

(Received 13th June, 1979)

The ultraviolet, infrared and ^{1}H NMR spectra of aromatic Schiff bases of the type X,Y-benzylidene-4-Z-aniline (X=H, 5-NO_2, 5-Br; Y=2-OH, 2-NH_2; Z=OH, NO_2) have been investigated. Regarding the formation of the keto-amine tautomeric form, the conclusion is drawn that the aniline-substituents play a determining role, but the aldehyde-substituents also influence the intensity of the visible band.

Several papers deal with the spectra [1—6], with the photochromic and thermochromic properties [7, 8] and with other behaviour [9—12] of the aromatic Schiff bases. In polar solvents a medium-intensity band appears in the 400—450 nm spectral region, which can be interpreted as due to enol-imine/keto-amine tautomeric equilibrium [13—15].

In an earlier paper [16] we reviewed the spectroscopic characteristics of numerous Schiff bases. It was concluded that the visible band appears if the following three conditions are fulfilled: a) the solvent is strongly polar, b) an OH group is present in the aldehyde ring in the *o*- or/and *p*-position, and c) a certain charge-density is attained on the N atom.

In this paper we discuss the spectra of the following compounds:

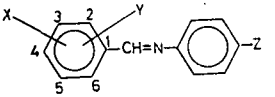

No.	X	Y	Z	m.p.
I	H	2—OH	OH	139.0
II	H	2—OH	NO_2	151.0
III	H	2—NH_2	NO_2	130.3
IV	5—NO_2	2—OH	OH	272.8
V	5—NO_2	2—OH	NO_2	230.3
VI	5—Br	2—OH	OH	224.6
VII	5—Br	2—OH	NO_2	200.7

The Schiff bases were prepared from their components in methanolic solution; the compositions were checked by C, N and H analysis. The ultraviolet, infrared and ^{1}H NMR spectra were recorded with a SPECORD UV—VIS and ZEISS UR—10 spectrophotometers and a JEOL 60 MHz instrument (TMS internal standard).

Table I

The ultraviolet, infrared** and ^{1}H NMR spectral data of the Schiff bases*

No.	nm and lg ε				νC=N	νNO$_2$	νC—O	γCH	δCHN	δOH
I[b]	430	348	270	~230	1613 s		1278 s	747 m	8.84	13.49
	2.60	4.20	3.91					833 m		9.53
II[a]		358	~320	~220	1607 s	1337 s	1267 s	760 m	8.69	12.58
		4.30			1561 s			847 m		
III[b]		367		230	1637 s	1303 s		757 m	8.10	7.82***
		4.50		4.26	1592 s			844 m		7.97
IV[b]	408	352	~317	232	1649 s	1337 s	1242 s	784 v	8.48	9.68
	3.70	4.42		4.35	1604 s			839 m	8.54	9.07
V[b]		364	~310	230	1629 s	1350 s	1292 s	752 m	8.66	12.07
		4.31		4.17	1593 s			860 m	8.72	
VI[b]	423	357		230	1623 s		1280 s	780 v	8.78	13.56
	2.81	4.34		4.53				832 m		9.56
VII[b]		363		220	1624 s	1342 s	1277 s	756 v	8.88	10.23
		4.40		4.52	1590 s			858 m		

* in CH_3OH;
** in KBr disk;
*** δ NH_2;
[a] in $CDCl_3$;
[b] in $CDCl_3$+DMSO

Table I presents the spectral characteristics, and Fig. 1 shows the u.v. spectra of IV and V. From these results the following conclusions can be drawn.

1. The ultraviolet spectra of methanolic solutions of I, IV and VI show a band with varying intensity between 400 and 430 nm. In III the 2—NH_2 group prevents

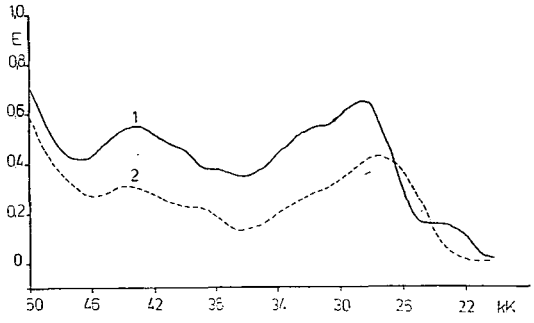

Fig. 1. Spectra of methanolic solutions. 1: IV, $c=2.48\cdot10^{-4}$ M, $d=0.1$ cm; 2: V, $c=2.09\cdot10^{-4}$ M, $d=0.1$ cm

the formation of the intramolecular H-bridge and the quinonoid form. In the cases of II, V and VII the strongly electron-withdrawing 4—NO_2 group ($\sigma = +0.778$) decreases the charge-density on the N-atom to such an extent that the keto-amine form cannot exist. It can be observed that, with the increase of the electron-withdrawing power of the aldehyde-substituents and with that of the electron-releasing power of the aniline-substituents, the intensity of the visible band increases. It can be stated that primarily the aniline-substituents play a structure-determining role, but the effect of the aldehyde-substituents cannot be neglected.

2. In the infrared spectra around 1650—1607, 1560—1604 and 1242—1292, and 1300—1350 cm^{-1} several bands can be found, which correspond to the νC—N, νC—O and νNO_2 stretching vibrations, respectively. From the infrared spectra measured with KBr pellets and in solution (CCl_4 or C_2Cl_4) the existence of the keto form is not provable. This corresponds to the experimental fact that the visible spectra of the solid substances show no band in the range mentioned.

3. In the ^1H NMR spectra the δCHN and δOH signals appear at 8.50—8.80 and 13.00—13.80 ppm, respectively. The molecules exist predominantly in the enol-imine form; in the presence of the keto-amine form the splitting of the δCHN signal and a significant change of the aromatic proton signals may be expected. For IV and V the δCHN signals are doublets, due probably to coupling with the 6—H proton. The two δOH signals of IV and VI are well separated.

The fact that the quinoid form cannot be proved by infrared and ^1H NMR methods does not totally exclude its presence, because the solvents used in the above-mentioned methods do not favour the formation of this structure.

References

[1] *Ebara, N.:* Bull. Chem. Soc. Japan, **33**, 534 (1960).
[2] *Minkin, V. I. et al.:* Dokl. Akad. Nauk, SSSR, **145**, 336 (1962).
[3] *Brocklehurst, P.:* Tetrahedron, **18**, 299 (1962).
[4] *Jaffe, H. H., S. J. Yeh, R. W. Gardner:* J. Mol. Spectr., **2**, 120 (1958).
[5] *Cohen, M. D., S. Flavian:* J. Chem. Soc., B, 321 (1967).
[6] *Claude, O., P. Rumpf:* Bull. Chem. Soc. France, **18**, 342 (1951).
[7] *Cohen, M. D., G. M. J. Schmidt:* J. Phys. Chem., **66**, 2442 (1963).
[8] *Cohen, M. D. et al.:* J. Chem. Soc., 2041, 2051 (1964).
[9] *Minkin, V. I. et al.:* Tetrahedron, **23**, 3651 (1967).
[10] *Minkin, V. I. et al.:* Zh. Obsch. Khim., **35**, 397 (1965).
[11] *Minkin, V. I., E. A. Medyantzeva:* Zh. Obsch. Khim., **35**, 1956 (1965).
[12] *Gray, G. W.:* Molecular Structure and the Properties of Liquid Crystals., Chap. 10, Acad. Press, N. Y. 1962.
[13] *Nagy P.:* Magyar Kémiai Folyóirat, **72**, 108 (1966).
[14] *Ledbetter, J. W.:* J. Phys. Chem., **70**, 2245 (1966).
[15] *Dudek, G. O., E. P. Dudek:* J. Amer. Chem. Soc., **86**, 4283 (1964).
[16] *Császár, J., J. Balog, A. Makáry:* Acta Phys. et Chem. Szeged, **24**, 473 (1978).

СПЕКТРЫ ШИФ—ОСНОВАНИЙ ТИПА X,Y-БЕНЗИЛИДЕНО-4-Z-АНИЛИНА

Й. Часар

Изучены УФ, ИК и ^1H ЯМР спектры ароматических Шиф-оснований типа X,Y-бензилидено-4-Z-анилина

(X = H, 5-NO_2, 5-Br, Y = 2-OH, 2-NH_2, Z = OH, NO_2).

Сделаны заключения относительно образования кето-аминной таутомерной формы при определяющей роли заместителей в анилине с учетом влияния заместителей в альдегиде на интенсивность полос видимого спектра.

LIGAND SUBSTITUTION AND COMPLEX STRUCTURE, XV. MAGNETIC AND SPECTRAL STUDIES OF $Ni[Hsal\text{-}pX.Ph]_2$ TYPE COMPLEXES

By

J. CSÁSZÁR

Institute of General and Physical Chemistry, Attila József University, Szeged, Hungary

(Received 6th July, 1979)

A study was made on the magnetic and spectral behaviour of $Ni[Hsal\text{-}pX.Ph]_2$ ($X=N(CH_3)_2$, OH, OCH_3, OC_2H_5, CH_3, C_2H_5, $NHCOCH_3$, H, F, Cl, Br, I, CN, NO_2) type complexes and conclusions were drawn regarding their structures in the solid phase and in solution.

It is well known [1—5] that the composition, physicochemical properties and stereochemistry of metal chelates are decisively influenced by the ligand substituents. The stereochemical forms of these complexes are labile, so very often the molecular configurations in solution are different from those in the solid state, and conformational equilibria exist between different forms. This structural lability implies that the free-energy difference between the different stereochemical forms is usually small. In the present work we discuss the magnetism and spectra of the following chelate complexes (structure I).

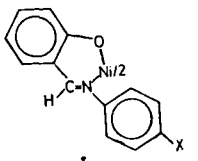

I.

No.	X	No.	X
I.	$N(CH_3)_2$	VIII.	H
II.	OH	IX.	F
III.	OCH_3	X.	Cl
IV.	OC_2H_5	XI.	Br
V.	CH_3	XII.	I
VI.	C_2H_5	XIII.	CN
VII.	$NHCOCH_3$	XIV.	NO_2

Experimental

The complexes were prepared by the known method of the reaction of bis-(salicylaldehyde)nickel(II).2 H_2O with the aniline derivatives in acetone solution; the products were purified by recrystallization from chloroform. The compositions were checked by C, N and H analyses.

The magnetic moments were determined at room temperature by the Gouy method; $Hg[Co(NCS)_4]$ was used for the calibration. The diamagnetic correction was calculated from literature data [6].

Reflectance and solution spectra were measured with a Beckman DU and a SPECORD UV—VIS spectrophotometer, respectively; analytical grade MgO and appropriately purified [7] solvents were used as references.

Results

Magnetic moments, stereochemistry and spectral data are summarized in Table I; the visible spectra of VII and XIII are illustrated in Fig. 1 and Fig. 2.

In the solid state VII and VIII ($\sigma=0$) are diamagnetic, while the other compounds show paramagnetism with about 2.80—3.32 BM; these values are in good agreement with the data of HOLM [3]. In the case of II the low magnetism

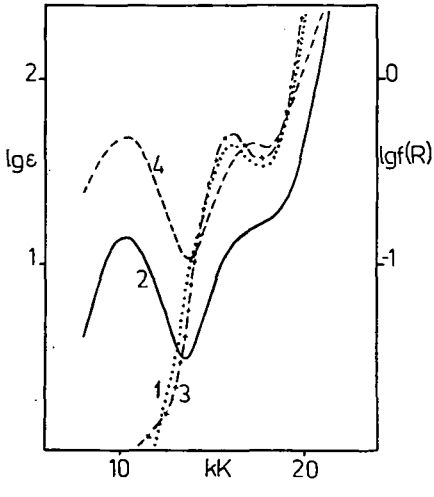

Fig. 1. Spectra of $Ni[Hsal\text{-}p\text{-}NHCOCH_3.Ph]_2$. 1: in $CHCl_3$; 2: in C_5H_5N; 3: reflection spectrum; 4: reflection spectrum of the bis-pyridine adduct.

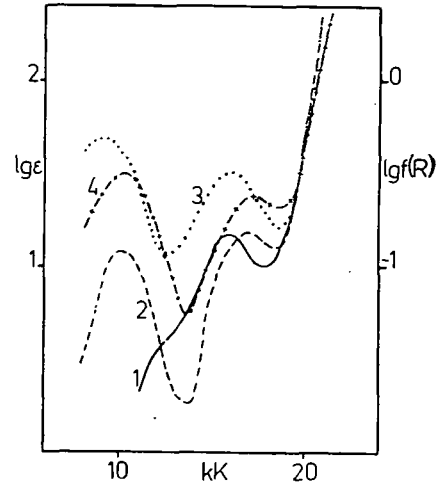

Fig. 2. Spectra of $Ni[Hsal\text{-}p\text{-}CN.Ph]_2$. 1: in $CHCl_3$; 2: in C_5H_5N; 3: reflection spectrum; 4: reflection spectrum of the bis-pyridine adduct.

(2.42 BM) can be interpreted in terms of a polynuclear structure; this is supported by the reflectance spectral studies.

In chloroform solution all the compounds studied are paramagnetic; with the exceptions of VII and VIII, the solution magnetism is lower than the solid-phase

paramagnetism; these complexes show "anomalous magnetic behaviour". This fact shows that, at room temperature, about 69—88% of all the species are paramagnetic, with a triplet ground state.

On the basis of the magnetic moments, conclusions can be drawn regarding the stereochemistry of the chelates. In the crystalline state VII and VIII have a square-planar arrangement. The other compounds probably have a strongly distorted octahedral structure; II is polynuclear with nickel-oxygen interaction (see Table I).

The systems formed in solution are very complicated. In noncoordinating solvents (*e.g.* $CHCl_3$) three species must be taken into account: a) diamagnetic, square-planar; b) paramagnetic, distorted tetrahedral molecules; and c) paramagnetic associates. These three species give rise to the following concentration and temperature-dependent conformational equilibrium [3, 4, 8]:

$$\text{associated form} \leftrightarrow \text{square-planar form} \leftrightarrow \text{tetrahedral form}$$

This equilibrium is displaced completely towards the right with increasing temperature or with decreasing concentration. The strong temperature-dependences of the solution moments and the spectral changes confirm the presence of the species presented in Table I.

The pyridine solutions of the chelates and the solid bis-pyridine adducts have very similar magnetic moments, of about 3.10—3.25 BM; these values correspond to the moments measured for six-coordinated nickel(II) complexes.

Similar conclusions can be drawn on the basis of the spectral investigations.

The reflectance spectra of VII and VIII are characteristic of square-planar nickel(II) complexes; the bands at about 16 kK are attributed to the $^1B_{1g} \leftarrow {}^1A_g$ transitions [9]. The other d—d bands are covered by the absorption of the ligand itself. For the other compounds two medium-intensity bands appear at 9—10 and 16—17 kK, which can be assigned to the NiO_2N_4 chromophores.

All the complexes studied have a medium-intensity band at *ca.* 16—17 kK in chloroform solution; these spectra indicate predominantly a square-planar arrangement. The intensities of these bands change with temperature to only a small extent; a similar change can be observed for the 10 kK bands. The changes of the intensity are difficult to interpret, because the characteristic bands of the square-planar and the distorted tetrahedral species, as well as those of the distorted tetrahedral form and the associates, appear in similar spectral regions.

The absorption spectra of the complexes in pyridine solution are very similar to the reflection spectra of the corresponding $Ni(SB)_2.py_2$ adducts. The bands measured at $\sim$10 (ν_1^*) and $\sim$17 (ν_2^*) kK can be assigned to the $^3B_{1g} \leftarrow {}^3B_{3g}$ and $^3B_{2g} \leftarrow {}^3B_{3g}$ transitions, respectively. The intensities of ν_1^* and ν_2^* show a strong temperature-dependence. With increasing temperature the equilibrium

$$Ni(SB)_2 + 2py \rightleftharpoons Ni(SB)_2 \cdot py_2$$

shifts toward to the left, and the intensity of ν_1^* decreases while that of ν_2^* remains nearly unchanged. The temperature effect is enhanced if the spectra are examined in an indifferent solvent containing pyridine or pyridine derivatives. The ν_2^* band of the adducts and the ν_1^* band of the planar species can be found at very near energies.

Table I

Magnetic and Spectral Data on the Complexes

No.	μ_{BM}		p %[2*]	Stereochem.[3*]		ν^{4*}_{max}			ν^{4*}_{max}			
	solid	$CHCl_3$ soln.		solid	$CHCl_3$ soln.	refl.		$CHCl_3$ soln.	refl. of py-add.		py soln. of chelate	
I	3.28	3.06	86	q0	P+dT+A	10.20;	16.90	16.85	~16.50;	10.22	10.30	
II	2.42	*	?	q0+A	?	~9.00;	~17.00	~16.90	18.00[5*]		10.50;	16.00
III	3.28	3.02	84	q0	P+dT+A	10.60;	16.80	16.70	10.30;	17.10	10.10;	~16.50
IV	3.24	3.10	88	q0	P+dT+A	10.40;	16.60	16.60	10.40;	17.30	10.20;	17.20
V	3.30	3.03	84	q0	P+dT+A	10.00;	16.90	16.40	10.08;	17.00	10.20;	17.20
VI	3.25	2.97	81	q0	P+dT+A	10.00;	16.80	16.60	10.00;	17.00	10.00;	17.10
VII	0	2.75	69	P	P+A	16,00		16.10	10.20;	17.10	10.20;	17.20
VIII	0	2.96	80	P	P+A	16,30		16.35	10.20;	17.30	10.20;	17.20
IX	3.27	2.93	79	q0	P+dT+A	9.90;	16.30	16.40	10.50;	17.30	10.22;	17.10
X	3.32	2.95	80	q0	P+dT+A	9.80;	17.00	16.10	10.30;	17.10	10.20;	17.30
XI	2.80	2.88	76	q0	P+dT+A	9.70;	16.60	16.20	10.35;	17.10	10.15;	17.20
XII	3.30	3.07	87	q0	P+dT+A	10.20;	16.70	16.30	10.40;	17.10	10.40;	16.90
XIII	3.18	3.04	85	q0	P+dT+A	~9.30;	16.10	15.80	10.20;	17.20	10.05;	17.00
XIV	3.26	*	?	q0	?	9.40;	16.40	~16.60	10.80;	17.70	10.30;	~16.80

* insoluble;
[2*] $p\% = 100\,(\mu^2_{BM}/3{,}3^2)$;
[3*] P: square-planar, A: associates, q0: quasi-octahedral, dT: distorted tetrahedral;
[4*] in kK;
[5*] broad, indistinct band

From these data a great decrease of symmetry can be deduced; this is also suggested by the very high values of the RACAH parameters; the octahedral energy functions cannot be used.

The chemical behaviour and stereochemistry of the nickel(II) chelates are governed by the electronic (electronegativity of Ni(II) and L; ligand field strength; nature of Ni—L bond) and steric factors (shape of ligand, crystal packing effect). In the case of the complexes studied in this work, the nature and position of X are the determining factors in the stereochemistry of the complexes, probably only through an electronic effect.

References

[1] *Yamada, S. et al.:* Coord. Chem. Rev., **3**, 247 (1968); **1**, 415 (1966) (and references therein).
[2] *Yamada, S. et al.:* Bull. Chem. Soc. Japan, **36**, 755 (1963); **40**, 1864 (1967); **39**, 994 (1966).
[3] *Holm, R. H.:* Advances in the Chemistry of the Coordination Compounds., Ed. S. Kirschner, McMillan Co., New York, 1961.
[4] *Sacconi, L.:* Transition Metal Chemistry. A Series of Advences., Ed. R. L. Carlin; M. Dekker Inc., New York, 1968. p. 341 (and references therein).
[5] *Császár, J., et al.:* Acta Chim. Hung., **86**, 9 (1975); **78**, 17 (1973); **86**, 3 (1975).
[6] *Lewis, L., R. G. Wilkins:* Modern Coordination Chemistry., Intersci. Publ. Co., New York, 1960.
[7] Technique of Organic Chemistry, VII. Organic Solvents, 2nd Ed., Intersci. Publ. Co., No. 4., 1955.
[8] *Sacconi, L., M. Ciampolini:* J. Amer. Chem. Soc., **85**, 1750 (1963).
[9] *Maki, G.:* J. Chem. Phys., **28**, 651 (1958); **29**, 1129 (1959).
[10] *Kannan, T. S., A. Chakravorty:* Inorg. Chem., **9**, 1153 (1970).

ИССЛЕДОВАНИЯ ВЛИЯНИЯ ЗАМЕСТИТЕЛЕЙ В ЛИГАНДАХ НА СТРУКТУРУ КОМПЛЕКСОВ, XV. ИЗУЧЕНИЕ МАГНИТНЫХ И СПЕКТРАЛЬНЫХ СВОЙСТВ КОМПЛЕКСОВ ТИПА $Ni[Hsal\text{-}pX.Ph]_2$

Й. Часар

Изучены магнитные и спектральные свойства комплексов $Ni[Hsal\text{-}pX.Ph]_2$ ($X = N(CH_3)_2$, OH, OCH_3, OC_2H_5, CH_3, C_2H_5, $NHCOCH_3$, H, F, Cl, Br, I, CN, NO_2) и сделаны заключения относительно их структуры в твердой фазе и растворах.

KINETICS OF THE THERMAL DECOMPOSITION OF AZOISOPROPANE

By

L. SZIROVICZA

Institute of General and Physical Chemistry,
Attila József University, Szeged, Hungary

(Received 26th September, 1979)

The gas-phase pyrolysis of azoisopropane (*iso*-C_3H_7-N=N-*iso*-C_3H_7; AIP) was studied at 494—546 K in a static system. Arrhenius equations were suggested for the following reactions:

$$\text{AIP} + \textit{iso}\text{-}C_3H_7 \rightarrow C_3H_8 + C_3H_6{\cdots}N{\cdots}N\text{-}\textit{iso}\text{-}C_3H_7 \qquad (1)$$

$$\log (k_1/\text{dm}^3\,\text{mol}^{-1}\text{s}^{-1}) = (6.7 \pm 0.2) - (27 \pm 2\ \text{kJ mol}^{-1})/2.3\ RT$$

$$\text{AIP} \rightarrow N_2 + 2\ \textit{iso}\text{-}C_3H_7 \qquad (i)$$

$$\log (k_i/\text{s}^{-1}) = (14.6 \pm 0.4) - (178 \pm 4\ \text{kJ mol}^{-1})/2.3\ RT$$

The disproportionation and combination rate constant ratio for the isopropyl radical was found to be $k_d/k_c = 0.8 \pm 0.1$. Results are discussed and compared with literature data.

Introduction

Azo compounds are good sources of radicals in gas reactions and their decompositions have been the subject of kinetic studies [1—4].

There have been several studies on the thermal decomposition of azoisopropane (hereafter AIP) [1, 5—7], although the quantitative results available so far differ somewhat.

Recent thermochemical data on AIP [8] suggest new investigations for the pyrolysis of AIP. The present work was undertaken for two purposes:

(a) measuring the kinetics of the hydrogen-abstraction reaction of *iso*-C_3H_7 from AIP; and

(b) measuring the kinetics of the unimolecular decomposition of AIP.

Experimental

The static reaction system and the analytical methods applied on the gas-chromatograph were described earlier [9, 10].

Azoisopropane was prepared by the RENAUD—LEITCH method [11] and purified by intensive washing with water and low-temperature distillation. It was 99.8% pure, containing acetone and diethyl ether as impurities.

Results and Discussion

The thermal decomposition of AIP was studied in a static reaction system in the range 494—546 K at pressures of about 6 kN m^{-2}. The following products were identified by gas-chromatography: nitrogen, propane, propylene, 2,3-dimethyl-butane (DMB), 4-methyl-pentene-1 (4 MPl), as well as C_2H_4 and CH_4 at higher temperatures.

A typical product composition is shown in Table I. Some polymer formation was also observed in the reactions.

Table I

Products of AIP decomposition
$T=500$ K; $[AIP]_0=4.53\cdot10^{-4}$ mol dm^{-3};
Conversion 10%

Products	%
N_2	40.6
C_3H_8	23.6
DMB	21.7
C_3H_6	14.0
4 MPl	0.1

The formation of the products can be understood from the reaction shown below:

$$AIP \rightarrow 2\ iso\text{-}C_3H_7 + N_2 \qquad (i)$$

Reaction (i) is the source of N_2 and *iso*-C_3H_7 radicals, which latter can react with each other in combination and disproportionation reactions:

$$2\ iso\text{-}C_3H_7 \rightarrow C_6H_{14}\ (DMB) \qquad (c)$$

$$2\ iso\text{-}C_3H_7 \rightarrow C_3H_8 + C_3H_6 \qquad (d)$$

It can be seen in Table II that the rate of formation of C_3H_8 ($R_{C_3H_8}$) is higher than that of propylene ($R_{C_3H_6}$). This means that, besides reaction (d), another source of propane formation should exist. This may be the hydrogen-abstraction reaction of *iso*-C_3H_7:

$$iso\text{-}C_3H_7 + AIP \rightarrow C_3H_8 + C_3H_6 \cdots N \cdots N\text{-}iso\text{-}C_3H_7 \qquad (1)$$

4-Methyl-pentene-1 can be formed by the following reactions:

$$iso\text{-}C_3H_7 + C_3H_6 \rightarrow C_3H_8 + C_3H_5\ (allyl) \qquad (2)$$

$$iso\text{-}C_3H_7 + C_3H_5 \rightarrow C_6H_{12}\ (4MPl) \qquad (3)$$

Reactions (2) and (3) were proved by decomposition of AIP in an excess of C_3H_6. It was observed that the rate of formation of 4MPl was proportional to the concentration of propylene.

In this study the rate constants of reactions (i) and (1) were determined. The procedure for the determinations is discussed below.

(a) *Rate Constant of Reaction (1)*

The rate of reaction (1) can be given by Eqn. (I):

$$R_{C_3H_8} - R_{C_3H_6} = k_1[iso\text{-}C_3H_7][AIP]_0 \qquad (I)$$

$R_{C_3H_8}$ and $R_{C_3H_6}$ are the initial rates of formation of C_3H_8 and C_3H_6, respectively; $[AIP]_0$ and k_1 are the initial concentration of AIP and the rate constant of reaction (1), respectively.

The rate of reaction (c) is given by Eqn. (II):

$$R_{DMB} = k_c[iso\text{-}C_3H_7]^2 \qquad (II)$$

where R_{DMB} and k_c are the initial rate of formation of DMB and the rate constant of isopropyl combination, respectively. Equation (III) can be obtained by substituting $[iso\text{-}C_3H_7]$ in Eqn. (I) by $R_{DMB}/k_c^{1/2}$ (originating from Eqn. (II)) and dividing by R_{DMB}:

$$\frac{R_{C_3H_8} - R_{C_3H_6}}{R_{DMB}} = \frac{k_1}{k_c^{1/2}} \frac{[AIP]_0}{R_{DMB}^{1/2}} \qquad (III)$$

If the reaction mechanism is correct, the ratio $(R_{C_3H_8} - R_{C_3H_6})/R_{DMB}$ should be linear as a function of $[AIP]_0/R_{DMB}^{1/2}$. The slope of the straight line is $k_1/k_c^{1/2}$.

The experimental results calculated with Eqn. (III) are shown in Fig. 1. Experimental data are collected in Table II. Ratios of k_d/k_c, together with $k_1/k_c^{1/2}$, are also shown in Table II. The ratios of $k_1/k_c^{1/2}$ were calculated with Eqn. (IV):

$$\frac{k_1}{k_c^{1/2}} = \frac{R_{C_3H_8} - R_{C_3H_6}}{R_{DMB}^{1/2}[AIP]_0} \qquad (IV)$$

The experimental results shown in Fig. 1 support reaction steps (c), (d) and (1).

From the temperature-dependence of $k_1/k_c^{1/2}$ shown in Table II, Arrhenius parameters can be calculated. The temperature-dependence of $k_1/k_c^{1/2}$ is shown in Fig. 2.

Figure 2 also depicts results of DURHAM AND STEACIE [12] and RIEM AND KUTSCHKE [13], measured in the photolysis of AIP. Recent results are in agreement with the literature data. The combination of the recent results and the literature data leads to the following equation:

$$\log(k_1/k_c^{1/2}\ dm^{3/2}mol^{-1/2}s^{-1/2}) = (1.9 \pm 0.2) - (27 \pm 2\ kJ\ mol^{-1})/2.3\ RT$$

Taking the value of $k_c = 10^{9.5}\ dm^3\ mol^{-1}\ s^{-1}$ from the paper of GOLDEN *et al.* [14], k_1 can be given as follows:

$$\log(k_1/dm^3mol^{-1}s^{-1}) = (6.7 \pm 0.2) - (27 \pm 2\ kJ\ mol^{-1})/2.3\ RT.$$

This value is compared with the literature data in Table III.

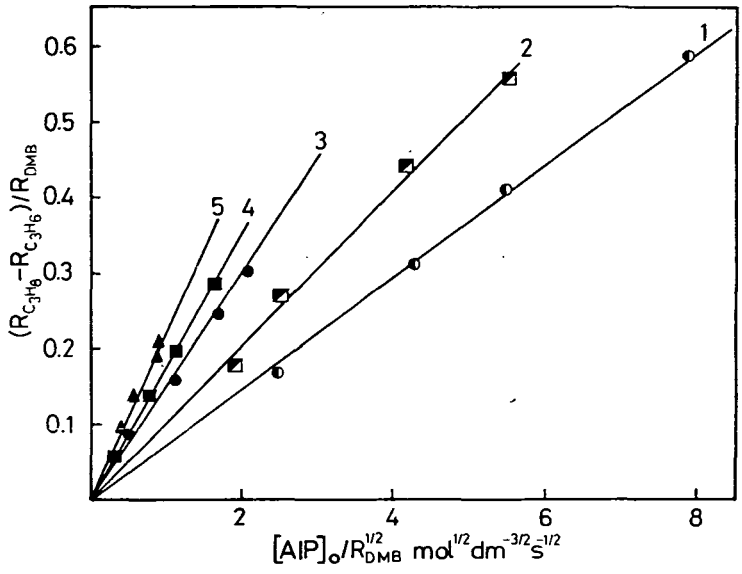

Fig. 1. $(R_{C_3H_8}-R_{C_3H_6})/R_{DMB}$ as a function of $[AIP]_0/R_{DMB}^{1/2}$. **1.** 494; **2.** 500; **3.** 523; **4.** 531; **5.** 546 K

Table II

Kinetic data for the determination of $k_1/k_c^{1/2}$ *and* k_d/k_c

T/K	$R_{C_3H_8}$	$R_{C_3H_6}$	R_{DMB}	$10^4[AIP]_0$	$k_1/k_c^{1/2}$	k_d/k_c
	10^8 R/mol dm^{-3} s^{-1}			mol dm^{-3}		
494	0.217	0.179	0.218	1.12	0.071	0.82
494	0.478	0.363	0.462	3.31	0.073	0.78
494	1.27	0.822	1.19	6.02	0.068	0.69
494	3.05	1.62	2.42	12.3	0.074	0.71
500	0.382	0.321	0.361	1.06	0.097	0.78
500	0.789	0.586	0.781	2.26	0.10	0.75
500	2.11	1.26	1.94	5.67	0.11	0.65
500	5.30	2.86	4.05	12.0	0.10	0.70
523	2.83	2.44	3.54	1.26	0.16	0.84
523	7.86	6.56	7.91	3.14	0.15	0.89
523	18.5	15.1	18.7	7.45	0.14	0.80
523	29.1	20.4	28.2	11.2	0.15	0.60
531	4.84	4.48	4.04	1.01	0.16	0.69
531	15.2	13.3	12.5	2.91	0.18	0.81
531	28.4	23.3	25.3	5.52	0.18	0.92
531	64.7	48.1	57.3	12.2	0.18	0.84
546	45.4	40.8	45.9	3.01	0.22	0.89
546	86.3	74.2	80.5	5.45	0.25	0.92
546	16.9	140	163	10.8	0.22	0.86
546	182	144	180	11.8	0.23	0.80

Dimensions of $k_1/k_c^{1/2}$ are dm$^{3/2}$ mol$^{-1/2}$ s$^{-1/2}$.

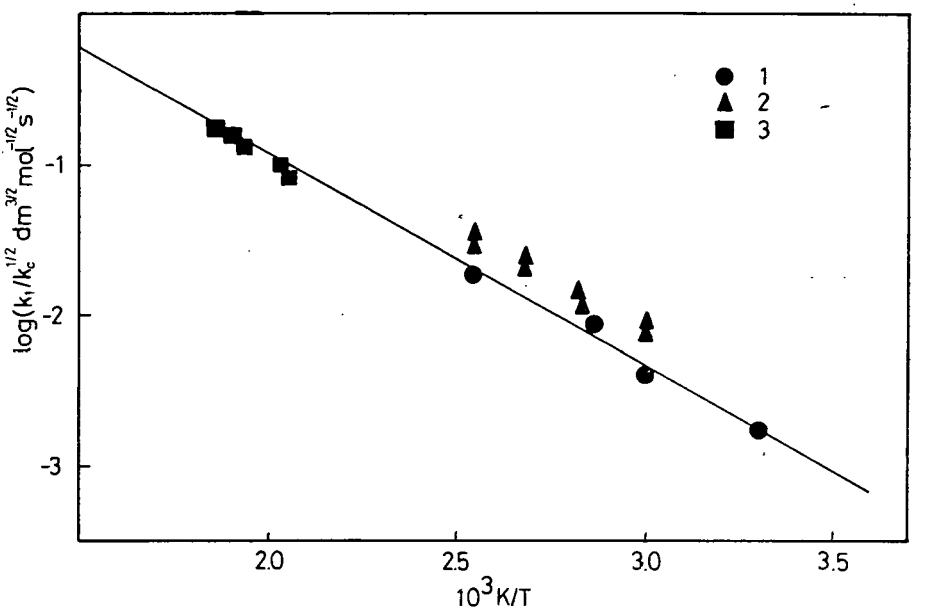

Fig. 2. Temperature-dependence of $k_1/k_c^{1/2}$. (1) Data of DURHAM and STEACIE [12]; (2) data of RIEM and KUTSCHKE [13]; (3) this work

Table III

Arrhenius parameters for AIP + *iso*-C_3H_7 → $C_3H_8 + C_3H_6$⋯N⋯N-*iso*-C_3H_7 (1)

$\log \frac{A}{dm^3\ mol^{-1}\ s^{-1}}$	$\frac{E}{kJ\ mol^{-1}}$	T/K	$\log \frac{k}{dm^3\ mol^{-1}\ s^{-1}}$ 500 K	Ref.
6.7	27	303—393	3.88	[12]
6.8	28	308—400	3.87	[13]
7.3	30	300—433	4.17	[14]
6.7±0.2	27±2	494—546	3.88	this work

(b) *Rate Constant of Reaction (i)*

Rate constants of reaction (i) were calculated from the rate of consumption of AIP. Reaction (1) was taken into account by correction, as reaction (1) is also a route of AIP consumption in the decomposition.

The consumption of AIP in the decomposition reactions obeys a first-order rate equation, as shown in Fig. 3. The slopes of the lines give the rate constant of AIP consumption (k_{AIP}).

The temperature-dependence of k_{AIP} was determined and the results are shown in Fig. 4. From this dependence the value of k_{AIP} can be given in the following Arrhenius equation:

$$\log(k_{AIP}/s^{-1}) = (15.4 \pm 0.2) - (186 \pm 2\ kJ\ mol^{-1})/2.3\ RT.$$

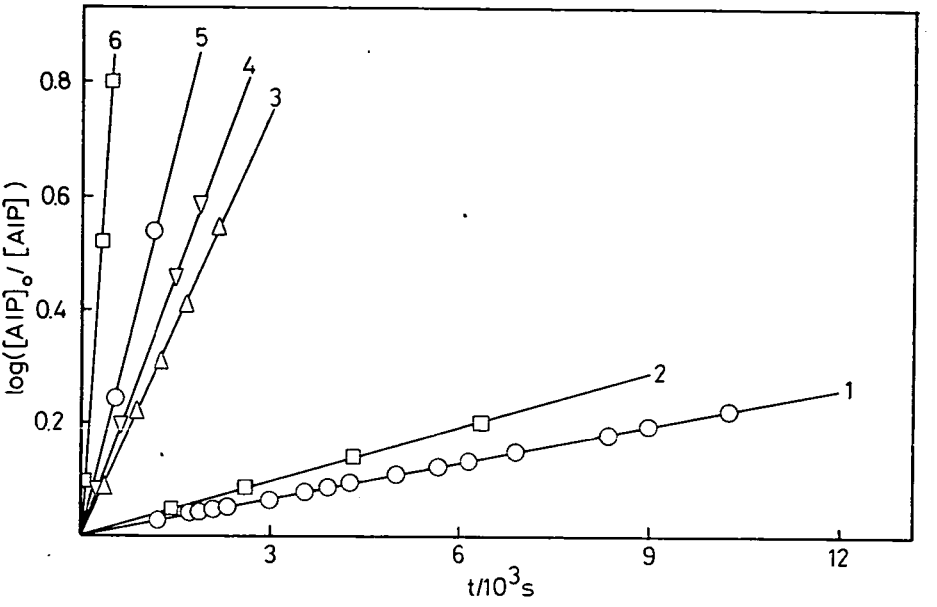

Fig. 3. Consumption of AIP in pyrolytic reactions at different temperatures. (1) 494; (2) 500; (3) 513; (4) 523; (5) 531; (6) 546 K

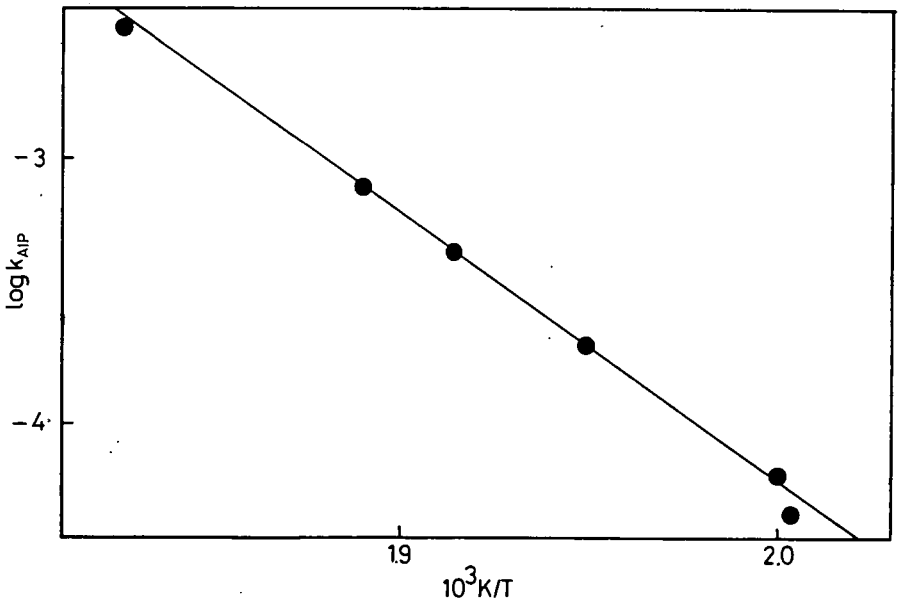

Fig. 4. Temperature-dependence of k_{AIP}

This rate constant is characteristic for the consumption of AIP in the decomposition reaction, which consists of two main processes, reactions (i) and (1).

The evaluation of the rate constant of reaction (i) is based on considerations in which the role of reaction (1) is estimated. From the experimental data the role of reaction (1) in the consumption of AIP can be given by the following formula:

$$x\% = \left(\frac{100\,R_1}{R_{AIP}}\right)_{t=0} \qquad (V)$$

The results of calculations are shown in Table IV.

Table IV

The role of the reaction AIP + *iso*-C_3H_7 → $C_3H_8 + C_3H_6{\cdots}N{\cdots}N$-*iso*-$C_3H_7$ (1) *in* AIP *decomposition*

T/K	10^4 [AIP]$_0$ / mol dm^{-3}	$10^8 R_{DMB}$	$10^8 R_{AIP}$	$10^9 R_1$	x %
		R/mol dm^{-3} s^{-1}			
494	3.24	0.61	1.29	2.94	22.8
500	3.20	1.02	2.21	4.07	18.4
523	3.06	7.58	15.3	14.1	9.2
531	3.01	12.5	28.9	18.9	6.5
546	2.93	44.0	90.2	42.0	4.6

From the known role of reaction (1), the value of k_i can be calculated with the following expression:

$$k_i = \frac{2.3}{t} \log \frac{[AIP]_0}{[AIP] + ([AIP]_0 - [AIP])(R_1)_0/(R_{AIP})_0}, \qquad (VI)$$

where $[AIP]_0$ and [AIP] are concentrations at zero time and time t, respectively; $(R_1)_0$ is the initial rate of reaction (1); and $(R_{AIP})_0$ is the initial rate of consumption of AIP.

The temperature-dependence of k_i can be given by the following Arrhenius equation:

$$\log(k_i/s^{-1}) = (14.6 \pm 0.4) - (178 \pm 4\ \text{kJ mol}^{-1})/2.3\ RT. \qquad (VI)$$

These Arrhenius parameters are compared with the literature data in Table V.

The Arrhenius parameters reported here are very different from those of BENSON and O'NEAL [1] and GOLDEN et al. [7].

BENSON and O'NEAL suggested an activation energy from thermochemical calculations. Their A factor was calculated from the experimental rate constant of RAMSPERGER [5] with their estimated activation energy. Heats of formation necessary for the calculation of the activation energy are shown in Table VI. BENSON and O'NEAL used thermochemical data of AIP calculated from the heat of combustion of AIP [15].

Recent data of ENGEL *et al.* [8] for the heat of combustion of AIP suggest that earlier data are probably erroneous. Thermochemical data on AIP were re-

Table V

Arrhenius parameters of reaction (i); AIP → N_2 + 2 iso-C_3H_7 (i)

log (A/s^{-1})	E / kJ mol^{-1}	−log (k/s^{-1}) T = 494 K	T/K	Ref.
13.75	171	4.34	523—563	[5]
13.68	171	4.41	503—673	[6]
16.4	198	4.54	—	[1]
16.6*	200*	4.55*		
18.1	213	4.43	625—854	[7]
13.7	170	4.28		
14.6±0.4	178±4	4.33	494—546	this work

* Preferred by the authors.

Table VI

Heats of formation for the calculation of the activation energy of reaction (i)

	AIP	iso-C_3H_7	iso-C_3H_7—N=N
ΔH_f^0 298 kJ mol^{-1}	87.5*	73.3	212.2*
	36.0**	73.3	140.7**

* Calculated from the data of Coates and Sutton [15].
** Calculated from the data of Engel *et al.* [8].

calculated in this work from the heat of combustion of AIP determined by ENGEL *et al.* [8].

Estimation of the activation energy of reaction (i) using the new thermochemical data results in 178 kJ mol^{-1}, in good agreement with the experimental data reported here.

Rate constants for reaction (i) determined in different laboratories are very similar. This means that the thermochemical calculations also make the recent value of the A factor probably correct.

References

[1] *Benson, S. W., H. E. O'Neal:* Kinetic Data on Gas Phase Unimolecular Reaction NSRDS-NBS **21**, 31 1970.
[2] *Strausz, O. P., J. W. Lown, H. E. Gunning:* Comprehensive Chemical Kinetics, 5. eds. C. H. Bamford and C. F. H. Tipper, Elsevier, New York, 1972.
[3] *Ramsperger, H. C.:* J. Amer. Chem. Soc. **51**, 2134 (1929).
[4] *Crawford, R. J., K. Tagaki:* J. Amer. Chem. Soc. **94**, 7406 (1972).
[5] *Ramsperger, H. C.:* J. Amer. Chem. Soc. **50**, 714 (1928).
[6] *Geiseler, G., J. Hoffman:* Z. Phys. Chem. N. F. **57**, 3 (1968).
[7] *Perona, M. J., P. C. Beadle, D. M. Golden:* Int. J. Chem. Kinet. **5**, 495 (1973).
[8] *Engel, P. S., J. L. Wood, J. P. Sweet, J. L. Margrawe:* J. Amer. Chem. Soc. **96**, 2381 (1974).
[9] *Szirovicza, L., F. Márta:* Int. J. Chem. Kinet. **8**, 897 (1976).
[10] *Szirovicza, L., F. Márta:* React. Kinet. Catal. Lett. **2**, 383 (1975).

[11] *Renaud, R., L. C. Leitch:* Canad. J. Chem. **32**, 545 (1954).
[12] *Durham, R. W., E. W. R. Steacie:* Canad. J. Chem. **31**, 377 (1953).
[13] *Riem, R. H., K. O. Kutschke:* Canad. J. Chem. **38**, 2332 (1960).
[14] *Berkley, R. E., G. N. C. Woodall, O. P. Strausz, H. E. Gunning:* Canad. J. Chem. **47**, 3305 (1969).
[15] *Coates, G. E., L. E. Sutton:* J. Chem. Soc. 1187 (1948).

КИНЕТИКА ТЕРМИЧЕСКОГО РАЗЛОЖЕНИЯ АЗОИЗОПРОПАНА

Л. Сировица

Изучен пиролиз в газовой фазе азоизопропана (изо-$C_3H_7N=N$-изо-C_3H_7, AIP) в статических условиях при температурах 494 и 546 К. Предложены уравнения Аррениуса для следующих реакций:

$$AIP + iso\text{-}C_3H_7 \rightarrow C_3H_8 + C_3H_6\text{-}N=N\text{-}iso\text{-}C_3H_7 \qquad (1)$$

$$\log(k_1/dm^3 mol^{-1} s^{-1}) = (6.7 \pm 0.2) - (27.2 \text{ kJ mol}^{-1})/2.3\ RT$$

$$AIP \rightarrow N_2 + iso\text{—}C_3H_7 \qquad (i)$$

$$\log(k_i/s^{-1}) = (14.6 \pm 0.4) - (178 \pm 4 \text{ kJ mol}^{-1})/2.3\ RT.$$

Найдено соотношение скоростей диспропорционирования и рекомбинации для изопропильного радикала равное $k_d/k_c = 0{,}80 \pm 0{,}1$. Обсуждены полученные результаты и сопоставлены с литературными данными.

HYSTERESIS AND INHIBITION EFFECT IN THE ANODIC OXIDATION OF *n*-PROPANOL

By

M. NOVÁK and CS. VISY

Institute of General and Physical Chemistry, Attila József University, Szeged, Hungary

(Received 12th October, 1979)

Experimental results are presented demonstrating a change in the inhibition effect of sorbate and its relation to the hysteresis of the current *vs.* potential curves.

In the study of the electrochemical transformation of organic compounds the determination of current *vs.* potential relationships is of essential importance. This determination generally encounters difficulties in the case of organic substances in comparison with inorganic redox systems, owing to the fact that in organic electrochemical processes the sorption of intermediates and/or products takes place, which can hardly be controlled. Therefore, the effect of sorption on the kinetics of reaction too can be determined only with difficulty. The experimental approach is not always clear enough to meet these difficulties and the reproducibility of the various results is not sufficient. In many cases it brings about such phenomena as the hysteresis of the potential *vs.* current curves, which unambiguously shows the need to get a better understanding of the change in the sorbed layer and its effect on the current-generating process.

As an example, in this paper some features which might lead to the hysteresis of current *vs.* potential curves are discussed for the anodic oxidation of *n*-propanol.

Experimental

The equipment was the same as previously described [1]. The working electrode was a platinum disc of 0.8 cm^2 geometric area, with a roughness factor of 4.75. It was rotated at 1000 rpm. Measurements were carried out in 1 mol dm^{-3} $HClO_4$ solution. As reference, a hydrogen electrode in the same solution was used. *n*-Propanol of analytical purity was distilled under a reduced nitrogen atmosphere and its purity was checked by gas-chromatography. Perchloric acid of Merck "Suprapur" grade was used. The triply-distilled water was redistilled pyrolytically [2] in a system attached to the cell.

The coverage values of the electrode were determined from the change in hydrogen capacity measured by means of cathodic potential sweeps at a rate of 20 Vs^{-1}.

Results and discussion

It is known that the strong sorption of primary alcohols is an irreversible process, and the sorbed species may not be considered as intermediates of the catalytic alcohol — aldehyde transformation [3—6].

The change in current with the growth in the amount of adsorbate can be illustrated by the current *vs.* coverage curve taken at $E=0.4$ V (Fig. 1). It can be seen that the kinetic pattern of the time-dependence of the current does not change even over a relatively large time range (curve *a*).

After a certain period of time (700 s), if the potential is switched from 0.4 V to more positive values, the resulting current *vs.* coverage relationships at the new potentials follow the pattern shown in Fig. 2. These curves reveal that the current is not only influenced by the change in the amount of sorbed species.

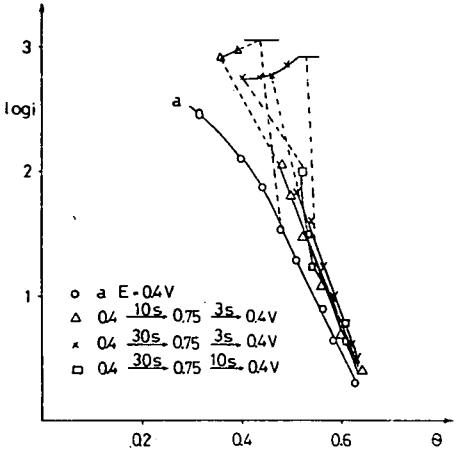

Fig. 1. Current *vs.* coverage relationships $a-E=0.4$ V
△, *x*, □-during the potential sequences given in the Figure

The situation is similar if the change in potential is the same, but the starting value of the coverage (θ°) is different before the potential step (Fig. 3). It can be seen that the current *vs.* coverage curves have two regions well distinguishable from each other. Those regions where the decrease in coverage occurs can not be considered as "stationary", although the current change in this period would imply so. These regions do not represent identical states, since at the same potential diffe-

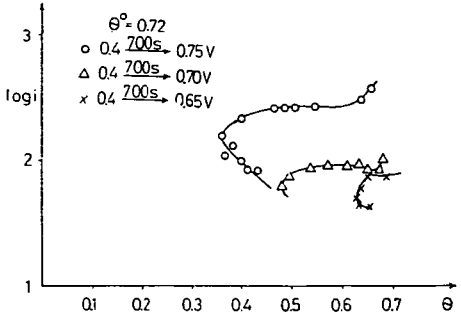

Fig. 2. Current *vs.* coverage curves after potential switchings from 0.4 V o — to 0.75 V, △ — to 0.70 V, X — to 0.65 V

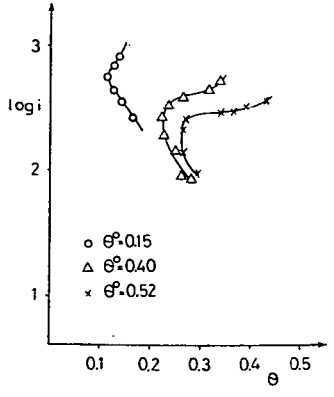

Fig. 3. Current *vs.* coverage relationships after potential switchings from 0.4 V to 0.75 V o — at $\theta^\circ=0.15$, △ — at $\theta^\circ=0.40$, X — at $\theta^\circ=0.52$

rent currents flow at the same value of the coverage, depending on the starting θ°.

On the basis of these observations, it is obvious that a polarisation curve recorded by means of the potential step method in the anodic direction, might show a hysteresis.

If the potential is switched back in the cathodic direction to 0.4 V, a similar difference arises (Fig. 1). At this potential no oxidation or reduction of sorbate takes place, as the charge required for its anodic oxidation is 1 *e/c* in the whole range of sorption [7]. It follows that coming back to 0.4 V provides a conservation of the previous state of the surface. Thus, the difference in current at the same coverage might be attributed to the different inhibiting effect on the catalytic alcohol — aldehyde reaction. As Fig. 1 shows, the inhibition is smaller than without potential change.

In Fig. 4, the results in Fig. 1 are presented as a function of time. It can be seen that the effect is not temporary, showing that the substance formed at 0.75 V is indeed not converted back into its initial state at 0.4 V.

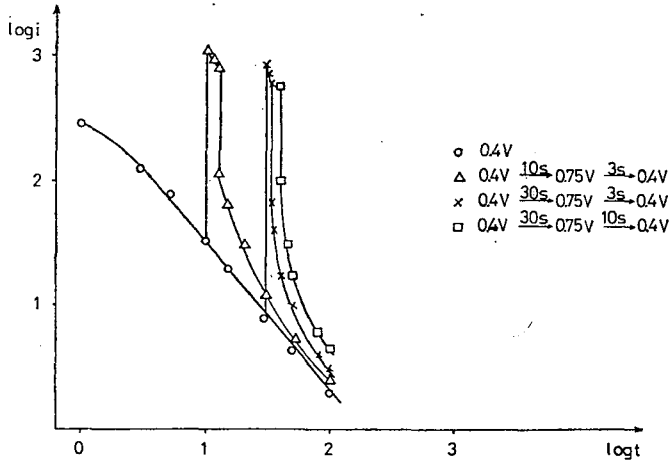

Fig. 4. Time-dependence of the current during the potential sequences given in the Figure

The reasons for the change in the inhibiting effect may be seen from measurements concerning the state of the sorbed species (Fig. 5). The oxidative desorption of the species at 0.75 V exhibits a constant charge/centre ratio, which is about 2—2.5 *e/c*.

On the basis of all these observations, it may be concluded that

(a) the layer produced by oxidizing the adsorbate formed at 0.4 V shows a lower inhibition effect at 0.4 V than the original state does;

(b) these changes in inhibition might lead to the hysteresis of the current *vs.* potential curves generally observed in the electrochemical investigation of organic compounds.

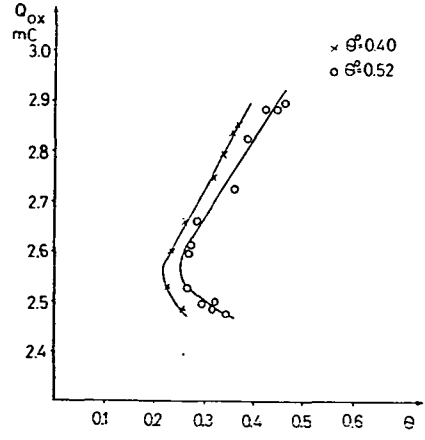

Fig. 5. Charges relating to the oxidation of sorbate as a function of covarage
X — $\theta°=0.40$, o — $\theta°=0.52$

References

[1] *Novák M., J. Lantos, F. Márta:* Acta Phys. et Chem. Szeged **18**, 147 (1972).
[2] *Conway B. E., H. Angerstein-Kozlowska, W. B. A. Sharp, E. E. Criddle:* Anal. Chem. **45**, 1331 (1973).
[3] *Rightmire R. A., R. L. Rowland, D. L. Boos, D. L. Beals:* J. Electrochem. Soc. **111**, 242 (1964).
[4] *Breiter B. W.:* Electrochemical Processes in Fuel Cells pp. 157—168 Springer-Verlag New York (1969).
[5] *Podlovchenko B. I., T. D. Glavisheva, V. F. Stenin, V. I. Levina:* Elektrokhimiya **9**, 1680 (1973).
[6] *Novák M., J. Lantos, F. Márta:* Acta Phys. et Chem. Szeged **18**, 151 (1972).
[7] *Novák, M.:* Dissertation (1973).

ГИСТЕРЕЗИС И ИНГИБИРУЮЩИЙ ЭФФЕКТ В АНОДНОМ ОКИСЛЕНИИ *н*-ПРОПАНОЛА

М. Новак и Ч. Виши

Представлены экспериментальные данные, показывающие изменения в ингибирующем действии сорбата и его связи с гистерезисом на кривых электрический ток — потенциал.

CHEMISTRY OF DIOLS AND CYCLIC ETHERS, XLV*. STERICALLY-HINDERED HYDROGEN-TRANSFER REACTIONS IN THE TRANSFORMATIONS OF 2-SUBSTITUTED 1,3-PROPANEDIOLS ON A COPPER CATALYST

By

Á. MOLNÁR and M. BARTÓK

Institute of Organic Chemistry, József Attila University, Szeged

(Received 28th September 1979)

During the transformations of 2-*n*-butyl-, 2-isopropyl-, 2-*tert*-butyl-, 2-cyclohexyl- and 2-phenyl-1,3-propanediol (I—V) on a copper catalyst, unsaturated aldehyde (and unsaturated alcohol) is also formed besides the saturated compounds. In the case of V, the formation of the unsaturated compounds is the characteristic reaction. The product distribution can be interpreted in terms of the steric and electronic properties of the substituents.

In the course of our earlier investigations in connection with the mechanisms of the metal-catalyzed reactions of 1,3-diols, it was established that in the presence of copper catalysts the 1,3-diols are transformed to oxo compounds containing the same number of carbon atoms, or are cleaved to give two molecules of oxo compound (Fig. 1) [1, 2].

The final step of the dehydration process occurs *via* a hydrogen-transfer reaction between the α,β-unsaturated oxo compounds formed and the starting diol. Our results relating to diols containing a cyclohexane skeleton [3] showed that

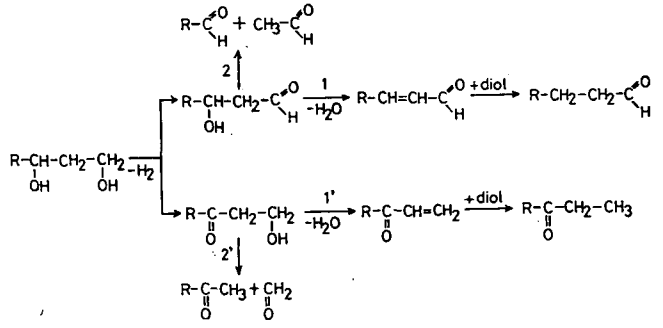

Fig. 1. Reaction pathways of 1,3-diols on copper catalysts.
Pathway 1 and 1′: dehydration Pathway 2 and 2′: dealdolization

* Part XLIV: *M. Bartók, Á. Molnár:* Acta Chim. (Budapest) **100**, 203 (1979).

with certain compounds [2-(1-hydroxyethyl)-1-cyclohexanol and 2-(1-hydroxybutyl)-1-cyclohexanol] this step is hindered, and thus the intermediate unsaturated oxo compounds also appear among the products.

In our recent investigations, some new examples of this hindered hydrogen-transfer have been found. The present paper describes results obtained during the transformations of some 2-substituted 1,3-propanediols (**I**—**V**).

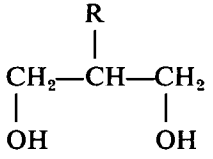

R =		
n-butyl	**I**
isopropyl	**II**
tert-butyl	**III**
cyclohexyl	**IV**
phenyl	**V**

Our preliminary studies with 2-isopropyl-1,3-propanediol (**II**) on three different copper catalysts (Cu/Al, Cu/SiO_2, and Cu) demonstrated the otherwise expected fact that the ratio of the saturated and unsaturated compounds depends on the nature of the catalyst (Table I). Accordingly, since our aim was to study how

Table I

Product distribution of 2-isopropyl-1,3-propanediol (**II**) *on copper catalysts (conversion 100%)*

Catalyst Temperature (C°)	Cu/Al 200	Cu/SiO_2 225	Cu 210
3-methylbutanal	8	15	19
2-isopropylpropenal	27	5	30
2,3-dimethylbutanal	37	50	21
3-methyl-1-butanol	6	13	13
2,3-dimethyl-1-butanol	12	14	6
2-isopropyl-2-propen-1-ol	5	—	8
unidentified	5	3	3

the properties of the substituent in position 2 (steric and electronic effects) influence the occurrence of the hydrogen-transfer, we carried out examinations on only a single catalyst. For this purpose the Cu catalyst prepared by reduction from CuO was selected, for, as indicated by the data in Table 1, this displayed the lowest activity in the hydrogen-transfer.

Experimental

Diols **I**, **II** and **IV** were prepared in a known way, by malonic ester synthesis and subsequent reduction with $Li[AlH_4]$. (**I**: b.p. 102—107 °C/5 torr; b.p. [4]: 105—108 °C/5 torr. **II**: b.p. 110—115 °C/5 torr; b.p. [5]: 114—116 °C/6 torr. **IV**: m.p. 93.5 °C; m.p. [5]: 94 °C.) In the preparation of **III**, the procedure described in [6] was followed, and the diol was then obtained by reduction (m.p. 59—61 °C; m.p. [5]: 61 °C). **V** was prepared by $Li[AlH_4]$ reduction of diethylphenylmalonate, obtained by the method described in [7] (m.p. 44—48 °C; m.p. [8]: 48.5—49 °C).

The experimental technique and the preparation of the Cu catalyst were reported earlier [2]. Products were identified with the aid of a GC technique and IR and NMR spectroscopy. The aldehydes were also identified via precipitation of (2,4-dinitrophenyl)-hydrazones.

The experimental results are summarized in Tables I—V.

Table II

Transformation of 2-n-butyl-1,3-propanediol (I) *on Cu catalyst at 250 °C (conversion 100%)*

Products	mol %
hexanal	22
2-methylhexanal	38
1-hexanol	16
2-methyl-1-hexanol	22
unidentified	2

Table III

Transformation of 2-tert-butyl-1,3-propanediol (III) *on Cu catalyst at 250 °C (conversion 100%)*

Products	mol %
3,3-dimethylbutanal	32
2-*tert*-butylpropenal	13
2,2,3-trimethylbutanal	14
3,3-dimethyl-1-butanol	34
2,3,3-trimethyl-1-butanol	2
2-*tert*-butyl-2-propen-1-ol	2
unidentified	3

Table IV

Transformation of 2-cychlohexyl-1,3-propanediol (IV) *on Cu catalyst at 270 °C (conversion 100%)*

Products	mol %
cychlohexylacetaldehyde	24
2-cyclohexylpropenal	26
2-cyclohexylpropanal	24
2-cyclohexylethanol	20
2-cyclohexyl-1-propanol	3
2-cyclohexyl-2-propen-1-ol	2
unidentified	1

Table V

Transformation of 2-phenyl-1,3-propanediol (V) *on Cu catalyst at 280 °C (conversion 100%)*

Products	mol %
phenylacetaldehyde	9
2-phenylpropenal	34
2-phenylpropanal	5
2-phenylethanol	21
2-phenyl-1-propanol	3
2-phenyl-2-propen-1-ol	22
unidentified	6

Discussion

The experimental results in Tables I—V, and the comprehensive data in Table VI, lead to the following findings:

Table VI

Product distributions of the transformations of compounds I—V *according to the reaction pathways*

Compound	Percentage amounts of products with the same number of carbon atoms as the diol			Percentage amounts of products obtained by dealdolization
	unsaturated	saturated	total	
I	—	60	60	38
II	38	27	65	32
III	15	16	31	66
IV	28	27	55	44
V	56	8	64	30

1. The straight-chain substituent (the *n*-butyl group in compound **I**) does not exert an inhibitory effect on hydrogen-transfer (Table II).

2. The branched-chain substituents (isopropyl and *tert*-butyl groups, **II** and **III**) impede hydrogen-transfer, and hence unsaturated aldehyde and (by reduction of this) unsaturated alcohol are also obtained in both cases (Tables I and III). In the case of **III**, the large bulk of the *tert*-butyl group not only affects this reaction, but at the same time increases the probability that the intermediate hydroxy-oxo compound will undergo further conversion by the other reaction pathway, *i.e.* dealdolization (Fig. 1, pathway 2 and 2'). The large extent of this side-reaction means that the effect of the *tert*-butyl group on hydrogen-transfer can not be examined, and accordingly can not be compared with that of the isopropyl group.

3. The cyclohexyl group influences hydrogen-transfer to a similar extent as do the branched-chain substituents (Table IV).

4. In the transformation of the diol (V) containing the phenyl group, strikingly large amounts of unsaturated compounds are formed (Table V). In our view, such

a marked increase in the inhibition can be ascribed to electronic factors. The conjugation effect between the phenyl group and the double-bond leads to such an electron-shift (e.g. the structure **A** in Fig. 2) that as a consequence the C—C double-bond becomes depleted in electrons. A similar situation results from the mesomerism between the C=C and C=O bonds (Fig. 2, **B**). The mechanism of the

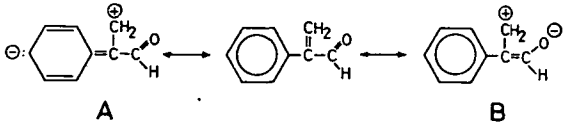

Fig. 2. Electron-shift effects occurring in 2-phenylpropenal

hydrogen-transfer was elucidated by EADON and SHIEKH [9]. In the first step, hydrogen is bound on the β-carbon atom of the α, β-unsaturated oxo compound, and therefore the above effects probably induce this significant phenomenon by decreasing the rate of this reaction step.

References

[1] *Bartók, M., Á. Molnár:* Kémiai Közlemények **45**, 335 (1976).
[2] *Molnár, Á., M. Bartók:* Acta Chim. (Budapest) **89**, 393 (1976).
[3] *Molnár, Á., M. Bartók:* React. Kinet. Catal. Lett. **3**, 421 (1975).
[4] *Pichat, L., C. Baret, M. Audinot:* Bull. soc. chim. France **1954**, 92.
[5] *Bartók, M., B. Kozma, A. S. Gilde:* Acta Phys. et Chem. Szeged **11**, 39 (1965).
[6] *Eliel, E. L., R.*[18]*O. Hutchins, M. Knoeber:* Org. Synth. **50**, 38 (1970).
[7] *Levene, P. A., G. M. Meyer:* Org. Synth. Coll. Vol. **II**, 288 (1943).
[8] *Adkins, H., H. R. Billica:* J. Amer. Chem. Soc. **70**, 3125 (1948).
[9] *Eadon, G., M. Y. Shiekh:* J. Amer. Chem. Soc. **96**, 2288 (1974).

ХИМИЯ ДИОЛОВ И ЦИКЛИЧЕСКИХ ЭФИРОВ, XLV.

Пространственно затрудненный переход водорода при превращении 2-замещённых 1,3-пропандиолов на медном катализаторе.

А. Молнар и М. Барток

При превращении 2-н-бутил-, 2-изопропил-, 2-трет-бутил-, 2-циклогексил-, 2-фенил-1,3-пропандиола (**I**—**V**) на медном катализаторе образуются ненасыщенный альдегид (и ненасыщенный спирт), кроме насыщенных соединений. В случае диола **V**, образование ненасыщенных соединений является характерным. Результаты объясняются пространственными и электронными факторами заместителей.

SYNTHESIS AND MELTING PROPERTIES OF CHOLESTERYL ESTERS OF *ORTHO-n*-ALKOXYBENZOIC ACIDS

By

J. A. SZABÓ, A. I. ZOLTAI, G. MOTIKA, P. M. AGÓCS and F. MIKLÓS

Department of Organic Chemistry, Attila József University, Szeged, Hungary

(Received 16th October, 1979)

The first ten compounds from the homologous series of cholesteryl esters of *ortho-n*-alkoxybenzoic acids have been synthetized, and their melting properties investigated with the aid of polarizing optical microscopy and differential scanning calorimetry (DSC).

In the literature a number of cholesterol benzoic acid esters showing liquid crystalline (mostly cholesteric) properties have been reported. Primarily the *para*-substituted benzoic acid esters have been synthetized, because their substituents are oriented in the direction of the molecular long axis (terminally-positioned substituents) [1, 2]. In the series of homologous *p*-alkoxybenzoic acid cholesteryl esters, the methyl, ethyl, *n*-propyl, *n*-butyl, *n*-pentyl and *n*-hexyl derivatives are enantiotropic cholesteric substances; all the others up to the octadecyl derivative show the enantiotropic C—S—Ch phase-sequence [3].

Little is known about the effects of the *meta*- and *ortho*-substituents. These substituents lie almost in the molecular plane, but not in the direction of the molecular long axis, and therefore they are called lateral substituents. VORA [4] has reported that the cholesterol *ortho*- and *para*-methoxybenzoates are non-mesomorphic, whereas the *ortho*-nitrobenzoate is monotropic smectic and enantiotropic cholesteric.

Recently a number of new series of homologous cholesterol derivatives have been reported, and their mesogenic properties have been studied [5], leading to the conclusion that there is no direct correspondence between the actual structures and the mesogenic properties. That is, from the properties of the first members of the series one cannot extrapolate to the properties of the second ones, etc. Therefore, it seemed reasonable for us to synthetize the title compounds and to study their melting properties.

The route of the preparation, as shown in Fig. 1, follows the sequence: salicylic acid (**I**) — methyl salicylate (**II**) — *ortho*-alkoxybenzoic acid ester (**III**) — *ortho*-alkoxybenzoic acid (**IV**) — *ortho*-alkoxybenzoyl chloride (**V**) — *ortho*-alkoxybenzoic acid cholesteryl ester (**VI**). Since all *ortho*-alkoxybenzoic acids (**IV**) investigated were liquids with high boiling points at atmospheric pressure, the corresponding methyl esters (**III**) and acid chlorides (**V**) were purified and the physical pro-

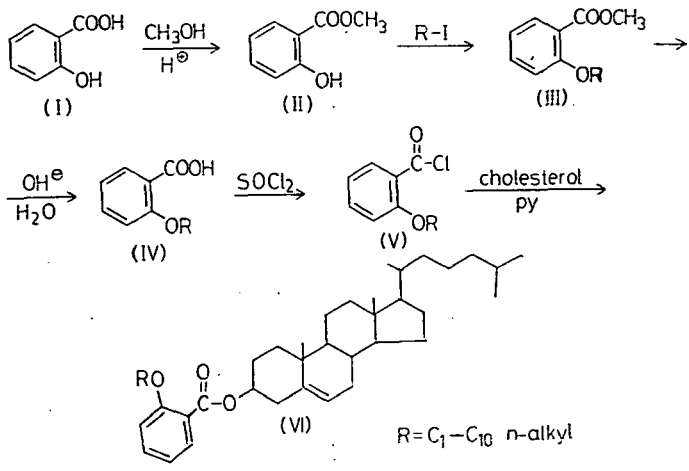

Fig. 1.

perties of the acid chlorides were registered; they are shown in Table I. The physical and analytical data on the cholesteryl esters (**VI**) are shown in Table II.

The melting properties of the compounds are closely similar to each other, with the exception of the methyl derivative. The methyl derivative has two melting points (99° and 120°, respectively), and on cooling a bluish-gray structureless appearance is observed under the microscope. DSC did not reveal any thermodynamic phase transition. With the lengthening of the alkyl chain in the case of the ethyl, *n*-propyl etc. derivatives, on heating only simple melting occured at the temperature values reported (see Table II). On cooling, the isotropic melt remains unchanged to the lowest temperatures investigated (about −20°) and subsequently forms a glass. All these compounds have an extremely low tendency to crystallize from their melts at temperatures down to −10° (several days).

Table I

Boiling points and some IR characteristics of ortho-n-alkoxybenzoyl chlorides

Substituent R	Bp. (°C/mm Hg)	IR $\nu_{C=0}$ (cm^{-1})	$\nu_{as\,COC}$ (cm^{-1})
methyl	105/3	1770	1286
ethyl	118/4	1768	1288
n-propyl	146/10	1770	1292
n-butyl	164/15	1772	1290
n-pentyl	167/11	1770	1288
n-hexyl	158/5	1770	1285
n-heptyl	175/17	1772	1285
n-octyl	179/4	1772	1288
n-nonyl	188/7	1770	1286
n-decyl	199/5	1770	1284

To summarize, in the case the *o*-alkoxybenzoic acid cholesteryl esters the methyl derivative shows a blue texture; the other derivatives were found to be nonmesogenic substances. All compounds investigated exhibited an extremely large temperature hysteresis.

Experimental

The melting points were determined with a PHMK (VEB Analytik, Dresden) hot stage. The thermal properties were studied with a Perkin—Elmer DSC 2 differential scanning calorimeter under nitrogen flushing, at 10°/min heating or cooling rates. The NMR and IR spectra were registered with JEOL 60 HL and Unicam SP 1000 spectrometers, respectively.

The preparation of 2-alkoxybenzoic acids (or its methyl esters)

To 35 ml 0.1 M methanolic sodium methylate solution, 0.1 mole (15.2 g) methyl salicylate and 0.12 mole of the corresponding alkyl iodide were added. The mixture was boiled under nitrogen, till TLC showed reaction to be complete (8—12 hours). After filtration of the inorganic substance the liquid was evaporated to one-half volume and the sodium iodide separating on cooling filtered on pump again.

(A) To the above filtrate, 10 ml water was edded and the mixture was extracted twice with 30 ml ethyl ether. The extracts were evaporated and hydrolyzed by boiling with aqueous methanolic KOH (about 1.5—8 hours). The solution was acidi-

Table II

Analytical and physical data of ortho-n-alkoxybenzoic acid cholesteryl esters (VI)

Substituent R	Formula	M. W.	Anal. calcd. C	Anal. calcd. H	Anal. found C	Anal. found H	M. p. °C	DSC C→I transition *(°C)
methyl	$C_{35}H_{52}O_3$	520.801	80.71	10.06	80.62	10.31	120.5—121**	99.0 and 120**
ethyl	$C_{36}H_{54}O_3$	534.828	80.85	10.18	81.05	10.26	120.2—121	119
n-propyl	$C_{37}H_{56}O_3$	548.855	80.97	10.28	80.93	10.17	91.5—92.8	93.5
n-butyl	$C_{38}H_{58}O_3$	562.882	81.09	10.39	80.96	10.46	73.8—75.1	74.0
n-pentyl	$C_{39}H_{60}O_3$	576.909	81.20	10.48	81.12	10.47	96.0—96.2	96.0
n-hexyl	$C_{40}H_{62}O_3$	590.336	81.30	10.58	81.15	10.75	91.7—92.8	92.0
n-heptyl	$C_{41}H_{64}O_3$	604.963	81.40	10.66	81.22	10.69	84.3—86	86.0
n-octyl	$C_{42}H_{66}O_3$	618.990	81.50	10.76	81.32	10.59	85.0—87.5	87.0
n-nonyl	$C_{43}H_{68}O_3$	633.017	81.59	10.83	81.42	10.80	79.0—81.0	80.0
n-decyl	$C_{44}H_{70}O_3$	647.044	81.68	10.90	81.41	10.72	44.0—46.0	45.5

* The temperatures of the C→I transition were extrapolated from the thermograms according to the linear slope method.

** At 98,5—99° melting to the isotropic melt was observed, and then at 103—6° the sample crystallized. On the thermogram two endothermic peaks appeared centered at about 101° and 122°, with a protracted exothermic peak at 103—115°

fied with aqueous HCl and extracted with ethyl ether. The extracts were shaked with lime-water and the calcium salicylate filtered off. To the filtrate conc. HCl was added and the mixture was extracted with benzene. Upon evaporation, the benzene solution yielded the crude *n*-alkoxybenzoic acids in sufficiently pure form to prepare the corresponding acid chlorides.

(B) The filtrate was evaporated completely and extracted with benzene. The extracts were distilled *in vacuo* and the methyl ester fraction collected. The methyl ester was hydrolyzed as above. This process was more convenient to prepare the alkoxybenzoic acids from the *n*-pentyl derivative up.

Preparation of ortho-alkoxybenzoic chlorides

At ambient temperatures 0.12 mole thionyl chloride was added to 0.1 mole alkoxybenzoic acids and the solution allowed to stand one day. The hydrogen chloride and the unreacted thionyl chloride were removed under moderate vacuum, and the acid chloride distilled as given in Table I.

Preparation of ortho-alkoxybenzoic acid cholesteryl esters

0.005 mole cholesterol was dissolved in 3.5 ml dry pyridine at ambient temperature, and then 0.006 mole *ortho*-alkoxybenzoic acid chloride dissolved in 5 ml dry benzene was added. The mixture was allowed to stand at room temperature for two (or more) days until no cholesterol spot was observed on TLC. Then the reaction mixture was poured into dilute HCl solution and extracted with benzene. The benzene extracts were washed in turn with water, with saturated aqueous $NaHCO_3$ solution and with water. After drying on anhydrous $CaCl_2$, the extracts were concentrated and purified on a silica column by eluting with benzene: chloroform (1:1) mixture. The pure fractions were collected, evaporated to dryness and crystallized from ethyl alcohol. The physical and analytical properties of esters prepared are given in Table II.

* * *

The authors acknowledge the financial support of the REANAL Chemical Works (Budapest).

References

[1] *Gray, G. W.:* Molecular Structure and the Properties of Liquid Crystals, Academic Press, New York, 1962.

[2] *Gray, G. W.:* Molecular Geometry and the Properties of Non-Amphiphilic Liquid Crystals, in Advances in Liquid Crystals, Ed.: G. H. Brown, Academic Press, New York, 1976, Vol. 2, pp. 1—72.

[3] *Dave, I. S., R. A. Vora:* Mol. Cryst. Liq. Cryst. **14**, 319 (1971) and *Demus D., H. Demus, H. Zaschke*: Flüssige Kristalle in Tabellen, Leipzig, 1974. p. 288—289.

[4] *Vora, R. A.:* Curr. Sci. **45**, (15) 538 (1976); Chem. Abstr. **86**, 4632f (1977).

[5] *Elser, W., R. D. Ennulat:* Selective Reflection of Cholesteric Liquid Crystals, in Advances in Liquid Crystals, Vol. 2 Ed.: G. H. Brown, Academic Press, New York, 1976. p. 97—125.

СИНТЕЗ И ТЕРМИЧЕСКИЕ ПРЕВРАЩЕНИЯ ЭФИРОВ ХОЛЕСТЕРИНА И *орто-н*-АЛКОКСИ БЕНЗОЙНЫХ КИСЛОТ

Й. А. Сабо, А. И. Золтаи, Г. Мотика, П. М. Агоч и Ф. Миклош

Синтетизированы первые десять членов гомологического ряда эфиров холестерина и *орто-н*-алкокси бензойных кислот и изучены их термические превращения методом поляризованной оптической микроскопии и дифференциально-сканирующей калориметрии (ДСК).

LIQUID CRYSTALS I. SYNTHESIS AND INVESTIGATION OF CHOLESTERYL FLUOROBENZOATES

By

P. M. AGÓCS, G. MOTIKA, J. A. SZABÓ and A. I. ZOLTAI

Institute of Organic Chemistry, Attila József University, Szeged

(Received 16th October, 1979)

Cholesteryl *ortho-* *meta-* and *para*-fluorobenzoates have been prepared. The temperatures, enthalpies and entropies of the phase transitions have been measured with the aid of differential scanning calorimetry. Optical examination of the compounds has proved that all derivatives are enantiotropic cholesteric liquid crystals.

Introduction

One of the first and foremost investigated compounds showing liquid crystalline properties is cholesteryl benzoate [1]. Substituted cholesteryl benzoates studied to date include the *ortho-*, *meta-* and *para*-substituted chloro, bromo, iodo, nitro, methyl and methoxy derivatives, and some other di- and tri-substituted compounds [2, 3].

It seems reasonable to complement these compounds with the synthesis of the cholesteryl fluorobenzoates and compare their liquid crystalline properties with the features of the other halogeno-derivatives.

Experimental

Preparation

Cholesteryl *ortho-*, *meta-* and *para*-fluorobenzoates were prepared by the reaction of the corresponding acid chloride and cholesterol in the presence of triethylamine. The crude products were crystallized from benzene-ethanol mixtures. The purities of the compounds were checked with thin-layer chromatography, IR spectroscopy and combustion analyses. The analytical data on the compounds prepared are shown in Table I.

Table I

Analytical Data on the Compounds

Compound	Formula	C %		H %	
		Found	Calc.	Found	Calc.
Ortho	$C_{34}H_{49}O_2F$	80.58	80.27	9.79	9.71
Meta	$C_{34}H_{49}O_2F$	79.88	80.27	9.66	9.71
Para	$C_{34}H_{49}O_2F$	80.41	80.27	9.65	9.71

Calorimetry

Measurements were made with a PERKIN—ELMER DSC—2 calorimeter, in a highly-purified nitrogen atmosphere. The thermal calibration of the instrument was made with bidistilled water and with an indium standard. The weight of the samples was altered in the range 3—5 mg, with ±0.001 mg accuracy. The heating and cooling rates were 10°/min and the sensitivity of the instrument was 5—10 mcal/sec. The temperatures of the phase transitions could be reproduced with an accuracy of ±0.4°. The calorimetric calibration was made with a known quantity of indium standard.

Optical examination

For the measurement of melting points and the determination of the textures of the mesophases, a PHMK (VEB Analytik, Dresden) hot-stage apparatus and an AMPLIVAL POL-U (Carl Zeiss, Jena) polarizing microscope (equipped with a hot stage) were applied.

Results and discussion

The thermograms of cholesteryl *ortho-*, *meta-* and *para*-fluorobenzoates are shown in Figs. 1, 2 and 3, respectively.

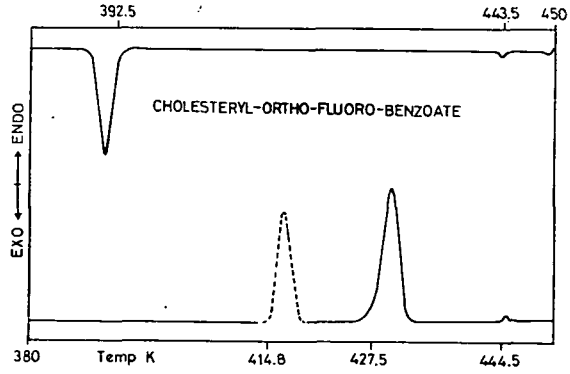

Fig. 1. Thermogram of cholesteryl *ortho*-fluorobenzoate

The lower parts of the diagrams show the phase transitions upon heating, and the upper regions of the diagram the phase transitions upon cooling. The full line means the first, and the dashed lines the second, *etc.* measurements in the heating mode (since differences may exist between the properties of solidified samples and those crystallized from solvents).

All three compounds show enantiotropic liquid crystalline phases. The thermal stabilities of the liquid crystalline states follow the sequence:

ortho < *meta* < *para.*

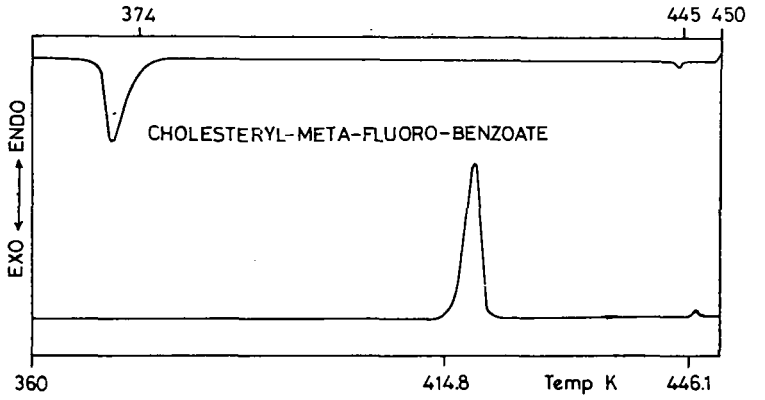

Fig. 2. Thermogram of cholesteryl *meta*-fluorobenzoate

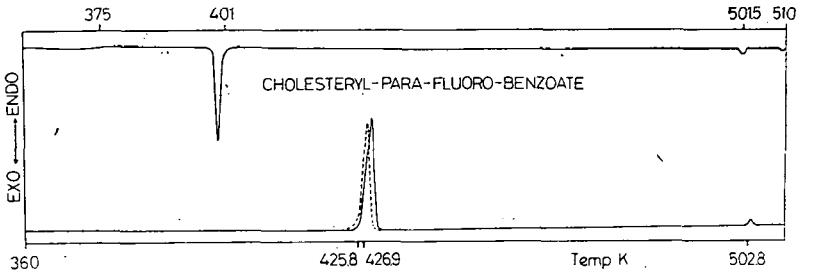

Fig. 3. Thermogram of cholesteryl *para*-fluorobenzoate

On the basis of the thermograms, the following phase transition schemes are characteristic for the changes in the state of the materials (Fig. 4).

Letter "C" means the crystalline state(s) of matter, symbol "Ch" represents the cholesteric mesophase, symbol "*I*" the isotropic liquid and symbol "*X*" the optically undetermined states.

Cholesteryl *ortho*-fluorobenzoate (Fig. 4, 2F) shows a simple enantiotropic cholesteric mesophase transition. The mesophase exists in a 31.3° temperature interval.

Cholesteryl *meta*-fluorobenzoate (Fig. 4, 3F) has two crystalline states. The "C_1" state comes from the crystallized sample, and the "C_2" state occurs when the sample is solidified from the isotropic melt. Thereafter, upon cooling and heating, only this latter state exists. Both states lead to an enantiotropic cholesteric state. This mesomorphic state is stable in a 31.5° temperature range.

Cholesteryl *para*-fluorobenzoate (Fig. 4, 4F) also has two crystalline states, but upon cooling after the cholesteric mesophase exists in an optically unobservable "X" state, and it follows the "C_2" crystalline state. The cholesteric mesophase is stable in a 77° interval.

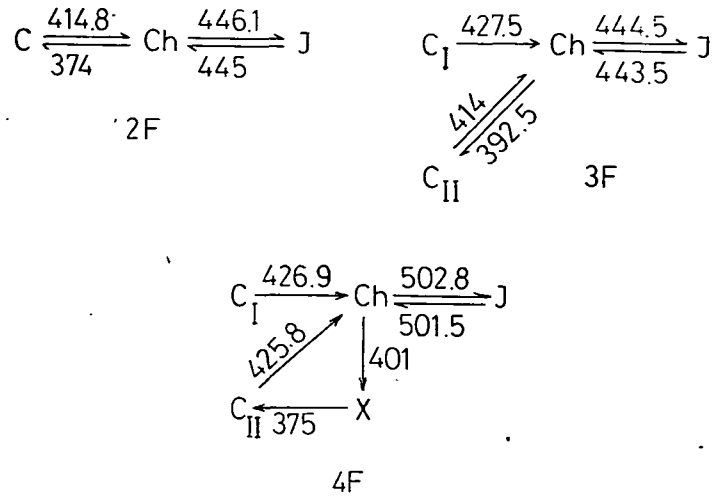

Fig. 4. Phase transition schemes of the compounds

The calorimetric values of the phase transitions were determined on the basis of the actual thermograms, because peak areas are proportional to the heat capacities of the phase transitions. The calculation was made with the following equation:

$$\Delta H = \frac{K \cdot A \cdot R}{W \cdot s}$$

Where ΔH = enthalpy change, R = sensitivity, K = instrument constant, W = weight of the sample, A = peak area, s = chart speed.

The peak areas were determined with a planimeter and also by weight measurement. The values of the enthalpy and entropy are shown in Table II.

Table II

Calorimetric Data on the Compounds

	ΔH (kcal/mol) C—Ch	ΔH (kcal/mol) Ch—I	Δs (kcal/mol K) C—Ch	Δs (kcal/mol K) Ch—I
Ortho	7.07*	0.13*	1.70×10^{-2}*	2.96×10^{-4}*
	5.83	0.13	1.40×10^{-2}	2.96×10^{-4}
Meta	9.78*	0.20*	2.29×10^{-2}*	4.46×10^{-4}*
	6.71	0.20	1.62×10^{-2}	4.46×10^{-4}
Para	7.72*	0.21*	1.81×10^{-2}*	4.25×10^{-4}*
	7.29	0.21	1.71×10^{-2}	4.25×10^{-4}

* Values obtained on first heating

Both the enthalpy and entropy change values increase in order:

$$ortho < meta < para$$

On the basis of the calorimetric data, it seems reasonable to compare mesomorphic features of the possible monohalogeno derivatives. In Table III the thermal stability values of cholesteryl benzoate and the monohalogeno derivatives are summarized; as the melting point in the case of non-mesomorphic substances, the thermal stability values well characterize the liquid crystalline phases.

Table III

Thermal Stability Values of the Cholesteryl Benzoates
(°C)

	H	F	Cl	Br	I
Ortho	178.0	173.0	146.0	134.0	112.0
Meta	178.0	171.4	147.0	142.0	130.0
Para	178.0	229.7	257.0	257.0	252.0

The data in Table III show that for the *ortho*- and *meta*-derivatives the thermal stability decreases with increase of the space requirements of the substituent. In the case of the *para*-derivatives such a tendency is not present. At extremely high temperatures all four *para*-substituted compounds give an isotropic liquid, leading to the conclusion that all the mesophases are very stable and therefore their stabilities are not influenced essentially by the nature of the substituent.

Comparing the thermal stability values of the corresponding *ortho*-, *meta*- and *para*-derivatives, it can be seen that the stability changes in the order:

$$ortho < meta < para$$

With the decrease of the space-filling of the substituent, the difference between the thermal stabilities of the *ortho*- and *para*-derivatives decreases. This tendency in the case of the fluoro-derivatives is such that the stability order changes:

$$meta < ortho < para$$

To summarize, we may conclude that on increase of the space-requirement of the halogeno substituent, the thermal stability decreases according to the position of the substituent, in the order:

$$ortho < meta < para$$

Acknowledgements

The authors thank OMFB (Hungarian Technical Development Committee) for the generous technical gift, and REANAL Chemical Factory, Budapest for substantial financial support.

Thanks are expressed to Dr. G. Bartók-Bozóki and Mrs. Éva Gács-Gergely for the combustion analyses, and to Mrs. J. Csányi-Kertész and Mr. A. Gajdacsi for technical assistance.

The authors wish to thank Dr. G. Dombi for the NMR and Mr. J. Kiss for the IR spectra and helpful discussions.

References

[1] *Reinitzer, F.:* Monatsh. Chem. **9**, 435 (1888).
[2] *Demus, D., H, Demus H. Zaschke:* Flüssige Kristalle in Tabellen, VEB Deutsche Verlag für Grundstoffindustrie, Leipzig, 1974.
[3] *Dave, J. S., R. A. Vora:* Indian J. Chem. **11**, 19 (1973).

ЖИДКИЕ КРИСТАЛЛЫ, I. СИНТЕЗ И ИССЛЕДОВАНИЕ ХОЛЕСТЕРИЛ-ФТОРОБЕНЗОАТОВ

П. М. Агоч, Г. Мотика, Й. А. Сабо и А. И. Золтаи

Синтетизированы *орто-*, *мета-* и *пара*-фторобензоаты Холестерина. Методом дифференциально-сканирующей калориметрии определены температуры, энтальпии и энтропии фазовых переходов. Оптические свойства изученных производных показывают, что все они являются энантиотропными жидкими кристаллами холестерина.

SYNTHESIS OF BRADYKININ ANALOGUES CONTAINING OPTICALLY-ACTIVE PIPECOLIC ACID

By

L. BALÁSPIRI, GY. PAPP, M. TÓTH, F. SIROKMÁN* and K. KOVÁCS

Institute of Medical Chemistry, University of Medicine, Szeged

(Received 25th October, 1979)

Seven structural analogues of bradykinin, containing optically-active L- and D-pipecolic acid**, were prepared and purified, and their physical constants were determined.

Slight changes in the structures of known peptide hormones by substituting amino acids of similar character for constituent amino acids are very important for investigation of the relationship between chemical structure and biological activity [1—3].

The amino acids substituted may be similar or not; they can be proteinogenic or nonproteinogenic. The known tissue hormone bradykinin

Arg-Pro-Pro-Gly-Phe-Ser-Pro-Phe-Arg

can be detected in the brain. Since this hormone contains three proline residues, it is easy to get more information by synthesis and biological study of bradykinin analogues containing one or more pipecolic acid residues in place of proline.

Up to now, numerous papers on the substitution of proline by optically-active pipecolic acid can be found in the literature of peptide chemistry. This synthesis may be achieved both classical and solid phase methods [4]. Among others, peptide analogues reported containing optically-active pipecolic acids include collagen models [5], oxytocin [6], angiotensin II [7], thyreotropin releasing hormone [8, 9], sequence-polypeptide [10] and model peptides [11]. Some others now under publication [12].

In order to fill gaps in the literature, special attention has been paid to the peptide chemical application of optically-active pipecolic acids [13]. Subsequently, the preparation of different protected and active derivatives of both L- and D-pipecolic acid was reported [14, 15] in detail. First, 3-L-pipecolic acid bradykinin appeared in the literature [16]; later, our research group reported 2-L- and 3-D-pipecolic acid

* Biological Center of the Hungarian Academy of Sciences, Szeged

** Nomenclature and abbreviations are those accepted by IUPAC—IUB for peptide chemistry: pip = pipecolic acid; Z = benzyloxycarbonyl; BOC = *t*-butyloxycarbonyl; OMe = methylester; ONb = = *p*-nitro-benzylester. Except for glycine, all proteinogenic amino acids are in the *L*-form.

Physical properties and analytical

Peptide	Method[2]	Purification[3]	Yield %
Z-Arg(NO_2)-L-Pip-Pro-Gly-Phe-Ser-L-Pip-Phe-Arg(NO_2)-OMe (**1**)	A	Aa	55
Arg-L-Pip-Pro-Gly-Phe-Ser-L-Pip-Phe-Arg (**2**)	A	Bd	44
Z-Arg(NO_2)-Pro-L-Pip-Gly-Phe-Ser-L-Pip-Phe-Arg(NO_2)-OMe (**3**)	A	Aa	52
Arg-Pro-L-Pip-Gly-Phe-Ser-L-Pip-Phe-Arg (**4**)	A	Bd	48
Z-Arg(NO_2)-D-Pip-Pro-Gly-Phe-Ser-Pro-Phe-Arg(NO_2)-ONb (**5**)	A	Ac	46
Arg-D-Pip-Pro-Gly-Phe-Ser-Pro-Phe-Arg(NO_2)-ONb (**6**)	A	Bd	70
Z-Arg(NO_2)-Pro-Pro-Gly-Phe-Ser-D-Pip-Phe-Arg(NO_2)-ONb (**7**)	A	Ac	50
Arg-Pro-Pro-Gly-Phe-Ser-D-Pip-Phe-Arg (**8**)	A	Bd	76
Z-Arg(NO_2)-Pro-Pro-Gly-Phe-Ser-L-Pip-Phe-Arg(NO_2)-ONb (**9**)	B	Ac	50
Arg-Pro-Pro-Gly-Phe-Ser-L-Pip-Phe-Arg (**10**)	B	Bd	84
Z-Arg(NO_2)-L-Pip-L-Pip-Gly-Phe-Ser-Pro-Phe-Arg-(NO_2)-OMe (**11**)	B	Aa	52
Arg-L-Pip-L-Pip-Gly-Phe-Ser-Pro-Phe-Arg (**12**)	B	Bd	39
Z-Arg(NO_2)-L-Pip-L-Pip-Gly-Phe-Ser-L-Pip-Phe-Arg(NO_2)-ONb (**13**)	B	Ac	52
Arg-L-Pip-L-Pip-Gly-Phe-Ser-L-Pip-Phe-Arg (**14**)	B	Bd	79

[1] all analogous are tabled
[2] A = stepwise condensation, B = fragment condensation
[3] A = silica gel column, B = Whatman CM 32 CMC-column, a = system 2, b = system 3, c = EtOAc-MeOH system, d = 0.01—0.5 M ammonium acetate
[4] A = acetic acid, D = dimethylformamide

bradykinin [17] and some fragments of further analogues [18, 19]. In this paper we describe the preparation of the following protected and free bradykinins: 2,7-L-pipecolic acid (**1—2**), 3,7-L-pipecolic acid (**3—4**), 2-D-pipecolic acid (**5—6**), 7-D-pipecolic acid (**7—8**), 7-L-pipecolic acid (**9—10**), 2,3-L-pipecolic acid (**11—12**) and 2,3,7-L-pipecolic acid bradykinins (**13—14**).

The first four analogues were synthesized in a stepwise manner, the others by a fragment condensation method. The biological data of these analogues will be published elsewhere [20].

Table I

data of the synthesized analogues[1]

M. p. °C	$[\alpha]_D$ c=1 T=24 °C[4]	Formula (Mol. weight)	Elemental analysis (N %) Calc. / Found / Amino acid analysis
128—137	−47° D	$C_{61}H_{83}O_{17}N_{17}$ (1326.5)	17.9 / 17.7
171—184	−80° A	$C_{58}H_{77}O_{11}N_{15}\times 3\ CH_3COOH$ (1268.3)	Arg 1.82 Pro 1.02 Pip 1.9 Gly 1.0 Pre 1.97 Ser 0.88
132—140	−50° D	$C_{61}H_{83}O_{17}N_{17}$ (1326.5)	17.9 / 17.7
176—186	−80° A	$C_{58}H_{77}O_{11}N_{15}\times 3\ CH_3COOH$ (1268.3)	Arg 1.8 Pro 1.02 Pip 1.8 Gly 1.0 Phe 1.97 Ser 0.83
138—140	−34° D	$C_{66}H_{84}O_{19}N_{18}$ (1433.5)	17.6 / 17.4
190—198	−58° A	$C_{57}H_{75}O_{11}N_{15}\times 3\ CH_3COOH$ (1254.3)	Arg 1.9 Pro 2.0 Pip 0.9 Gly 1.0 Phe 2.1 Ser 0.9
134—138	−34° D	$C_{66}H_{84}O_{19}N_{18}$ (1433.5)	17.6 / 17.4
190—200	−58° A	$C_{57}H_{75}O_{11}N_{15}\times 3\ CH_3COOH$ (1254.3)	Arg 1.84 Pro 1.86 Pip 0.8 Gly 1.0 Phe 1.88 Ser 0.91
140—150	−47° D	$C_{66}H_{84}O_{19}N_{18}$ (1433.5)	17.6 / 17.5
168—178	−80° A	$C_{57}H_{75}O_{11}N_{15}\times 3\ CH_3COOH$ (1254.3)	Arg 1.81 Pro 1.86 Pip 0.9 Gly 1.0 Phe 1.96 Ser 0.8
125—136	−48° D	$C_{61}H_{83}O_{17}N_7$ (1326.5)	17.9 / 17.6
165—175	−76° A	$C_{58}H_{77}O_{11}N_{15}\times 3\ CH_3COOH$ (1268.3)	Arg 1.82 Pro 0.9 Pip 1.8 Gly 1.0 Phe 1.98 Ser 0.88
117—124	−40° D	$C_{68}H_{88}O_{19}N_{18}$ (1461.6)	17.2 / 17.1
191—200	−82° A	$C_{59}H_{79}O_{11}N_{15}\times 3\ CH_3COOH$ (1282.4)	Arg 1.87 Pip 2.79 Gly 1.0 Phe 2.04 Ser 0.81

Experimental

Melting points were determined with a Kofler-block and optical rotations with a Zeiss-polarimeter. Amino acid analysis was performed on a Czechoslovakian HD-1200 E analyser after hydrolysis in 6 N HCl.

IR spectra were taken in KBr on a Unicam SP 200 instrument. TLC on Kiesel G plates was used for purity control and identification in the following systems:

1. *n*-butanol—acetic acid—water 4:1:1

2. ethyl acetate—pyridine—acetic acid—water 60:20:6:11
3. ethyl acetate—pyridine—acetic acid—water 80:20:6:11
4. ethyl acetate—pyridine—acetic acid—water 90:20:6:11
5. chloroform—methanol 8:2
6. chloroform—methanol—acetic acid 85:10:5.

The protected analogues were purified on a Merck Kieselgel 60 (0.063—0.2) column, eluted with system 2 or 3 or with ethyl acetate—methanol. The free peptides were purified by ion-exchange chromatography on a Whatman CM 32 carboxymethyl-cellulose column, eluted with a 0.01—0.5 M ammonium acetate gradient. Development of the TLC was carried out with ninhydrin, chlorine/*o*-toluidine and Sakaguchi reagent.

All data of described analogues can be found in Table I.

*Methyl benzyloxycarbonyl-arginyl(nitro)-*L*-pipecolyl-prolyl-glycyl-phenylalanyl-seryl-*L*-pipecolyl-phenylalanyl-nitroargininate* (**1**)

1.37 g (1.5 mmole) protected octapeptide ester [19] was treated with excess of trifluoroacetic acid at room temperature for 1 hour. The acid was evaporated in vacuum and the remaining trifluoroacetate of the octapeptide ester precipitated with ether, filtered, and dissolved in 8 ml dimethylformamide, cooled to −5 °C, and neutralized with triethylamine. 389 mg (1.65 mmole) benzyloxycarbonyl-(nitro)arginine was added, followed by 190 mg (1.65 mmole) N-hydroxysuccinimide (HOSu) and 310 mg (1.5 mmole) dicyclohexylcarbodiimide (DCCI). The reaction mixture was stirred at 0 °C for 4 hr, and then at room temperature for 24 hr. After filtering off the dicyclohexylurea, the filtrate was evaporated in vacuum, and the residue was triturated with ether, washed in turn with water, acetone and ether, and dissolved in methanol for column chromatography. The fractions were evaporated in vacuum, triturated in ether and dried.

*Arginyl-*L*-pipecolyl-prolyl-glycyl-phenylalanyl-seryl-*L*-pipecolyl-phenylalanyl-arginine triacetate* (**2**)

620 mg (**1**) was dissolved in dioxan—methanol 5:1, and 0.5 ml 2 N NaOH was added. After a 4-hr stirring at room temperature, 0.5 ml 2 N H_2SO_4 was added, and the mixture was evaporated in vacuum till half volume, poured into ice-water, filtered and washed with ether. The residual powder was dissolved in acetic acid—methanol 3:1, and the solution was hydrogenated in the presence of 10% Pd-C and Pd-black catalysts in a bubbling-apparatus at room temperature. The catalysts were filtered off and the filtrate was evaporated in vacuum. The residue was dissolved in start buffer (pH 5) and chromatographed. The main peak was collected and liophilized. The latter process was repeated twice from dilute acetic acid and water.

*Methyl benzyloxycarbonyl-arginyl(nitro)-prolyl-*L*-pipecolyl-glycyl-phenylalanyl-seryl-*L*-pipecolyl-phenylalanyl nitroargininate* (**3**)

1.0 g (1.0 mmole) protected octapeptide ester [19] was treated with trifluoroacetic acid, and the trifluoroacetate of the octapeptide ester, coupled with benzyloxycarbonyl(nitro)arginine in the presence of HOSu and DCCI, was worked up and chromatographed as described for (**1**).

*Arginyl-prolyl-*L*-pipecolyl-glycyl-phenylalanyl-seryl-*L*-pipecolyl-phenylalanyl-arginine triacetate* (**4**)

150 mg (**3**) was hydrolyzed, hydrogenated, chromatographed and worked up as described for (**2**).

*p-Nitrobenzyl benzyloxycarbonyl-arginyl(nitro)-*D*-pipecolylprolyl-glycyl-phenylalanyl-seryl-prolyl-phenylalanyl-nitro-nitroargininate* (**5**)

1.2 g (1.0 mmole) protected octapeptide ester [19] was treated with trifluoroacetic acid, and the trifluoroacetate of the octapeptide ester, coupled with benzyloxycarbonyl-(nitro)arginine in the presence of HOSu and DCCI, was worked up as described for (**1**), chromatographed in ethyl acetate—methanol and worked up similarly.

*Arginyl-*D*-pipecolyl-prolyl-glycyl-phenylalanyl-seryl-prolyl-phenylalanyl-arginine triacetate* (**6**)

143 mg (**5**) was hydrogenated as described for (**2**) (but only in the presence of Pd-black catalyst) and the crude product was chromatographed and worked up similarly.

*p-Nitrobenzyl benzyloxycarbonyl-arginyl(nitro)-prolyl-prolyl-glycyl-phenylalanyl-seryl-*D*-pipecolyl-phenylalanyl-nitroargininate* (**7**)

1.2 g (1.0 mmole) protected octapeptide ester [19] was treated with trifluoroacetic acid, and the trifluoroacetate of the octapeptide ester, coupled with benzyloxycarbonyl-(nitro)arginine in the presence of HOSu and DCCI, was worked up as described for (**1**), with chromatography in ethyl acetate—methanol as for (**5**).

*Arginyl-prolyl-prolyl-glycyl-phenylalanyl-seryl-*D*-pipecolyl-phenylalanyl-arginine triacetate* (**8**)

380 mg (**7**) was hydrogenated, chromatographed, and worked up as described for (**6**).

p-Nitrobenzyl benzyloxycarbonyl-arginyl(nitro)-prolyl-glycyl-phenylalanyl-seryl-L-pipecolyl-phenylalanyl-nitroargininate (**9**)

1.54 g (1.5 mmole) protected hexapeptide ester [19] was dissolved in acetic acid — HBr. After 1 hr the solution was evaporated in vacuum, solidified with ether, washed with ether and dried. The crude product hydrobromide of the hexapeptide ester was dissolved in dimethylformamide, cooled to −15 °C and neutralized with N-methyl morpholine. From 840 mg benzyloxycarbonyl-arginyl(nitro)-prolyl-proline the azide was prepared in situ at −15 °C. The two cooled solutions were poured together and stirred for 48 hr at 0 °C, and then filtered, evaporated in vacuum, dissolved for chromatography, and worked up as described for (**5**).

Arginyl-prolyl-prolyl-glycyl-phenylalanyl-seryl-L-pipecolyl-phenylalanyl-arginine triacetate (**10**)

800 mg (**9**) was hydrogenated, chromatographed, and worked up as described for (**6**).

Methyl benzyloxycarbonyl-arginyl(nitro)-L-pipecolyl-L-pipecolyl-glycyl-phenylalanyl-seryl-prolyl-phenylalanyl-nitroargininate (**11**)

1.35 g (1.5 mmole) protected hexapeptide ester [19] was treated with acetic acid—HBr, and the hydrobromide of the hexapeptide ester, coupled with 864 mg benzyloxycarbonyl-arginyl(nitro)-L-pipecolyl-L-pipecolic acid (converted in situ to the azide), and worked up and chromatographed as described for (**9**).

Arginyl-L-pipecolyl-L-pipecolyl-glycyl-phenylalanyl-seryl-propyl-phenylalanyl-arginine triacetate (**12**)

540 mg (**11**) was hydrogenated, chromatographed, and worked up as described for (**2**).

p-Nitrobenzyl benzyloxycarbonyl-arginyl(nitro)-L-pipecolyl-L-pipecolyl-glycyl-phenylalanyl-seryl-L-pipecolyl-phenylalanyl-nitroargininate **13**

1.56 g (1.5 mmole) protected hexapeptide ester [19] was treated with acetic acid — HBr, and the hydrobromide of the hexapeptide ester, coupled with 864 mg benzyloxycarbonyl-arginyl(nitro)-L-pipecolyl-L-pipecolic acid (converted in situ to the azide), and worked up and chromatographed as described for (**9**).

Arginyl-L-pipecolyl-L-pipecolyl-glycyl-phenylalanyl-seryl-L-pipecolyl-phenylalanyl-arginine triacetate **14**

700 mg (**13**) was hydrogenated, chromatographed, and worked up as described for (**6**).

* * *

The authors are indebted to thanks to the microanalytical and infrared laboratory of the Organic Chemistry Institute of Attila József University, Szeged, for elemental and infrared analyses, to Mr. R. Ferenczi for amino acid analysis, and to Miss I. Bagi and J. Fülöp for technical assistance.

References

[1] *Schröder, E., K. Lübke:* "The Peptides", Vol. 2. Acad. Press, New York—London, 1966.
[2] *Rudinger, J.:* "Drug Design", Vol. 1. Acad. Press, New York—London, 1971.
[3] *Sheppard, B.* (senior reporter): "Amino-acids, Peptides, and Proteins." A Special Periodical Report. The Chemical Society, London. Vol. 1—9. (1969—1977).
[4] *Merrifield, R. B.:* J. Amer. Chem. Soc. **85**, 2149 (1963).
Merrifield, R. B.: Advances in Enzymology **32**, 221 (1969).
[5] *Katchalski, E., A. Berger, J. Kurtz:* Internat. Symposium on Protein Structure and Crystallography, Madras, 1963.
[6] *Bespalova, Z. D., O. A. Kairov, U. F. Martinov, V. U. Natosky, M. I. Titov, E. I. Sachamtova:* Vest. Leningrad. Univ. Ser. Fiz. Khim. **21**, 157 (1966).
[7] *Chaturvedi, N. C., W. K. Park, R. R. Smeby, F. M. Bumpus:* J. Med. Chem. **13**, 177 (1970).
[8] *Bankowski, K., S. Drabarek:* Acta Polon. Pharm. **33**, 81 (1976).
[9] *Baláspiri, L., Zs. Csapó, M. Fekete, G. Telegdy, K. Kovács:* unpublished results.
[10] *Fairweather, R., J. H. Jones:* J. C. S. Perkin I. **1972**, 2475.
[11] *Vicar, J., M. Budésinsky, K. Blaha:* Coll. Czechosl. Chem. Commun. **38**, 1940 (1973).
Vicar, J., J. Smolikova, K. Blaha: Coll. Czechosl. Chem. Commun. **38**, 1957 (1973).
[12] *Baláspiri, L., A. Török, Zs. Csapó, I. Nógrádi, K. Kovács:* unpublished results.
[13] *Kovács, K., B. Penke, J. Czombos, J. Petres, L. Baláspiri:* Acta Phys. et Chem. Szeged **17**, 61 (1971).
[14] *Baláspiri, L., B. Penke, J. Petres, K. Kovács:* Monatshefte **101**, 1177 (1970).
[15] *Baláspiri, L., Gy. Papp, K. Kovács:* Monatshefte **103**, 581 (1972).
[16] *Nicolaides, E. D., H. A. DeWald, M. K. Craft:* Ann. N. Y. Acad. Sci. **104**, 14 (1963).
[17] *Neubert, K., L. Baláspiri and G. Losse:* Monatshefte **103**, 1575 (1972).
[18] *Baláspiri, L., Gy. Papp, P. Pallai and K. Kovács:* Acta Phys. et Chem. Szeged **20**, 105 (1974).
[19] *Baláspiri, L., B. Penke, Gy. Papp and K. Kovács:* Acta Phys. et Chem. Szeged **20**, 465 (1974).
[20] *Baláspiri, L., J. Lonovics, K. Kovács:* unpublished results.

СИНТЕЗ АНАЛОГОВ БРАДИКИНИНА, СОДЕРЖАЩИХ ПИПЕКОЛИНОВУЮ КИСЛОТУ

Я. Балашпири, Дь. Папп, М. Тот, Ф. Широкман и К. Ковач

Описан синтез, очистка и физические характеристики аналогов брадикинина, содержащих оптически активную — L- и D-пипеколиновую кислоту.

INFRARED SPECTROSCOPIC EXAMINATION OF HUMIC ACIDS I.

By

S. SIPOS and É. SIPOS

Institute of Colloid Chemistry, Attila József University Szeged, Hungary

(Received 18th October, 1979)

The infrared spectroscopic examination is highly applicable to determine the functional groups, bond-types and structures of humic acid samples of different origins, if the samples are divided into several homogeneous fractions with a suitable method.

The products obtained in the fractionation of humic acid extracted from Oroszlány brown coal display characteristic values. With the increase in the number of the fractions, the molecular weight rises and increasingly intense peaks appear in the infrared spectrum. In parallel with the increase in the molecular weight, besides the development of the aliphatic side-chains, the increase in the aromatic nature is striking. The infrared spectra of the fractions of humic acid extracted from compost soil indicate a considerably different structure compared with that of brown coal humic acid. In these samples the aromatic character dominates.

Infrared spectroscopy is one of the currently most important research and analytical methods, and is widely used in structural examinations. In the past decade an increasing number of papers have been published on the structural examination of humic materials by infrared spectroscopy.

According to certain research workers [1—3], humic materials originating from different places differ in the proportions of certain functional groups, but the similarity of their spectra indicates materials of similar structure. BUTLER and LADD [4] carried out a detailed analysis of the differences in humic acid preparations obtained by different extraction procedures. They found that the method applied during extraction results in essential differences in the infrared spectrum. According to DORMAAR [5], the infrared spectra of different soil humic acids depends to a great extent on the structure of the soil, the thickness of the layer and the molecular weight of the sample. ISHIWATARI [6] examined the structures of fulvic and humic acids extracted from the sediment of lakes and from the soil, also applying spectroscopic methods. He compared the functional group, the molecular weight and the element analysis data. He found that in the visible and ultraviolet regions there is no essential difference in the spectra of the samples; however, in the infrared region, significant differences can be found, depending on the extent of humification. KHAN [7] examined heat-treated humic acid fractions. He observed that heat-treatment does not cause a significant change in the infrared spectrum. GOH and STEVENSON [8] compared synthetic and natural humic acids on the basis of their infrared spectra. Certain synthetic materials (*e.g.* catechol and benzoquinone types) show a slight, but others a strong similarity with soil humic acids. NUTTER and DAVIS [9] examined

preparations obtained by ultrafiltration, as well as metal humate complexes. On the basis of their experimental data, they declared that the course of complex-development can be followed very well by means of the infrared technique.

During the past few years we have carried out series of measurements in which infrared spectroscopy was used to establish the chemical compositions of coal samples of different ages and products made from them and to characterize certain preparations. The method proved applicable in the determination of the characteristic bonds of the samples examined and the nature of the functional groups; it was also possible to deduce the quantity of the latter. With this method it was possible to choose the optimum extracting conditions for certain preparations and, complemented by analytical procedures, to trace the degree of carbonification of coals. These examinations were reported earlier [10—13].

Colloid chemical examinations of humic acids extracted from coals [14—17] proved that, for a clearer picture of the structure, the preparations obtained, must be fractionated further, since they show considerable heterodispersity in their original state. This heterodispersity can be observed in the infrared spectra of the humic materials where only a few, mainly broad overlapping bands can be observed.

Since our previous examinations revealed that, as a result of the interaction of the functional groups, the broad bands in the infrared spectra taken before fractionation are compound ones, our aim was further gel-chromatrographic fractionation and examination of the resulting humic acid preparations. The infrared spectra of the fractions were compared with those of the humic acid samples before fractionation.

Our investigations were carried out on a humic acid sample extracted from Eocene brown coal from Oroszlány. The methods of extracting the humic acids [18] and purifying the crude products [19] were described earlier. For comparison, a humic acid extracted from a compost soil was also examined; this was purified by similar operations as for the coal humic acid.

To obtain preliminary information, infrared spectra were taken of the two materials. Figures 1 and 2 show only a few, mainly broad overlapping bands. Such spectra suggest that heterodisperse materials were obtained in the extraction. This is supported by gel-fractionation examinations on the same materials, whose distribution curves indicate considerable heterogeneity. Gel-fractionation examinations were carried out as described previously [20].

For infrared spectroscopy, 1—2 mg sample was homogenised with 200 mg KBr in an agate mortar. Pellets were then formed at 11 atm pressure. Spectra of the pellet preparations were taken with a Spectromom 2000 spectroscope over a 5-minute measuring time in the 650—4000 cm^{-1} wavenumber range. The applied concentration and layer thickness gave band transmission values within the 20—70% region.

Preparative fractionation was carried out on the two humic acid samples on a Sephadex G-75 column, 6 cm in diameter and 40 cm in height [20]. 5 fractions of coal humic acid and 4 of compost humic acid were obtained. The quantity of each fraction was 2—3 mg. With molecular weight standards and calibration curves the molecular weights of the fractions were calculated from the gel-fractionation data, and then, on the basis of the percentage compositions of the fractions, the harmonic means of the molecular weights of the two humic acids were obtained. These data are given in the Table I.

Table I

Molecular weight fractions at different samples

Sample	Number and molecular weight of fractions ($M \cdot 10^{-3}$)					Harmonic mean molecular weight ($M \cdot 10^{-3}$)
	1	2	3	4	5	
Oroszlány brown coal humic acid	1.5	5	10	25	40	7.5
Compost soil humic acid	4.0	12	25	60	—	24.0

It is evident from the Table that the brown coal humic acid contains fractions of considerably lower molecular weight than the soil humic acid. As regards the similarity or difference of their structures, an answer can be expected from the infrared spectra.

The spectra taken of the humic acid extracted from Oroszlány brown coal, as well as of the 5 fractions of this sample, are shown in Fig. 1. The characteristic bond and group frequencies in Fig. 1 were evaluated on the basis of the literature and our own experience, as follows.

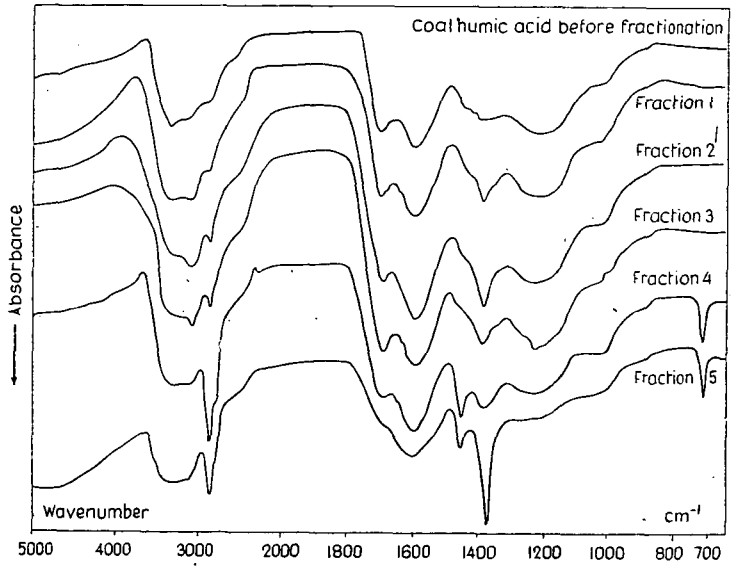

Fig. 1. Infrared spectra of coal humic acid fractions

No sharp peaks can be observed in the infrared spectrum of the sample before fractionation. Only in the 3000—3500 cm^{-1} region can there be found a very broad diffuse band, which is of a similar structure in the case of the fractions, too. A small peak can be observed at 3100 cm^{-1} only in the cases of the 2nd and 3rd fractions. This is due to the presence of amides. A smaller broad band is found around 1700 cm^{-1}, and a larger one near 1600 cm^{-1}. The former corresponds to the C=O

of the carboxyl goups of the humic acid, the latter to the valency vibrations of the carboxylate ion. A slight shoulder can also be found at 1400 cm^{-1}, and a very flat, broad band near 1200 cm^{-1}. The identification of these bands is uncertain with such great heterodispersity.

In the first fraction of this sample a small sharp shoulder appears at 2850 cm^{-1}; this becomes more and more intense in the later fractions. In the 4th fraction a very intense, long peak can be found at the same wavenumber. In the 5th fraction the intensity of the peak decreases slightly. This peak indicates the presence of aliphatic (CH, CH_2 and CH_3) groups. This tendency is well supported by the data shown in Table 1: with the increase in the number of fractions, the molecular weight increases as well. In the higher fractions sharper peaks can be observed, which proves the presence of humic acids of greater molecular weight (more aliphatic chains). There is a seemingly contradictory fact in connection with this tendency, *i.e.* the intensity of the band decreases in the 5th fraction. At the same time, a very sharp peak appears in this fraction at 1360 cm^{-1}; this is due to the presence of aromatic carboxylic acids. (This peak appears in very weak form in the 4th fraction). Furthermore, there is a sharp band at 720 cm^{-1}; according to the literature, this corresponds to a C—C skeletal vibration and to a $(CH_2)_n$ grouping, where $n=4$ or more. In the case of fractions 1—4 the vibration of the carboxylic C=O groups can be observed in the range 1700—1720 cm^{-1}, with increasing intensity between fractions 1 and 3. In the 4th fraction this peak is smaller, and it has disappeared completely in the 5th fraction. In the 4th and 5th fractions a sharp peak appears at 1460 cm^{-1}. This corresponds to the deformation vibrations of the CH_2 and CH_3 groups on aromatic rings. This is in accordance (especially in the case of the 5th fraction) with the development of the aromatic character found in the region of 1360 cm^{-1}. According to the spectrum, besides the aromatic characteristics, sidechains can also be found on the ring in the case of these two fractions of highest molecular weight. Each fraction has a characteristic band of the same width and intensity around 1600 cm^{-1}. This corresponds to the C=C bond and the carboxylate ion valency vibration. The presence of these bands might mean that the system contains not only covalent bonds, but also ionic COO^- groups. This fact is well supported by some of our metal ion-induced aggregation examinations carried out previously [21], in which it was found that a proportion of the metal humates are ionically bound.

In the 3rd fraction a small peak can be observed at 1240 cm^{-1}; this indicates the presence of phenolic OH groups. There is a shoulder at 1020 and 1030 cm^{-1} in the case of the 1st, 3rd and 4th fractions, which might mean silicate-contamination or polysaccharides in the sample.

Similary to the coal humic acid sample, the humic acid sample extracted from compost soil shows a spectrum containing scarcely evaluable, flat, broad bands before fractionation. After fractionation, however, evaluable, characteristic bands appear in the spectra of the fractions. These can be seen in Fig. 2. On comparison of these spectra with those demonstrated in Fig. 1, the difference is obvious. The fractions of soil humic acid show completely different characteristic values. Only the region above 3000 cm^{-1} is similar to the spectrum of the fraction of brown coal humic acid. The 3500—3600 cm^{-1} region for the soil humic acid differs slightly from this, *i.e.* here the broad band is divided into two parts. It may be assumed

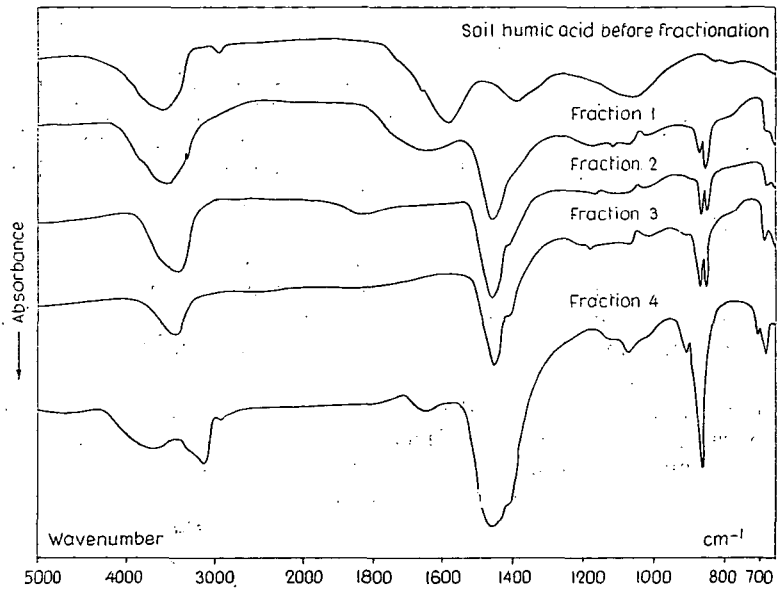

Fig. 2. Infrared spectra of soil humic acid fractions

that in this fraction the humic acid in the solid sample has a cyclic dimeric structure, and its OH valency vibration band is different from that of the other intermolecularly-associated compounds.

The 1720 and the 1620 cm^{-1} bands in the spectrum of the coal humic acids, which prove the presence of carboxyl groups and carboxylate ions, are absent here from each fraction. However, the deformation vibrations of the CH_3 and CH_2 groups on the aromatic ring appear as very intense bands in the spectra of each fraction, at 1450 cm^{-1}. In the 2nd, 3rd and 4th fractions, the valency vibration of aromatic carboxylic acids can be observed with a small shoulder at 1380—1400 cm^{-1}. The mainly aromatic nature of the samples is proved by the characteristic value of the deformation vibration at 860 cm^{-1}, which appears with increasing intensity, parallel with the increase in the number of the fraction; this is typical of 1,3,5-tri-substituted aromatic compounds. A band characteristic of substituted aromatic compounds can be found with the same tendency at 680 cm^{-1}. In the 3rd fraction there is only a small shoulder at 1060 cm^{-1}, but in the 4th it is a small peak; it is characteristic of polysaccharides indicative of plant fossil remains. It is absent from the earlier fractions, probably because of decomposition. In the 3rd fraction, and to a smaller extent in the 2nd fraction, there is a deformation vibration at 1220 cm^{-1}, characteristic of the C—N and N—H groups.

The 2850 cm^{-1} region, indicating aliphatic character, shows absorption in the form of a small shoulder in the 4th fraction, which has the highest molecular weight.

The examinations permit the statement that the infrared spectra of the humic acid samples before fractionation cannot be evaluated unambiguously, owing to their heterodispersity. The broad bands found in these spectra are highly complex

as a result of the interaction of the functional groups of the fractions; the characteristic bond and group frequencies overlap.

The products obtained in the fractionation of humic acid extracted from Oroszlány brown coal display characteristic values. With the increase in the number of the fractions, the molecular weight rises and increasingly intense peaks appear in the infrared spectrum. In parallel with the increase in the molecular weight, besides the development of the aliphatic side-chains, the increase in the aromatic nature is striking.

The infrared spectra of the fractions of humic acid extracted from compost soil indicate a considerably different structure compared with that of brown coal humic acid. In these samples the aromatic character dominates. The intensity increase of the band runs parallel with the increasing molecular weight in the case of these samples, too.

To summarize, it can be stated that the infrared spectroscopic examination is highly applicable to determine the functional groups, bond-types and structures of humic acid samples of different origins, if the samples are divided into several homogeneous fractions with a suitable method.

References

[1] *Theng, B. K., J. Wake, A. M. Posner:* J. Soil. Sci. **18**, 349 (1967).
[2] *Visser, A. S.:* J. Soil. Sci. **15**, 202 (1964).
[3] *Dormaar, J. F., M. Metche, F. Jacquin:* Soil. Biol. Biochem. **2**, 285 (1970).
[4] *Butler, J. H., J. N. Ladd:* Aust. J. Soil Res. **7**, 229 (1969).
[5] *Dormaar, J. F.:* Goderma **1**, 37 (1967).
[6] *Ishiwatari, R.:* Adv. in Org. Geochem. Proc. of 3rd Internat. Conf. 285 (1970).
[7] *Khan, S. U.:* J. Soil Sci. **112**, 401 (1971).
[8] *Goh, K. M., F. J. Stevenson:* J. Soil Sci. **112**, 392 (1971).
[9] *Nutter, Jr., E. Davis:* Geochim. et Cosmochim. **40**, 369 (1976).
[10] *Sipos, S., Siposné É. Kedves, T. Széll:* Szegedi Tanárképző Főiskola Tudományos Közleményei 177 (1965).
[11] *Siposné Kedves É., S. Sipos:* Szegedi Tanárképző Főiskola Tudományos Közleményei 207 (1969).
[12] *Siposné Kedves É., S. Sipos:* Szegedi Tanárképző Főiskola Tudományos Közleményei 141 (1973).
[13] *Sipos, S., Siposné É. Kedves:* Szegedi Tanárképző Főiskola Tudományos Közleményei 157 (1971).
[14] *Sipos, S., Siposné É. Kedves, I. Dékány:* Szegedi Tanárképző Főiskola Tudományos Közleményei 223 (1970).
[15] *Sipos, S., Siposné É. Kedves:* Szegedi Tanárképző Főiskola Tudományos Közleményei 157 (1972).
[16] *Sipos, S., I. Dékány, A. Deér, É. Sipos, I. Horváth:* Acta Phys. et Chem. Szeged **20**, 437 (1974).
[17] *Sipos, S., É. Sipos, I. Dékány, A. Deér, I. Horváth:* International Peat Symposium, Gdansk 111 (1974).
[18] *Sipos, S., Siposné É. Kedves, I. Dékány, A. Deér, T. Meisel, B. Lakatos:* Agrokémia és Talajtan **23**, 313 (1974).
[19] *Sipos, S., W. Rochus:* Kongress Report **4**, 351 (1976). Posnan
[20] *Sipos, S., É. Sipos, I. Dékány, A. Deér, J. Meisel, B. Lakatos:* Acta Agron. Acad. Sci. Hung. *27*, 31 (1978).
[21] *Sipos, S., Siposné É. Kedves, I. Dékány, B. Lakatos:* VI. Szénkémiai Ankét Monográfia, Budapest. 61 (1972).

ИНФРАКРАСНАЯ СПЕКТРОСКОПИЯ ГУМИНОВЫХ КИСЛОТ, I

Ш. Шипош и Э. Шипош

Авторы провели ИК-спектроскопическое изучение различных фракций гуминовых кислот, разделенных гель-хроматографией. ИК-спектры фракций сравнивали со спектром исходных образцов. Найдено, что только фракционированные образцы имеют спектры, обладающие характерными полосами пригодными для соответствующего отнесения. Показано, что в гуминовой кислоте из других углей, вместе с увеличением молекулярного веса, наряду с появлением алифатических боковых цепей появляется также ароматический характер. В фракциях гуминовых кислот из компостных почв показана преобладающая роль ароматических участков. Использованный метод, по полученным данным, показывает его применимость для определения структуры и состава различных гуминовых кислот.

ИССЛЕДОВАНИЕ ИНИЦИИРУЮЩЕЙ АКТИВНОСТИ ФУНКЦИОНАЛЬНО-ЗАМЕЩЕННЫХ МОНО- И ДИПЕРЕКИСЕЙ ПРИ ПОЛИМЕРИЗАЦИИ СТИРОЛА В МАССЕ И ЭМУЛЬСИИ

В. И. ГАЛИБЕЙ

Кафедра физико-химии полимеров университета им. И. И. Мечникова, Одесса

Т. А. ТОЛПЫГИНА

Кафедра общей химии института инженеров морского флота, Одесса

И. А. АНДОР

Кафедра общей и физической химии университета им. Аттилы Йожефа, Сегед

(Поступило в редакцию 25 сентября 1979 г.)

Исследована связь между строением и инициирующей активностью при полимеризации стирола ряда моно- и диперекисей с функциональными группировками. Показано, что увеличение числа оксиэтиленовых группировок в центральной части молекулы диперекисей не сказывается на инициирующей активности при полимеризации в массе, но приводит к возрастанию скорости эмульсионной полимеризации.

В последнее время значительное внимание уделяется синтезу и исследованию органических перекисей, содержащих различные функциональные группировки [1—3]. Введение заместителей в молекулу перекиси в первую очередь сказывается на ее термической устойчивости — основной характеристике перекисных инициаторов. Полимеры, полученные с применением функционально, замещенных перекисей и содержащие реакционно-способные концевые группы могут принимать участие в различных макромолекулярных реакциях (сшивание, блок-сополиконденсация [4], взаимодействие с красителями [5]) и иметь лучшую адгезию к полярным субстратам [6].

Настоящая работа посвящена исследованию связи между строением и инициирующей активностью при полимеризации стирола в эмульсии и массе ряда алифатических моно- и диперекисных соединений, содержащих сложноэфирные функциональные группировки.

В качестве объектов исследования выбраны моноперекисные соединения общего строения:

$$ROC(CH_2)_xCOOC(CH_2)_xCOR, \quad \text{где} \quad R = CH_3;\ C_2H_5;\ x = 2, 3,$$

а именно перекиси бисметоксисукцинила (I), бисэтоксисукцинила (II), бисэтоксиглутарила (III); а также диперекиси общего строения

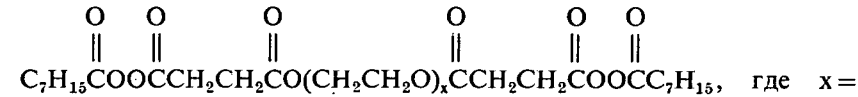

где x = 1, 9, 13,

а именно: α,ω-ди-о,о-каприлил-(бисперокисукцинил)этиленгликоль (IV), α,ω-ди-о,о-каприлил-(бисперокисукцинил)нонаэтиленгликоль (V), α,ω-ди-о,о-каприлил-(бисперокисукцинил)тридекаэтиленгликоль (VI).

Синтез перекисей проводили по методике [7—8]. Содержание основного продукта составляло 96—100%. Методика проведения эксперимента описана ранее [9]. Константы инициирования ($k_{ин}$) полимеризации рассчитывали по основному уравнению полимеризации из значений скоростей полимеризации ($v_{пол}$) и соотношения констант роста и обрыва ($k_p/k_0^{0,5}$) [10]. Термоустойчивость перекисей оценивали по константам скорости разложения ($k_{разл}$) в этилбензоле в атмосфере аргона.

Кинетические измерения показали, что разложение всех перекисей подчиняется уравнению первого порядка. Результаты термолиза перекисей приведены в табл. I, там же приведены значения $k_{разл}$ перекиси бутирила (ПМК), взятые из [11].

Таблица 1

Кинетические параметры термического разложения перекисей в этилбензоле

Перекись	$K_{разл} \cdot 10^5$, сек$^{-1}$ при температурах, °С						E_a, ккал/моль
	65	75	80	85	90	95	
I			4,8	9,3	17,0	31,0	31,2
II			6,0	12,0	20,0	35,0	30,6
III			10,0	18,3	36,3	59,6	31,2
IV	1,5	4,1		21,9		69,2	28,8
V	1,7	6,6		17,8		97,2	27,9
VI	1,3	4,5		19,1			30,6
ПМК		7,0		27,8			29,8

Сопоставление термоустойчивости исследуемых моноперекисных соединений I—III с термоустойчивостью незамещенной ПМК указывает на стабилизирующее влияние сложноэфирного заместителя, обладающего отрицательным индукционным эффектом. Увеличение расстояния между перекисной и сложноэфирной группировками приводит к возрастанию константы скорости термического разложения, которая, однако, у III остается меньшей, чем у незамещенной ПМК.

Диперекиси IV—VI распадаются несколько медленнее ПМК, но быстрее моноперекисей I—III. Это связано с тем, что у моноперекисей перекисная связь подвергается двухстороннему стабилизирующему влиянию сложноэфирных группировок, в то время как у диперекисных соединений обе перекисные связи стабилизируются аналогичными сложноэфирными группировками только с одной стороны.

Как следует из табл. I, количество оксиэтиленовых группировок, расположенных в центральной части молекулы диперекиси, практически не влияет на термоустойчивость перекисных связей.

Изучена полимеризация стирола в массе, инициированная исследуемыми перекисями. Результаты эксперимента приведены в табл. II.

Как следует из сопоставления данных табл. I и II, в ряду алифатических диацильных моно- и диперекисей скорости инициирования изменяются в том же порядке, что и скорости их термического разложения.

В случае инициирования полимеризации диперекисью IV характеристическая вязкость ([η]) полистиролов возрастает по ходу процесса от 0,22 до 0,76 (при концентрации 0,05 осново-моль/л), т. е. в значительно большей степени, чем при инициировании диацильными моноперекисями [11—12]. Резкое нарастание [η] образующихся полимеров на глубоких стадиях превращения объясняется не только реакцией передачи цепи на полимер, но и возможностью дальнейшего роста макромолекул полистирола, полученных в присутствии диперекисей, за счет разложения концевых перекисных групп. Так, по данным иодометрии у полистирола, полученного в присутствии IV и выделенного на глубине превращения 10% на макромолекулу приходится в среднем около одной перекисной группы; у полимера, выделенного на глубине превращения 90%, концевые перекисные группы практически полностью отсутствуют.

Таблица II

Кинетические параметры полимеризации стирола в массе

Инициатор	Температура, °С	Концентрация инициатора, осново-моль/л	$v_{пол} \cdot 10^4$, моль/л·сек	$k_{ин} \cdot 10^4$, сек$^{-1}$
I	95	0,05	13,4	
		0,0125	7,1	
		0,005	4,16	2,04
		0,001	1,96	
II	95	0,05	15,5	
		0,025	11,3	
		0,0125	7,73	2,6
		0,005	4,82	
		0,001	2,11	
III	95	0,05	22,5	
		0,025	15,0	
		0,0125	10,5	5,14
		0,001	3,23	
IV	85	0,1	13,4	
		0,05	10,0	
		0,025	7,3	1,6
		0,0125	5,6	
V	85	0,0134	7,88	3,4
	95	0,0134	16,7	11,5
VI	85	0,0134	7,34	3,0
	95	0,0134	15,1	9,2

Образование «активных» полимеров на начальных стадиях полимеризации и последующее разложение концевых перекисных групп в ходе полимеризации, сопровождающееся дальнейшим ростом макромолекул, подтверждено анализом ИК-спектров. В спектре полистирола, выделенного на глубине превращения 10%, имеется полоса поглощения в области 1760 $см^{-1}$ и дублет полос в области 1800—1830 $см^{-1}$, характерных для карбонильного поглощения сложных эфиров и диацильных перекисей, соответственно [13]. В полистироле, выделенном на глубине превращения 90%, присутствует только полоса сложноэфирного карбонильного поглощения (1760 $см^{-1}$) [14].

Ранее [15] было показано, что диперекиси, содержащие оксиэтиленовые группировки, обладают поверхностно-активными свойствами. Увеличение полярной части молекулы диперекиси за счет перехода от производных этиленгликоля (IV) к производным нонаэтиленгликоля (V) и тридекаэтиленгликоля (VI) увеличивает водорастворимость перекисей и уменьшает их растворимость в мономере. Исследование поверхностных свойств водных растворов соединения V показало, что диперекись понижает поверхностное натяжение воды до 40 $эрг/см^2$.

Нам представлялось интересным исследовать эмульсионную полимеризацию стирола, инициированную такого типа перекисными соединениями.

Эмульсионную полимеризацию проводили при 60° в дилатометрах с магнитной мешалкой. Соотношение фаз мономер: вода составляло 1: 9. В качестве эмульгатора применяли оксиэтилированный эфир ангидросорбита лауриновой кислоты (твин-20). Необходимое количество инициатора рассчитывали на фазу мономера, эмульгатора — на водную фазу.

Для выяснения оптимальной концентрации эмульгатора предварительно была изучена зависимость скорости полимеризации от концентрации твина-20 в присутствии постоянного количества перекиси бензоила (ПБ). Концентрацию эмульгатора варьировали в пределах 1—5%. Для работы была выбрана концентрация эмульгатора 2%, как сравнительно низкая и гарантирующая постоянство скорости процесса при незначительных колебаниях концентрации твина-20. Экспериментальные результаты по изучению зависимости скорости эмульсионной полимеризации от природы и концентрации инициатора приведены на рисунке.

Как видно из рисунка, увеличение концентрации инициатора в области низких концентраций приводит к возрастанию скорости полимеризации, затем кривая, проходя через максимум, понижается и достигает определенного предела. Для ПБ и плохо растворимой в воде диперекиси IV максимум скорости полимеризации небольшой и лежит в области 0,005—0,01 осново-моль/л мономера. Для соединения V максимальное значение скорости полимеризации сдвинуто в сторону больших концентраций (0,01—0,02 осново-моль/л). Для хорошо растворимого в воде соединения V скорость полимеризации достигает значительно большей величины, чем для плохо растворимых ПБ и IV. Такое различие в скорости эмульсионной полимеризации не связано с термической устойчивостью перекисей. Возрастание скорости полимеризации в ряду диперекисных соединений, обладающих поверхностно-активными свойствами, с увеличением полярной части их молекул, а следовательно, и водорастворимости, по-видимому, связано с возможностью более легкого перехода в водную фазу и поступ-

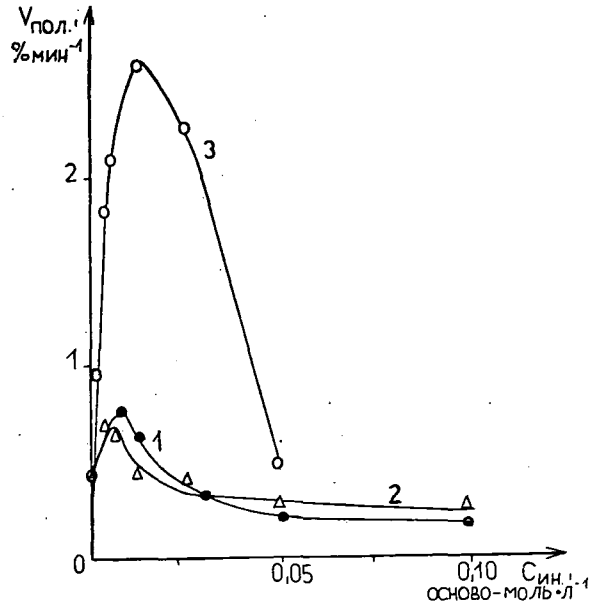

Рис. 1. Зависимость скорости полимеризации стирола от концентрации инициатора; соотношение фаз 1: 9, концентрация эмульгатора твина-20 — 2%, температура 60 °С: I—IV, 2 — ПБ, 3 —V.

ления в мицеллы эмульгатора, где при их ориентации в поверхностном слое создаются условия для более легкого термолиза.

Несмотря на значительное различие в скоростях полимеризации, молекулярные массы полимеров, образующихся в присутствии диперекисных соединений IV и V, близки и закономерно уменьшаются с возрастанием концентрации инициаторов.

Таким образом, увеличение числа полярных оксиэтиленовых группировок в центральной части молекулы диперекиси не сказывается на ее инициирующей активности при полимеризации в массе и повышает активность диперекиси при инициировании эмульсионной полимеризации стирола.

Литература

[1] *Антоновский, В. Л.:* Органические перекисные инициаторы, «Химия», Москва, 1972, ст. 378.
[2] *Рахимов, А. И.:* Химия и технология органических перекисных соединений, «Химия», Москва, 1979, ст. 128.
[3] *Галибей, В. И., И. Лабади, И. А. Андор:* Acta Phys. et Chem. Szeged, **23**, 287 (1977).
[4] *Колесников, Г. С., Л. К. Яралов:* Успехи химии, **34**, 454 (1965).
[5] *Виноградова, С. В., И. П. Антонова-Антипова:* сб. Прогресс полимерной химии, «Наука», Москва, 1969, ст. 375.
[6] *Берлин, А. А., В. Е. Басин:* Основы адгезии полимеров, «Химия», Москва, 1969, ст. 247.
[7] *Галибей, В. И., Т. А. Толпыгина, И. С. Волошановский:* Изв. высших учебных заведений, Химия и химическая технология, **19**, 1032 (1976).

[8] *Галибей, В. И.:* Ж. общ. хим., **44**, 2363 (1974).
[9] *Галибей, В. И., А. И. Юрженко, С. С. Иванчев:* Укр. хим. ж., **29**, 1282 (1963).
[10] *Багдасарьян, Х. С.:* Теория радикальной полимеризации, «Наука», Москва, 1966, ст. 34.
[11] *Галибей, В. И.:* Изучение ацильных перекисей как инициаторов полимеризации, Канд. дисс., Одесский госуниверситет, 1965, ст. 101.
[12] *Иванчев, С. С., В. И. Галибей, А. И. Юрженко:* Высокомолек. соед., **7**, 74 (1965).
[13] *Иванчев, С. С., А. И. Юрженко, Ю. Н. Анисимов:* Ж. физ. химии, **39**, 1900 (1965).
[14] *Holly, S., P. Sohár:* Infravörös spektroszkópia (Инфракрасная спектроскопия), Műszaki Könyvkiadó, Budapest, 1968. 83. o.
[15] *Галибей, В. И., Л. В. Дудник, Т. А. Толпыгина, А. Б. Петрова, В. И. Соколова:* Высокомолек. соед., А **19**, 1321 (1977).

INVESTIGATION OF SUBSTITUTED MONO- AND DIPEROXIDES AS INITIATORS IN THE BULK AND EMULSION POLYMERIZATION OF STYRENE

V. I. Galibej, T. A. Tolpygina, J. A. Andor

The authors have investigated the correlation between the structure and initiating activity of different substituted mono- and diperoxides for the polymerization of styrene. It was shovn that the increase of ethyleneoxy groups in the peroxyde molecule had no effect on the initiating activity in the bulk polymerization, while, in the case of emulsion polymerization a rate increase was observed.

ADSORPTION OF POLY(VINYL ALCOHOL) AND ITS EFFECT ON THE ELECTROSURFACE CHARACTERISTICS OF SOME OXIDES

By

B. E. PLATONOV[1], A. A. BARAN[2], and T. A. POLISCHUK[1]

(Received 16th October, 1979)

The adsorption of poly(vinyl alcohol) (PVA) from dilute (up to 3 g/l) aqueous and electrolyte solutions onto some oxides, and its effects on the surface charge density σ and the ζ-potential, have been studied. With rise of the acetate group content (from 2% to 18%) in the PVA molecule the adsorption increases on Fe_2O_3 and gives a maximum at 12% on ZnO. The adsorption values on ZnO, NiO, Fe_2O_3, ZrO_2 and MnO_2 increase with the pH, whereas on SiO_2 the opposite picture is observed. The assumption is made that on the surface of oxides with high points of zero charge (ZnO) the PVA adsorbs on the water layer tightly bound with the surface, without squeezing out the water molecules. The adsorption data are explained from the standpoint of the formation and adsorption of aggregates of macromolecules. The effect of PVA adsorption on the ζ-potential of quartz is due to the shift of the slipping plane toward the solution as a result of the formation of thick polymer sheaths around the particles, whereas for ZnO this effect operates together with the changing of the surface charge density.

Introduction

The increasing interest in polymer-containing disperse systems is due to the important role of these systems in different branches of modern technology. Water-soluble polymers are widely used as effective flocculants and stabilizers, soil-improvers and structure-regulating agents, *etc.* In particular, poly(vinyl alcohol) (PVA) is used in the ceramic, metallic and oxide power industries, and in the building materials industry as plastifiers and adhesives. The development of a scientific basis for the regulation and prognosis of the properties of such dispersions presupposes the investigation of PVA adsorption on the surface of oxides. Valuable information on the structure of adsorption layers may be obtained from electrosurface measurements.

Technical oxides represent complex multicomponent systems with different contaminations and with low specific surfaces; therefore, as the first stage, we have studied the adsorption of PVA from dilute (up to 3 g/l) solutions onto the surfaces of the individual oxides which are the main components of such materials. In some cases the adsorption measurements were completed by electrokinetic and potentiometric experiments.

[1] Teacher's Training College, Kiev, U.S.S.R.

[2] Institute of Colloid Science and Water Pollution, Control of the Ukranian Academy of Sciences, Kiev.

Experimental

Materials. Industrial samples of PVA were used. The parameters of the macromolecules in aqueous solutions, determined from viscosimetric data, are listed in Table I. The polymer was dissolved at 80° during 3—4 hours. PVA working solutions were prepared from stock solutions of 10 g/l concentration. Since the structure and the properties of PVA solutions change with time, the applied solutions were stored for 7 days before use. The polymer and salt solutions were mixed one day before the experiments.

Table I

The Characteristics of the Samples of Polyvinyl Alcohol

Sample of PVA	The content of the acetate groups, %	$[\eta]$, dl/g	$\overline{M}$
PVA-1	2	0.70	56,000
PVA-2	12	0.59	50,000
PVA-3	18	0.57	59,000
PVA-4	18	0.76	98,000

Industrial oxides of zinc, zirconium, iron and silicon were investigated. According to spectral analysis, the admixture content was not more than 0.3% in Fe_2O_3, and less than 0.1% for other oxides. The BET surface areas for ZnO, Fe_2O_3, ZrO_2 and SiO_2 were 4.4, 9.0, 2.2 and 175 m^2/g, respectively. For electrokinetic measurements quartz powder with a particle diameter of 45—80 nm was used. The quartz was preliminarily ground, washed with concentrated HCl and distilled water, ignited and fractionated.

All the reactants were of chemical grade and were used without further purification.

Methods. The adsorption values were calculated from the material balance of PVA in the solution before and after its contact with the adsorbent. The polymer concentration was determined by a colorimetric method according to [1]. The solid phase was separated from the solution by centrifugation at 2000 g during 3—4 min. The contact time in all adsorption, electrokinetic and potentiometric experiments was 24 hours.

The electrokinetic potential was determined by the potential streaming method described in detail in [2]. Under the experimental conditions the value of the Rel criterion [3] ($Rel = e^{\psi\sigma/2} - 1/\varkappa a$, where a is the mean radius of the capillary, $\varkappa$ is the reciprocal Debye thickness, and $\bar{\psi}_\delta$ is the dimensionless Stern potential $= \psi ez/kT$; for ψ_δ the measured ζ-potential without polymer addition was taken) was considerably smaller than unity; therefore, the correction on polarization of the electric double layer (DL) could be neglected [3], and the ζ-potential values could be estimated according to the Smolouchowsky formula. The conductivity of ZnO particles themselves is insignificant ($\approx 10\%$) in comparison to the general conductivity of a moisture-saturated diaphragm. Nevertheless, taking into consideration such a complication, the obtained values of ζ were used only for qualitative assessment of the effect of PVA adsorption on the DL structure of a ZnO surface.

Potentiometric titration was conducted by the rapid titration method in KCl solutions, as described in [4, 5]. In the case of ZnO the titration was restricted to pH=8—10, and the correction for dissolution was introduced according to [6]. The following points of zero charge (p.z.c.) (in pH units) were obtained: SiO_2 3.1; ZrO_2 4.0; ZnO 8.9; Fe_2O_3 6.0; these values are in good accordance with data reported in the literature.

pH measurements were carried out with glass electrodes and a "pH—340" pH-meter.

The viscosity of polymer solutions was measured with an Ubbelohde viscosimeter at 25°.

Results

Adsorption isotherms. Figures 1 and 2 show the adsorption isotherms of PVA samples with different acetate group contents on zinc oxide and iron oxide surfaces. For PVA-1 and PVA-2 on ZnO they are characterized by a rapid rise in the low concentration region, reaching a plateau at high concentration. The shapes of the isotherms for PVA-3 and PVA-4 are more complex, with a maximum and a minimum (Fig. 1). Depending on the adsorption values on ZnO, the samples investigated

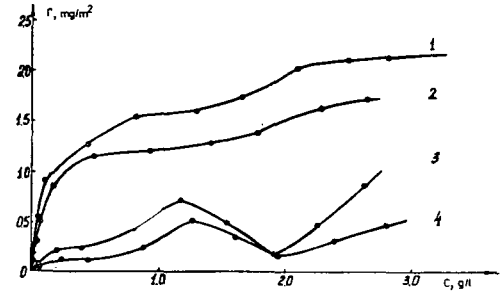

Fig. 1. Adsorption isotherms of PVA on ZnO surface: PVA-2 (1), PVA-1 2), PVA-3 (3), PVA-4 (4)

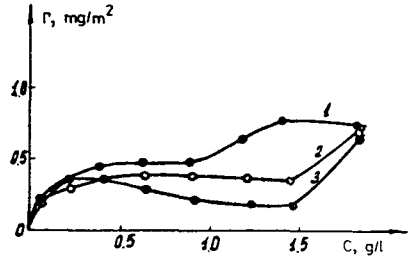

Fig. 2. Adsorption isotherms of PVA on Fe_2O_3 surface: PVA-4 (1), PVA-2 (2), PVA-1 (3)

can be arranged in the order PVA-2>PVA-1>PVA-3≈PVA-4. The adsorption value increases with the molecular weight more weakly than with the change of the acetate group content of the molecule (Fig. 1). For iron oxide the adsorption values Γ follow the sequence PVA-4>PVA-2>PVA-1. The analogous range for PVA adsorption on aerosil particles was obtained in [7]. The Γ values on Fe_2O_3 are less than on ZnO. This may be due to the considerable aggregation of particles in iron oxide suspensions with polymer additions.

The different adsorption behaviours of the oxides are revealed in the dependence of Γ on the pH (Figs. 3 and 4). In the case of zirconium oxide the adsorption increases with the pH. Such a dependence was obtained for PVA adsorption on zinc, aluminium, nickel and manganese oxides as well, whereas for iron and titanium oxides Γ depends only slightly on the pH. Silica is the only oxide for which the decrease of PVA adsorption with rising pH was observed (Fig. 4).

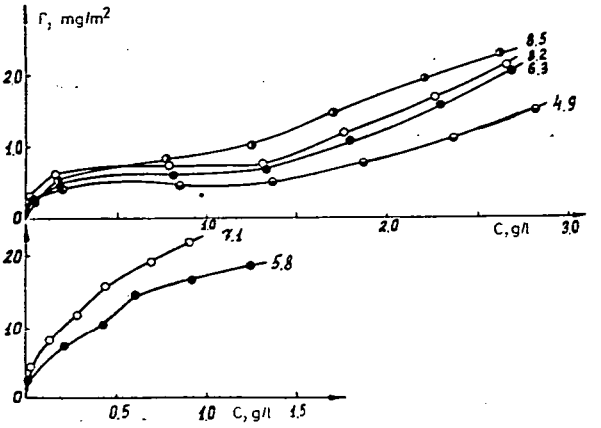

Fig. 3. Adsorption isotherms of PVA-1 on ZnO surface. pH values are indicated

The adsorptions of PVA-2 and PVA-4 from salt solutions onto the ZnO surface are shown in Fig. 5. The increase of the KCl concentration has practically no influence on the shapes of the isotherms at low PVA content (under 0.1 g/l), but at high polymer concentrations it leads first to the decrease and then to the gradual increase of the adsorption values. At the same time, with the increase of the KCl concentration the bends in the adsorption isotherms disappear or become smooth, then they appear again and shift to lower PVA contents (Fig. 5).

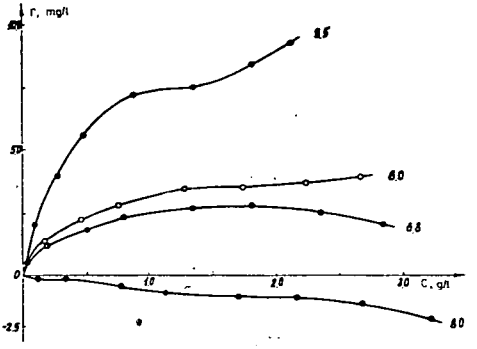

Fig. 4. Adsorption isotherms of PVA-1 on aerosil surface. pH values are indicated

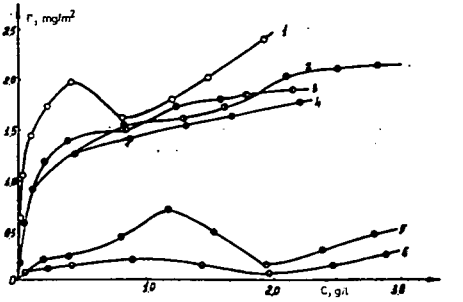

Fig. 5. Adsorption isotherms of PVA on ZnO surface from aqueous salt solution. Curves 1, 2, 3, 4 — PVA-2; 5, 6 — PVA-4. Concentration of KCl in the solutions: 1 — 10^{-2} M; 2,5 — 0; 3 — 10^{-3} M; and 4, 6 — $5 \cdot 10^{-4}$ M

Surface charge density. The potentiometric titration of SiO_2 in KCl solutions shows that PVA adsorption does not change the surface charge density σ of silica. The adsorption of PVA-1 from 10^{-2} M KCl shifts the p.z.c. of zinc oxide to higher pH and, consequently, σ to more positive values.

Electrokinetic potential. PVA adsorption affects the ζ-potential of oxide surfaces considerably, but in a rather complicated way (Figs. 6 and 7). In the case of SiO_2, for all the KCl concentrations investigated the marked decrease of ζ at low PVA content (under 0.2 g/l) region is observed. Then, with the increase of the PVA content, the dependence of the ζ-potential on the polymer concentration shows a maximum and a minimum. These extrema regions become less pronounced with the increase of the electrolyte concentration in the system. The complex character of the $\zeta(C_{PVA})$ plot for zinc oxide is observed too (Fig. 7). For example, small additions of PVA-4 cause the increase of ζ to values higher than the initial ones. In general, the elevation of the ionic strength leads to the decrease of the ζ-potential, which at high polymer concentrations reaches a value of zero.

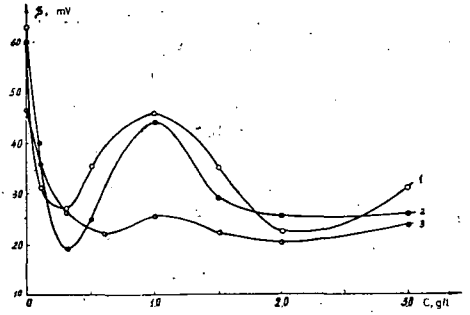

Fig. 6. Dependence of the ζ potential of quartz on the PVA-2 concentration in KCl solution: 1 — 0; 2 — $5 \cdot 10^{-4}$; 3 — 10^{-3} M KCl

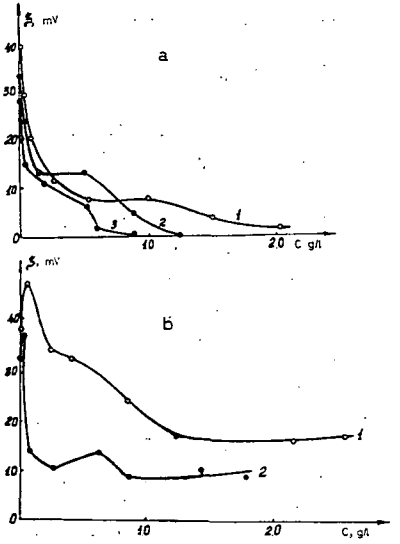

Fig. 7. Dependence of the ζ potential of ZnO on the equilibrium concentration of PVA in KCl solutions: a) PVA-2; b) PVA-4. Concentration of KCl: 0 (1), $5 \cdot 10^{-4}$ (2), 10^{-3} M (3)

Despite the rather complex character of the $\zeta(C_{PVA})$ dependences, in general a correlation exists between the adsorption and electrokinetic data: the addition of better adsorbable samples of PVA causes a more marked decrease of the ζ-potential; the shift of the bend in the $\zeta(C_{PVA})$ curves in KCl solutions corresponds to the shift of the bend in the adsorption isotherms (*cf.* Figs. 5 and 7).

Discussion

According to [9], the second virial coefficients of PVA in aqueous solutions, depending on the acetate group content in a molecule, may be put in the following order $A_2(12\%) > A_2(2\%) > A_2(18\%)$. In other words, the quality of water as a solvent for the polymers studied decreases in this sequence. Thus, it might be ex-

pected that the adsorption values would increase in this order. However, the experimental data point to the opposite picture (Fig. 1). This is, perhaps, explained by two factors.

A number of papers [9, 10] indicate that in aqueous solutions a tightly-bound adsorbed water layer (so-called W-layer) is present on oxide surfaces; this is not destroyed even by the addition of 90—95% of such organic solvents as alcohol, acetone, or dioxane [10], *i.e.* solvents which can firmly bind the water molecules with H-bonds. Thus, it is quite reasonable to suppose that in the cases under consideration the polymer adsorbs on the water layer bound with the surface due to the formation of hydrogen-bonds. A polymer possessing a greater affinity for water will adsorb better. The additional polarization of the water molecules in the W-layer affords the hydrogen-bond with it energetically more advantageously than with the water molecules in the liquid phase. Such a mechanism is the more probable because, as follows from [11], the energy of hydration of oxide surfaces increases with the increase of the p.z.c. This is especially valid for zinc oxide, which has a high value of the p.z.c. (8.9 pH units in our case).

On the other hand, it is known [12, 13] that aqueous PVA solutions have a complicated supermolecular structure which depends, among other factors, on the polymer concentration. At low PVA concentration the adsorption of individual macromolecules predominates and the formation of the supermolecular structure is the competitive process. In this region, polymer samples having a greater affinity for the solvent and giving less aggregates in solution, *i.e.* PVA-1 and PVA-2, will adsorb better. With the increase of the PVA concentration, the formation and adsorption of polymer aggregates will play a greater and greater role, which leads to the bends and extrema in the adsorption isotherms. In PVA-3 and PVA-4 solutions the formation of supermolecular structures begins at lower polymer contents than in the cases of PVA-1 and PVA-2. This results in smaller adsorption values for PVA-3 and PVA-4, narrowing the plateau at low polymer concentration, and in the complicated forms of the adsorption isotherms for these samples.

The assumption concerning the adsorption of polymer on the bound water layer is not strictly valid for iron oxide, on which the adsorption of PVA increases with the acetate group content per molecule. As in the case of the adsorption of PVA on silica [7], such regularities may be explained by the fact that even at low PVA-4 concentrations the degree of aggregation of macromolecules is high, and their adsorption leads to the large values of Γ for this sample. At the same time, the competition between adsorption and aggregation of macromolecules leads to a considerable decrease of Γ at PVA-1 concentrations higher than 0.4 g/l (Fig. 2).

The point of view exists that the adsorption of PVA on the surface of silica [14, 15] or metal oxides [16] is due to the formation of hydrogen-bonds between the OH groups of the polymer chain and non-dissociated acidic (basic) centers of the surface. If this is valid, the increase of Γ with approach to the pH of the p.z.c. should be expected (taking into account the shift of the p.z.c. by polymer adsorption). This model is in accordance with our results obtained for zinc, nickel, aluminium and silicon oxides (Fig. 4). At the same time, it does not explain the dependence of Γ on the pH for iron and titanium oxides and, especially, for oxides with low p.z.c. (MnO_2, ZrO_2); for these two oxides the adsorption of PVA continues to increase while the pH value rises by four units in comparison with the

p.z.c. (Fig. 3). The mechanism of adsorption of PVA on the surface of mineral oxides will be considered in detail in the following publications.

The standpoint on the adsorption of aggregates of macromolecules gives a reasonable explanation of the effect of electrolytes on the adsorption of PVA. With rising electrolyte concentration the quality of the solvent becomes worse; this effect promotes the formation of aggregates. The competition between the processes of aggregation and adsorption in $5 \cdot 10^{-4}$ M KCl is intensive, and this causes the decrease of Γ (Fig. 5). The disappearing of bends in the isotherms is evidence of the decrease in the adsorption of the aggregate. With further increase of the KCl content, the quality of the solvent gets poorer, which intensifies the adsorption of aggregates. This process is revealed in the PVA concentrations, which are the lower, the higher the concentration of salt. Accordingly, the bend in the isotherm shifts to smaller PVA concentrations and the Γ value begins to increase sharply (Fig. 5). Thus, the concept on the formation and adsorption of polymer aggregates developed by Lypatov and co-workers [17] enables us to explain the peculiarities of PVA adsorption from aqueous and electrolyte solutions onto the surfaces of oxides.

In [18—20] it was shown that the effect of adsorption of non-ionic polymers on the ζ-potential of disperse particles is due to the changes of the surface charge density and the shift of the slipping plane into solution as the result of formation of thick polymer sheaths around particles. The fact that PVA does not change the σ of SiO_2 shows that the decrease of the ζ-potential with polymer adsorption in this case is due to the second factor mentioned. The appearance of extrema in the $\zeta(C_{PVA})$ curves is connected with the changing of the polymer layer thickness, which reflects the changing of the dimensions of adsorbable kinetic units. In contrast, the appearance of extrema regions in the $\zeta(C_{PVA})$ curves is due to the simultaneous operation of both factors considered. The shift of σ to more positive values when PVA adsorption occurs leads to the increase of positive ζ-potentials; this is observed in experiments at really low electrolyte concentrations (Fig. 7). With increase of the PVA content in the system, the effect of the shift of the slipping plane predominates and the ζ potential decreases.

The increase of the ionic strength of the solution affects the structure of the double layer and the structure of the polymer sheath as well. With the assumption that the slipping plane coincides with the polymer sheath boundary, the calculated values of the thickness of the PVA-2 layer on the surface of quartz are 15—100 Å, depending on the KCl and PVA concentrations in solution. Despite some increase of polymer adsorption with electrolyte addition, the thickness of the adsorption layer decreases, which probably reflects the accumulation of less compact aggregates on the surface. Hence, the decrease of the ζ-potential of SiO_2 in an aqueous salt solution of PVA-1 is due not only to the thickening of the polymer adsorption layer, but to the compression of the DL as well. The latter factor promotes the falling of the ζ-potential in the case of zinc oxide too (Fig. 7).

The data presented in this work demonstrate the correlation between non-ionic polymer adsorption and the electrosurface characteristics of oxides. The mechanism of adsorption and its effect on the parameters of the double layer are probably not the same for different oxides. The further investigation of this problem is of great theoretical and practical interest.

Information for Contributors

1. Manuscripts should be submitted to Prof. Pál Fejes, Institute of Applied Chemistry, József Attila University, Szeged, Rerrich tér 1, Hungary, H-6720.
2. The manuscripts must not exceed in any case 32 pages (Figures, legends, Tables and Summary included). Manuscripts should be submitted in duplicate.
3. The format of the text: A/4, double spaced, 25 lines per page and 50 characters per line. Title: all capital characters; underlined twice. Subtitle(s) should be written in new line(s) in normal writing, underlined also twice, first characters: capital. (See the following example).

STEREOCHEMICAL STUDIES

Studies on Cyclic-2-Hydroxycarboxylic Acids

By

PÁL KISS

Research Institute for Industrial Chemistry, Budapest
(Received.....)

4. After these comes the summary, which is followed by the text proper. If the parts of the paper are separated by secondary titles like: Introduction, Experimental etc., the following rule holds: secondary titles of equal rank are to be written in new lines, the first word with capital letter, otherwise running text underlined once.
   Example:
   Introduction
   Experimental part
5. The names of the authors in the running text are written in capital letters. Exceptions are the names in connection with scientific instruments, etc. where only the first letter should be capital.
6. Citations in the text with reference to the selected literature at the end of the paper are to be made with squared brackets, like: [5], [4, 9], [4—9].
7. To make printing easier, mathematical formulas are to be simplified as much as possible. Reference to mathematical equations is made by numbers in parenthesis, like: (16).
8. Tables should be typed on separate pages. Please supply numbers and titles for all tables (Numbering occurs with Roman numerals: Table I).
   Throughout the whole text the IUPAC nomenclature should be used.
   Insert of Tables in the text will be indicated at the appropriate place of the margin, like this: Table I.
9. Figures must be drawn clearly with Chinese ink on oily drawing paper, the thickness of lines as well as size of letters and symbols should be selected with care, the minimum size is nearly 0,3 cm.
   The maximum width of Figures is 24 cm, however, Figures of width equal or less than 12 cm are preferred.
   Please, use upwright writing on the Figures.
   In the case of real numbers points are used instead of commas.
   The place of Figures in the text is indicated on the margin like this: Figure 13.
   Please supply legends for all figures and compile these on separate sheets. Indicate only the number of the Figures in the original drawing, for this purpose use blue pencil.
10. Literature will be given under the heading References, like this: (on a separate sheet at the end of the manuscript)
    [1] Allinger, N. L., M. T. Tribble: J. Phys. Chem. 33, 1565 (1976).
    [2] Abraham, J. K., H. S. Hoover: Principles of Competitive Oxidation. Mc Graw-Hill, New York, 1977, p. 133.

INDEX